Emergent Fisher Halos from Information Geometry

Preliminary Open Access Preprint for Dissemination

J. R. Dunkley

December 15, 2025

Abstract

We develop a scalar theory of gravity in which the apparent dark matter halo of a galaxy is the response of a Fisher information vacuum to the presence of baryonic matter. The starting point is a local Fisher energy functional for a scalar field $\sigma_{\rm F}$ on an information manifold for the vacuum, with baryons entering as a source. The Fisher energy admits a Bogomolny type completion that fixes the halo profile via a Fisher bound rather than empirical fitting. The scalar sector is formulated as a dissipative gradient flow generated by a Fisher operator $G_{\rm F}$ embedded in the Universal Information Hydrodynamics framework, with reversible currents $J_{\rm F}$ encoded by a bounded entropy correction obtained by viewing $\sigma_{\rm F}$ as the logit of a Bernoulli occupation number on the Bogoliubov Kubo Mori information manifold. This yields a Fisher Bogomolny equation for the halo at fixed baryon distribution and a Fisher free energy with a saturation mechanism that prevents runaway halo growth, while also producing inequalities and scaling relations that bound halo masses and accelerations and identify characteristic Fisher acceleration and surface density scales. In spherical symmetry the Fisher Bogomolny equation produces cored or cuspy halos depending on a Fisher temperature parameter T_F controlling bounded entropy: in the cold limit $T_F \to 0$ the profiles approach Navarro Frenk-White like cusps, while for T_F of order unity the solutions match Burkert type cores. A Bernoulli bounded entropy model reproduces this cusp to core transition and fits cored profiles. On realistic baryon distributions taken from the SPARC sample, a single halo amplitude per galaxy obtained from a linear Fisher susceptibility model captures many rotation curves, especially in low surface brightness and dwarf galaxies, while $G_{\rm F}$ acting on high surface density discs generates baryon compressed profiles and characteristic acceleration and surface density scales consistent with observed disc galaxy trends. Gravity in this regime is described by the combined acceleration of baryons and Fisher halo, with the halo realised as the Fisher minimiser of the free energy under the given baryon source and the Fisher sector acting as a universal information theoretic susceptibility of the vacuum to matter.

Contents

1 Introduction

The dynamics of galaxies are dominated at large radii by an effective mass distribution that is not accounted for by luminous baryons. Rotation curves remain approximately flat far beyond the optical disc, and gravitational lensing maps reveal mass concentrations offset from baryonic components in cluster collisions. Standard approaches address this by postulating a new form of matter, or by modifying the law of inertia or the Poisson equation. Both strategies introduce new degrees of freedom or new constants which are constrained empirically but not determined by an underlying geometric or information theoretic principle.

In earlier work on the converse Madelung problem the Schrödinger equation was reconstructed from minimal information theoretic axioms, with the quantum potential arising as a Fisher information term in a hydrodynamic representation [1, 2].

In Universal Information Hydrodynamics the same Fisher structure governs the irreversible part of a general GKLS generator on a state space equipped with a monotone metric and a symplectic form [3]. The combined generator $K = G + J$ splits into a symmetric Fisher part G and a skew part J which encodes reversible currents, and the pair is constrained by an information geometric structure that admits a Fisher–Kähler realisation on suitable coadjoint orbits.

This suggests treating gravity at galactic scales as the response of a Fisher information vacuum to the presence of baryonic matter. Instead of introducing a new particle species with an arbitrary density profile, one introduces a scalar Fisher field σ_{F} on physical space whose gradients encode the local Fisher energy stored in vacuum degrees of freedom. Baryons act as sources in a Fisher free energy functional, and the resulting scalar field equation is fixed by the Fisher structure and its Bogomolny completion rather than by phenomenological fitting. The apparent halo is then an emergent property of the Fisher vacuum, determined by a small set of geometric parameters and the baryon distribution.

1.1 Fisher information and hydrodynamic form

The Fisher information of a probability density $\rho(x)$ on $\mathbb{R}^d$,

$$I[\rho] = \int_{\mathbb{R}^d} \frac{|\nabla\rho(x)|^2}{\rho(x)}\,\mathrm{d}x,$$

plays a distinguished role among information measures. It is the unique metric tensor on the statistical manifold of probability distributions [8] that is monotone under coarse graining, and it appears as the quadratic form governing small fluctuations around a reference distribution.

In the Madelung representation of quantum mechanics a wave function $\psi = \sqrt{\rho}\,\mathrm{e}^{iS}$ gives rise to a phase field S and a density field ρ, and the kinetic energy can be written as the sum of a classical part $\int \rho|\nabla S|^2$ and a Fisher part proportional to $I[\rho]$ [7, 9].

In Universal Information Hydrodynamics this structure is lifted to the space of density matrices equipped with a monotone quantum metric such as the Bogoliubov Kubo

Mori (BKM) metric. The irreversible part of a GKLS generator can be written as a gradient flow with respect to this metric, and the Fisher information functional plays the role of a Lyapunov functional. The reversible part generates Hamiltonian or symplectic flows on the same manifold. The pair (G, J) is constrained by a Fisher Kähler structure on suitable coadjoint orbits, so that the state space carries both a Riemannian Fisher metric and a compatible symplectic form.

This geometric framework suggests that any effective field theory for large scale dynamics in a medium built from such degrees of freedom should inherit a Fisher structure. In particular, if the vacuum is treated as a medium with internal states described by a Fisher Kähler manifold, then long wavelength excitations of that vacuum will be governed by effective Fisher energy functionals and gradient flows derived from the underlying metric.

This extends to the metric sector itself. In Section 7 we show that the natural Fisher metric on the configuration space of spatial geometries is the DeWitt supermetric. Imposing refoliation invariance on the associated reversible generator uniquely fixes the Hamiltonian constraint to be that of General Relativity. Consequently, the Einstein–Hilbert action is recovered not as an external assumption, but as the rigid dynamical backbone of the theory, ensuring that the scalar halo embeds covariantly into standard spacetime dynamics.

1.2 Scalar Fisher gravity

The simplest way to encode the response of the Fisher vacuum to baryonic matter is through a real scalar field $\sigma_{\mathrm{F}}(x)$ on physical space, with an energy functional of the form

$$\mathcal{F}[\sigma_{\mathrm{F}}; \rho_b] \;=\; \int_{\mathbb{R}^3} \Big\{ \alpha(x)\, |\nabla \sigma_{\mathrm{F}}(x)|^2 + V_{\mathcal{I}}\big(\sigma_{\mathrm{F}}(x)\big) - \kappa\, \sigma_{\mathrm{F}}(x)\, \rho_b(x) \Big\}\, \mathrm{d}^3x.$$

Here ρ_b is the baryon density, where α is a Fisher stiffness that encodes the local information metric of the vacuum, V_I is an effective bounded entropy potential that arises from the underlying BKM geometry, and κ has the potential so that the scalar-baryon coupling $-\kappa\, \sigma_F \rho_b$ contributes with the correct physical units in the Fisher free energy.

The field equation obtained by varying (1.2) with respect to σ_{F} is a nonlinear elliptic equation of Fisher type. In the weak field regime it can be written schematically as

$$-\nabla \cdot \big(2\alpha(x) \nabla \sigma_F(x)\big) + \frac{dV_I}{d\sigma_F}(x) = \kappa \rho_b(x).$$

The Fisher gravitational acceleration associated to the scalar sector is then defined by

$$g_{\mathrm{F}}(x) \;=\; \lambda_F\, \nabla \sigma_{\mathrm{F}}(x),$$

where λ_F is a Fisher coupling scale. The total acceleration governing slow test particles is the sum of the Newtonian baryon acceleration g_{N} and the Fisher halo acceleration g_{F},

$$g_{\mathrm{tot}}(x) \;=\; g_{\mathrm{N}}(x) + g_{\mathrm{F}}(x).$$

In spherical symmetry this produces a Fisher halo contribution to the circular velocity that can be expressed as a Green function of the baryon acceleration, and in general disc geometries it can be treated as a nonlocal susceptibility kernel.

The central questions are how the Fisher energy functional is fixed by information geometry, how the bounded entropy potential arises from a Bernoulli or BKM geometry, and how the resulting scalar theory compares to observed galactic rotation curves and halo profiles.

1.3 Information geometric origin of the Fisher halo

In Universal Information Hydrodynamics the generator K of the dynamics on state space decomposes into a symmetric part G and a skew part J,

$$K = G + J,$$

where G is a Fisher gradient operator determined by a monotone metric, and J is a Hamiltonian vector field determined by a symplectic form. On diagonal sectors associated with classical probability distributions, G reduces to a Fisher diffusion operator, while J encodes reversible currents.

When the scalar field σ_{F} is interpreted as the logit of a Bernoulli occupation number $p(x)$ on a local two level system, the effective potential $V_{\mathcal{I}}(\sigma_{\mathrm{F}})$ inherits a bounded entropy structure from the BKM geometry of the two level density matrix. The Fisher mobility vanishes at $p = 0$ and $p = 1$, so the Fisher diffusion generated by G cannot drive the system beyond these bounds. The reversible sector J can be interpreted effectively as giving rise to a Fisher temperature parameter T_F in the scalar free energy, controlling the weight of the bounded entropy term relative to the gradient term in this phenomenological reduction.

The halo is not an arbitrary profile but a distinguished solution of a Fisher Bogomolny equation derived from the structure of G and the bounded entropy geometry. The cusp to core transition is then controlled by T_F and by the baryon density, with low temperature and high surface density favouring cusps, and higher temperature and low surface density favouring cores.

1.4 Structure of the paper

The paper is organised as follows. Section 2 introduces the scalar Fisher field, the Fisher free energy functional and its Bogomolny completion in the presence of a baryon source. We derive the scalar field equation and its spherical reduction, identify the Fisher halo acceleration in terms of the scalar gradients, and record basic functional analytic properties and simple solar system bounds for the scalar sector.

Section 3 constructs a bounded entropy potential for σ_F by treating it as the logit of a Bernoulli occupation number on a BKM manifold. This produces a Fisher temperature parameter T_F that controls the strength of the entropy term, and we analyse a family of spherical Bernoulli halos that interpolate between cuspy and cored profiles as T_F and the baryon density are varied.

Section 4 describes numerical solvers for the scalar Fisher halo equation in spherical symmetry and on three-dimensional grids. We present parameter sweeps over T_F and stiffness profiles that illustrate the cusp-to-core transition and the emergence of Burkert-like cores and NFW-like cusps in the Bernoulli model.

Section 5 develops a Fisher susceptibility description of disc galaxies, treating the halo as a nonlocal response to baryonic acceleration. We derive the Baryonic Tully-Fisher Relation from the Bogomolny scaling, establish structural inequalities and Freeman-type surface density bounds, and introduce a pair of Fisher gap and response indices that define a "Fisher spectrometer" for galaxies.

Section 6 presents the numerical implementation of the one-parameter Fisher fit to the SPARC galaxy sample. We analyze the results across low, intermediate and high density subsamples, demonstrating the transition from a soft to a stiff vacuum response and confirming the universality of the effective Planck-weighted stiffness profile.

Section 7 details the relativistic completion of the theory. We derive Einstein geometrodynamics directly from Fisher–DeWitt kinematics, showing that the Einstein-Hilbert action is the unique reversible generator compatible with the information geometry. We further demonstrate that the reversible "Kähler current" sector suppresses gravitational slip, ensuring the model remains consistent with weak lensing observations.

Section 8 discusses cluster-scale Fisher halos and colliding systems. We show that the scalar sector naturally accommodates Bullet-type phenomenology where lensing peaks track collisionless components, and discuss implications for dwarf galaxy clustering.

Section 9 summarises the main results, outlines the guardrails and failure modes of the effective theory, and places the scalar Fisher gravity picture within the broader Universal Information Hydrodynamics programme.

1.5 Guardrails and failure modes

The scalar Fisher halo model developed below is intended to be a necessity statement inside a specific class of Fisher free energies, baryon sources and weak field regimes. This subsection records the main analytic and phenomenological guardrails under which the results are claimed to hold, together with simple failure modes that would falsify or constrain the present formulation. The spirit is the same as the scope and guardrails discussion in [2, 3], adapted to the scalar halo setting.

Analytic guardrails for the scalar Fisher sector. Throughout we work with the scalar free energy (1.2)

$$F[\sigma_F;\rho_b] = \int_{\mathbb{R}^3} \Big(\alpha(x)|\nabla\sigma_F(x)|^2 + V_I(\sigma_F(x)) - \kappa\sigma_F(x)\,\rho_b(x)\Big)\,\mathrm{d}^3x,$$

with a stiffness profile $\alpha(x)$ and a bounded entropy potential V_I induced by the Bernoulli construction in Section 3. The functional analysis in Section 2, the Bogomolny completion, and the radial flow statements in Section 4 are made under three structural hypotheses.

First, the potential sector is assumed to be C^2, bounded below, and strictly convex on the range of σ_F explored by physically relevant halos. In the Bernoulli model of

Section 3 this corresponds to keeping the bounded entropy channel in a single well regime, so that the second variation $V_I''(\sigma_F)$ is non negative along the halo branch. Strongly non convex choices of V_I, for example double well deformations of the Bernoulli potential, would spoil the coercivity of the second variation and can lead to multiple competing local minima. In such cases the uniqueness and stability of the minimiser are not covered by the present arguments.

Second, the Fisher stiffness is taken to be local and uniformly elliptic. We assume that $\alpha(x)$ is measurable and satisfies

$$0 < \alpha_{\min} \leq \alpha(x) \leq \alpha_{\max} < \infty$$

on the region where ρ_b and ρ_F are non negligible. This keeps the Euler-Lagrange equation in the class of uniformly elliptic second order operators and allows standard maximum principles and regularity theory to be applied. Nonlocal kernels or stiffness profiles that vanish inside the halo, which would effectively change the tangent norm in the sense of [2], are outside the present scope and can break the Fisher curvature picture imported from the density manifold.

Third, the baryon source ρ_b is assumed to have finite total mass and to belong to a mild regularity class, such as $L^1(\mathbb{R}^3) \cap L^p(\mathbb{R}^3)$ with $p > 3/2$, or to be a smooth, radially decreasing profile with reasonable decay at large radius. This covers the coarse grained SPARC discs and simple cluster models used later. Highly singular or strongly oscillatory sources, for example distributions with Dirac spikes or fractal structure at very small scales, are not treated here. The halo theory is intended as a coarse grained description on kiloparsec scales and is not claimed to resolve stellar scale clumpiness.

Astrophysical scope and parameter hierarchy. The present paper works in a weak field, quasi Newtonian regime in which the metric remains general relativistic and the Fisher sector enters only through an additional energy density in the Poisson equation. The scalar field modifies the total acceleration by an extra contribution $g_F = -\lambda_F \nabla \sigma_F$, but it does not introduce new tensorial degrees of freedom or alter the local light cones. Precision tests of the metric sector and gravitational wave propagation (such as GW170817) are therefore inherited from general relativity provided the Fisher contribution to the Newtonian potential is small on solar system and binary pulsar scales. Section 5 and the solar system bounds in Section 2 are written under this separation of roles.

On the data side, sharp claims in this paper are restricted to rotationally supported disc galaxies with well measured baryon profiles, essentially the SPARC sample, and to simple cluster scale toy models. Elliptical galaxies with strongly anisotropic velocity tensors, violently interacting systems, and a full Fisher cosmology are deliberately left for future work. The Fisher scalar sector can in principle be extended into those regimes, but this paper does not claim that such an extension has been carried out.

A further guardrail concerns parameter counting. Motivated by the universality pattern in [3], we work with a small set of global Fisher parameters such as a coupling scale λ_F, a Fisher temperature T_F, and one or two parameters in the stiffness profile $\alpha(r)$, together with at most a single susceptibility-like amplitude per galaxy when fitting rotation curves. Allowing additional per galaxy knobs, highly flexible radial profiles for α, or ad hoc modifications of the bounded entropy map would move the model into the class of over parameterised halo fits that the present approach is designed to avoid.

Falsifiers and breakdown scenarios. Within these guardrails the scalar Fisher halo picture has several clean failure modes.

First, the Bogomolny completion and bounded entropy sector give inequalities that bound the halo response to a given baryon source. At fixed ρ_b and Fisher parameters there are upper bounds on the total Fisher halo mass and on central slopes or core surface densities. If a robust population of galaxies were to exhibit inferred halo masses or inner densities that systematically exceed these bounds for all admissible choices of the global Fisher parameters, the present scalar halo model would be falsified or would require a different potential sector.

Second, once a parameter hierarchy is fixed, the scalar Fisher theory predicts specific relations between baryon distributions and rotation curves, including the shape of the radial acceleration relation and the slope and zero point of the baryonic Tully Fisher relation for a given choice of λ_F and T_F. If a full SPARC scale analysis were to show that no single choice of global Fisher parameters plus one amplitude per galaxy can jointly reproduce these relations while respecting the mass and slope bounds, then the current formulation of the Fisher scalar sector would be in tension with the data.

Third, the wider UIH framework imposes Fisher monotonicity under coarse graining and links Fisher curvature scales to hypocoercive indices measured in quantum and statistical systems [2, 3]. If fitting galactic halos forced the Fisher scalar into a regime of effective gaps or spectral exponents that is grossly incompatible with Fisher channels in laboratory systems, in a way that cannot reasonably be attributed to scale separation, the cross scale universality story that motivates Fisher halos would be weakened.

Fourth, on cluster scales the scalar Fisher model implies that effective mass distributions inferred from lensing should track a combination of baryons and Fisher halo in a way consistent with the static or slowly evolving scalar equation. If future observations of clean, dissociative cluster collisions were to show that lensing mass robustly tracks only the hot gas, or moves in a way that cannot be reconciled with a quasi static Fisher scalar coupled to the baryon density, the simple coupling adopted here would have to be revised.

Finally, there are explicit non claims. The present paper does not cover our work on Fisher cosmology for the cosmic microwave background, large scale structure and lensing. It does not address strong field quantum gravity or black hole interiors. It does not attempt to derive a unique microscopic model of the Fisher vacuum degrees of freedom beyond the assumption that their state space carries a Fisher Kähler structure with a bounded entropy scalar sector. Reading the scalar Fisher halo as a complete replacement for general relativity or for all dark sector phenomenology would therefore be outside the scope that this guardrail subsection is intended to define.

1.6 Relation to existing approaches

It is useful to locate the scalar Fisher halo model within the landscape of existing attempts to explain galactic and cluster scale mass discrepancies. Standard cold dark matter treatments postulate a new collisionless particle species whose phase space distribution is evolved under gravity and feedback. In phenomenological applications this is often encapsulated by flexible profile families such as NFW or Einasto halos, with two or more shape parameters per galaxy.

Modified dynamics frameworks instead alter the relation between acceleration and force or the structure of the Poisson equation, typically introducing a new acceleration scale and an interpolating function that control the transition between Newtonian and modified regimes. Emergent gravity proposals appeal to entropic or holographic considerations [11, 12] to generate additional forces from coarse grained microscopic degrees of freedom.

The scalar Fisher construction developed here can be read as an alternative corner of the same phenomenological space. Rather than adding a new particle species or modifying the inertial law directly, we treat the apparent halo as the response of a Fisher information vacuum whose state space already carries a monotone information metric and a Fisher Kähler structure in other contexts. The free energy is fixed by this Fisher geometry and by a bounded entropy channel, and the halo profile is determined by a Bogomolny completion and a scalar field equation rather than by choosing a density profile by hand. Once a small set of global Fisher parameters and a simple stiffness hierarchy are fixed, the scalar sector is constrained to live inside the corresponding Fisher Bogomolny and bounded entropy bounds.

From a practical point of view the scalar Fisher model occupies an intermediate position between fully empirical halo fitting and tightly prescribed modified gravity. It retains the Newtonian and weak field GR limit for the metric sector, and uses the Fisher scalar only to supply an additional quasi static potential determined by the baryon distribution. At the same time, the Fisher free energy and its Bogomolny structure restrict the space of allowed halos more strongly than generic profile fits. A systematic quantitative comparison with cold dark matter fits, MOND type laws and emergent gravity constructions on common galaxy and cluster samples is left for future work, but the present framework is designed so that such comparisons can be made at the level of Fisher parameters and inequalities rather than ad hoc profiles.

Remark (Quantum potential as Korteweg capillarity). In the converse Madelung analysis [1, 2] the Fisher curvature term appears in the Hamiltonian as a quadratic gradient energy

$$F_{\mathrm{F}}[\rho] = 4\alpha_Q \int_{\mathbb{R}^d} |\nabla\sqrt{\rho(x)}|^2 \, \mathrm{d}x,$$

with associated Euler-Lagrange potential

$$Q_{\alpha_Q}(\rho) = -2\alpha_Q \, \frac{\Delta\sqrt{\rho}}{\sqrt{\rho}}.$$

Written in momentum form, the contribution of F_{F} can be expressed as the divergence of a symmetric stress tensor Π^{F} whose entries are built from ρ, $\nabla\rho$ and $\nabla^2\rho$. This stress has the same structure as the classical Euler-Korteweg capillarity stress for a compressible fluid with a density-dependent capillarity coefficient, so that the Bohm-Madelung "quantum potential" Q_{α_Q} may be viewed as the capillary pressure associated with an internal surface tension of the probability fluid. In particular, the Madelung hydrodynamics sit inside the well-studied class of capillary (Euler-Korteweg) fluids; the Fisher term penalises sharp gradients of ρ rather than introducing any new long-range interaction.

We will only use this observation at the level of interpretation. No additional assumptions from the Korteweg theory are required in what follows.

Remark. The Fisher stiffness $Z(\sigma_F)$ is positive by construction and the bounded entropy potential $V_I(\sigma_F)$ is built from the Bernoulli entropy, so the scalar sector admits a standard relativistic completion. A covariant formulation and the corresponding energy conditions are recorded in Section 2.8.

2 Scalar Fisher gravity and Bogomolny structure

In this section we develop the scalar Fisher description of gravity in the weak field regime. We start from a local Fisher energy functional for a scalar field σ_{F} on $\mathbb{R}^3$ coupled to a baryon density ρ_b, and we derive the associated Bogomolny type bound and scalar field equation. The construction is deliberately minimal and local, and will be refined later when bounded entropy and Bernoulli geometry are introduced.

2.1 Fisher free energy for a scalar halo

We consider a real scalar field $\sigma_{\mathrm{F}}\colon \mathbb{R}^3 \to \mathbb{R}$ and a non negative baryon density $\rho_b\colon \mathbb{R}^3 \to \mathbb{R}_{\geq 0}$. The Fisher free energy is taken to be of the form

$$\mathcal{F}[\sigma_{\mathrm{F}}; \rho_b] \;=\; \int_{\mathbb{R}^3} \Big\{ \alpha(x)\, |\nabla \sigma_{\mathrm{F}}(x)|^2 + U\big(\sigma_{\mathrm{F}}(x)\big) - \kappa\, \sigma_{\mathrm{F}}(x)\, \rho_b(x) \Big\}\, \mathrm{d}^3x,$$

where $\alpha(x) > 0$ is a stiffness profile, U is a scalar potential, and κ is a coupling constant with potential.

The interpretation is that the gradient term encodes the Fisher energy stored in spatial variations of the scalar field, while the potential U encodes local constraints from the underlying information geometry of the vacuum. Consistent with the thermodynamic structure of Universal Information Hydrodynamics [3], the scalar field σ_F can be viewed as a dimensionless chemical potential.

In this picture the linear coupling $-\kappa\sigma_{\mathrm{F}}\rho_b$ has the standard form of a Gibbs mixing contribution, representing the work required to insert baryonic matter ρ_b into the vacuum fluid.

We will use this as the canonical effective coupling between the Fisher vacuum sector and baryons in the present scalar theory.

A simple field redefinition makes the stiffness role of α more transparent in the constant coefficient case. For $\alpha(x) \equiv \alpha_0$ one can write

$$\phi(x) \;=\; \sqrt{2\alpha_0}\, \sigma_F(x),$$

so that

$$\alpha_0\, |\nabla \sigma_F|^2 \;=\; \frac{1}{2}\, |\nabla \phi|^2, \qquad -\kappa\, \sigma_F\, \rho_b \;=\; -\,\frac{\kappa}{\sqrt{2\alpha_0}}\, \phi\, \rho_b.$$

In this normalisation the gradient term takes the canonical form $\frac{1}{2}\int |\nabla\phi|^2 d^3x$, and the effect of α_0 is to set the overall size of an effective matter coupling

$$g_{\text{eff}} \;=\; \frac{\kappa}{\sqrt{2\alpha_0}}.$$

Larger Fisher stiffness therefore corresponds to a more weakly coupled scalar response to a given baryon distribution, while smaller stiffness enhances the response. When $\alpha(x)$ varies slowly with position the same interpretation holds locally up to derivative corrections from $\nabla\alpha$, which can be treated as higher order terms in the weak field, slowly varying regime.

The Euler Lagrange equation for σ_{F} obtained by varying (2.1) is

$$-\nabla\cdot\big(2\alpha(x)\,\nabla\sigma_{\text{F}}(x)\big) + U'\big(\sigma_{\text{F}}(x)\big) \;=\; \kappa\,\rho_b(x),$$

interpreted in a weak sense when ρ_b is a finite measure rather than a smooth function.

The Fisher gravitational acceleration associated to the scalar sector is defined as the gradient of the field,

$$g_{\text{F}}(x) \;=\; \lambda_F\,\nabla\sigma_{\text{F}}(x),$$

where λ_F is a positive constant. For a test particle in the weak field regime, the total acceleration is the sum of the Newtonian baryon acceleration g_{N} and the Fisher acceleration,

$$g_{\text{tot}}(x) \;=\; g_{\text{N}}(x) + g_{\text{F}}(x).$$

Microscopic origin of the stiffness scale. In Fisher regularised Madelung dynamics the quadratic Fisher form that controls density gradients carries a fixed coefficient $\alpha = \hbar^2/(2m)$, determined by matching the hydrodynamic equations to the Galilean dispersion relation for a free particle [1].

In that setting the same coefficient sets the scale of the quantum regulariser and ties the Fisher curvature of the density directly to the inertial mass m [2]. Scalar sectors that descend from such microscopic dynamics inherit this Fisher coefficient in the overall scale of their gradient term. After the canonical rescaling that brings the scalar Fisher energy to the form $\frac{1}{2}\int |\nabla\phi|^2\, d^3x$, the coefficient α_0 moves into the effective matter coupling $g_{\text{eff}} = \kappa/\sqrt{2\alpha_0}$ and can be interpreted as setting an inverse squared coupling for the scalar response. In this way the stiffness profile $\alpha(x)$ appearing in the halo model can be viewed, at least at the level of scale setting, as the large scale imprint of the same Fisher regulariser that controls the underlying Madelung sector.

In the remainder of this section we choose U so that the gradient term and source term admit a Bogomolny completion, leading to a Fisher bound and a first order equation for σ_{F} in spherical symmetry.

2.2 Spherical symmetry

We now specialise to static, spherically symmetric configurations. Write

$$\sigma_{\text{F}}(x) = \sigma_{\text{F}}(r), \qquad r = |x|,$$

and assume a spherically symmetric baryon density

$$\rho_b(x) = \rho_b(r).$$

The free energy (2.1) becomes

$$\mathcal{F}[\sigma_{\rm F}; \rho_b] \;=\; 4\pi \int_0^\infty \left\{\alpha(r)\, \sigma_{\rm F}'(r)^2 + U\big(\sigma_{\rm F}(r)\big) - \kappa\, \sigma_{\rm F}(r)\, \rho_b(r)\right\} r^2\, {\rm d}r.$$

where a prime denotes a derivative with respect to r.

The Euler Lagrange equation (2.1) reduces to

$$-\frac{1}{r^2}\frac{\rm d}{{\rm d}r}\big(2\alpha(r)\, r^2 \sigma_{\rm F}'(r)\big) + U'\big(\sigma_{\rm F}(r)\big) \;=\; \kappa\, \rho_b(r).$$

This can be interpreted as a balance between Fisher diffusion, local potential forces, and the baryon source.

The baryon mass enclosed within radius r is

$$M_b(r) \;=\; 4\pi \int_0^r \rho_b(s)\, s^2\, {\rm d}s,$$

so that

$$\rho_b(r)\, r^2 \;=\; \frac{1}{4\pi}\, \frac{{\rm d}M_b}{{\rm d}r}(r).$$

The Newtonian baryon acceleration in the radial direction is

$$g_{\rm N}(r) \;=\; -\frac{G M_b(r)}{r^2}\, \hat{r},$$

where $\hat{r}$ is the radial unit vector. The Fisher halo acceleration is

$$g_{\rm F}(r) \;=\; \lambda_F\, \sigma_{\rm F}'(r)\, \hat{r},$$

and the total circular velocity for a test particle in the equatorial plane is

$$v_{\rm c}^2(r) \;=\; r\, |g_{\rm N}(r) + g_{\rm F}(r)|.$$

2.3 Cold Fisher limit and Bogomolny completion

In the cold Fisher limit the bounded entropy potential is negligible, so we set

$$U(\sigma_{\rm F}) = 0.$$

The free energy reduces to

$$\mathcal{F}_{\rm cold}[\sigma_{\rm F}; \rho_b] \;=\; 4\pi \int_0^\infty \left\{\alpha(r)\, \sigma_{\rm F}'(r)^2 - \kappa\, \sigma_{\rm F}(r)\, \rho_b(r)\right\} r^2\, {\rm d}r.$$

Using (2.2), the source term can be written as

$$-4\pi\kappa \int_0^\infty \sigma_{\mathrm{F}}(r)\, \rho_b(r)\, r^2\, \mathrm{d}r \;=\; -\kappa \int_0^\infty \sigma_{\mathrm{F}}(r)\, \frac{\mathrm{d}M_b}{\mathrm{d}r}(r)\, \mathrm{d}r.$$

An integration by parts gives

$$-\kappa \int_0^\infty \sigma_{\mathrm{F}}(r)\, \frac{\mathrm{d}M_b}{\mathrm{d}r}(r)\, \mathrm{d}r \;=\; -\kappa\big[\sigma_{\mathrm{F}}(r)\, M_b(r)\big]_0^\infty + \kappa \int_0^\infty \sigma_{\mathrm{F}}'(r)\, M_b(r)\, \mathrm{d}r.$$

Assuming that $M_b(r)$ vanishes at the origin and that $\sigma_{\mathrm{F}}(r)$ does not diverge faster than $1/r^2$ at infinity, the boundary term can be treated as a finite surface contribution.

Substituting (2.3) into (2.3) gives

$$\mathcal{F}_{\mathrm{cold}}[\sigma_{\mathrm{F}};\rho_b] \;=\; 4\pi \int_0^\infty \alpha(r)\, \sigma_{\mathrm{F}}'(r)^2\, r^2\, \mathrm{d}r + \kappa \int_0^\infty \sigma_{\mathrm{F}}'(r)\, M_b(r)\, \mathrm{d}r - \kappa\big[\sigma_{\mathrm{F}}(r)\, M_b(r)\big]_0^\infty.$$

The integrand in the bulk can be written as a quadratic in σ_{F}',

$$4\pi\alpha(r)\, r^2\, \sigma_{\mathrm{F}}'(r)^2 + \kappa\, M_b(r)\, \sigma_{\mathrm{F}}'(r) \;=\; 4\pi\alpha(r)\, r^2 \left(\sigma_{\mathrm{F}}'(r) + \frac{\kappa\, M_b(r)}{8\pi\alpha(r)\, r^2}\right)^2 - \frac{\kappa^2 M_b(r)^2}{16\pi\, \alpha(r)\, r^2}.$$

Therefore

$$\begin{aligned}\mathcal{F}_{\mathrm{cold}}[\sigma_{\mathrm{F}};\rho_b] \;&= 4\pi \int_0^\infty \alpha(r)\, r^2 \left(\sigma_{\mathrm{F}}'(r) + \frac{\kappa\, M_b(r)}{8\pi\alpha(r)\, r^2}\right)^2 \mathrm{d}r \\ &\quad - \int_0^\infty \frac{\kappa^2 M_b(r)^2}{16\pi\, \alpha(r)\, r^2}\, \mathrm{d}r - \kappa\big[\sigma_{\mathrm{F}}(r)\, M_b(r)\big]_0^\infty.\end{aligned}$$

The first term is non negative, so we obtain the Fisher Bogomolny bound

$$\mathcal{F}_{\mathrm{cold}}[\sigma_{\mathrm{F}};\rho_b] \;\geq\; -\int_0^\infty \frac{\kappa^2 M_b(r)^2}{16\pi\, \alpha(r)\, r^2}\, \mathrm{d}r - \kappa\big[\sigma_{\mathrm{F}}(r)\, M_b(r)\big]_0^\infty.$$

It is convenient to isolate the radial integral in this expression as a Fisher charge functional of the baryon distribution.

Writing the radial reduction in the form of a general Bogomolny completion, one can identify a weight

$$w(r) = 8\pi\, \alpha(r)\, r^2, \qquad q(r) = \frac{\kappa\, M_b(r)}{8\pi\, \alpha(r)\, r^2},$$

so that the pure Fisher charge takes the specialised form

$$Q_F^{\mathrm{grav}}[\rho_b] \;:=\; \frac{1}{2}\int_0^\infty w(r)\, |q(r)|^2\, \mathrm{d}r \;=\; \int_0^\infty \frac{\kappa^2 M_b(r)^2}{16\pi\alpha(r) r^2}\, \mathrm{d}r.$$

In terms of Q_F^{grav} the cold Fisher bound can be written

$$\mathcal{F}_{\mathrm{cold}}[\sigma_{\mathrm{F}};\rho_b] \;\geq\; -\,Q_F^{\mathrm{grav}}[\rho_b] \;-\; \kappa\, \sigma_{\mathrm{F}}(r) M_b(r)\Big|_0^\infty.$$

For the class of baryon profiles and scalar configurations considered here the boundary term either vanishes under the standard regularity and decay conditions or can be controlled as a finite surface contribution. In that regime $Q_F^{\mathrm{grav}}[\rho_b]$ depends only on the enclosed baryon mass profile and plays the role of a configuration independent lower scale for the cold Fisher free energy, in direct analogy with the pure Fisher charge $Q_F[q]$ in the abstract scalar setting.

The bound is saturated if and only if the first order Fisher Bogomolny equation holds:

$$\sigma_{\mathrm{F}}'(r) \;=\; -\frac{\kappa\, M_b(r)}{8\pi\,\alpha(r)\,r^2}.$$

Any solution of (2.3) that satisfies suitable boundary conditions at the origin and infinity is therefore a global minimiser of the cold Fisher free energy for the given baryon distribution.

> *Remark.* The Bogomolny equation (2.3) relates the radial derivative of the Fisher scalar field directly to the enclosed baryon mass. Up to the stiffness profile $\alpha(r)$ and the coupling κ, the Fisher halo is completely determined by the baryonic mass profile. The effective Fisher halo mass and acceleration then follow from the scalar gradient. Unlike standard dark matter halos, where the mass and scale radius are free fitting parameters, the Bogomolny nature of the Fisher halo implies its profile is entirely rigid: once the baryon source and global stiffness are set, the halo mass distribution is geometrically necessitated.

2.4 Cold Fisher halos as scalar EPI extremals

The scalar information sector developed in the Fisher–Kähler paper provides a general template for Extreme Physical Information (EPI) functionals on a Fisher type state space [5, 9, 10]. In that setting a real scalar field $\sigma(x)$ carries a Fisher gradient energy with weight $w(x)$, couples linearly to an external source $q(x)$, and is endowed with a bounded entropy $S_{\mathrm{bnd}}[\sigma]$. The pure Fisher free energy

$$F_0[\sigma] := \frac{1}{2}\int_X w(x)\,|\nabla\sigma(x)|^2\,d\mu(x) - \int_X w(x)\,\nabla\sigma(x)\cdot q(x)\,d\mu(x)$$

admits an exact Bogomolny completion

$$F_0[\sigma] = \frac{1}{2}\int_X w\,|\nabla\sigma - q|^2\,d\mu - Q_F[q], \qquad Q_F[q] := \frac{1}{2}\int_X w\,|q|^2\,d\mu,$$

so that $F_0[\sigma] \geq -Q_F[q]$ with equality if and only if the BPS condition $\nabla\sigma = q$ holds almost everywhere. Identifying

$$I_{\mathrm{sc}}[\sigma] := \frac{1}{2}\int_X w\,|\nabla\sigma|^2\,d\mu, \qquad J_{F,\mathrm{sc}}[\sigma] := \int_X w\,\nabla\sigma\cdot q\,d\mu,$$

one may view $F_0 = I_{\mathrm{sc}} - J_{F,\mathrm{sc}} - Q_F[q]$ as an EPI functional in which the Fisher data information I_{sc} is pumped from the source information $J_{F,\mathrm{sc}}$. BPS configurations

saturate the Fisher charge $Q_F[q]$ and realise maximal information extraction in this channel.

The cold Fisher halo functional

$$F_{\mathrm{cold}}[\sigma_F;\rho_b] = 4\pi \int_0^\infty \left(\alpha(r)\,\sigma_F'(r)^2 - \kappa\,\sigma_F(r)\,\rho_b(r)\right) r^2\,dr$$

is a special case of this scalar EPI structure. Introducing the enclosed baryon mass $M_b'(r) = 4\pi r^2 \rho_b(r)$ and integrating by parts, one finds

$$F_{\mathrm{cold}}[\sigma_F;\rho_b] = 4\pi \int_0^\infty \alpha(r)\,\sigma_F'(r)^2 r^2\,dr + \kappa \int_0^\infty \sigma_F'(r) M_b(r)\,dr - \kappa\left[\sigma_F(r) M_b(r)\right]_0^\infty.$$

If we now specialise the scalar sector to $X = \mathbb{R}^3$ with spherical symmetry and set

$$w(r) := 8\pi\,\alpha(r)\,r^2, \qquad \sigma(r) := \sigma_F(r), \qquad q(r) := -\frac{\kappa\,M_b(r)}{8\pi\,\alpha(r)\,r^2}\,\hat{r},$$

then the bulk term in F_{cold} takes the EPI form

$$F_{\mathrm{cold}}^{\mathrm{bulk}}[\sigma_F;\rho_b] = I_{\mathrm{sc}}[\sigma_F] - J_{F,\mathrm{sc}}[\sigma_F],$$

with the same data and source functionals $I_{\mathrm{sc}}, J_{F,\mathrm{sc}}$ as in the abstract scalar theory. Using the Bogomolny completion one can equivalently write

$$F_{\mathrm{cold}}[\sigma_F;\rho_b] = \frac{1}{2}\int_0^\infty w(r)\,|\sigma_F'(r) - q_r(r)|^2\,dr - Q_F[q] - \kappa\left[\sigma_F(r) M_b(r)\right]_0^\infty,$$

where $Q_F[q]$ is the pure Fisher charge of the baryon source. For baryon profiles and scalar configurations satisfying the usual regularity and decay conditions the surface term can be treated as a finite boundary contribution, so the cold Fisher bound reduces to

$$F_{\mathrm{cold}}[\sigma_F;\rho_b] \geq -Q_F[q] - \kappa\left[\sigma_F(r) M_b(r)\right]_0^\infty.$$

The Fisher Bogomolny equation

$$\sigma_F'(r) = -\frac{\kappa\,M_b(r)}{8\pi\,\alpha(r)\,r^2}$$

is precisely the radial component of the scalar BPS condition $\nabla\sigma = q$ for this choice of weight and source. In the cold limit $T_F \to 0$ a Fisher BPS halo is therefore exactly an EPI extremal in the scalar sector: the baryon mass profile $M_b(r)$ plays the role of the external information source q, and the Fisher halo profile σ_F is the field configuration that saturates the pure Fisher charge $Q_F[q]$ and realises maximal information transfer from the baryons into the scalar Fisher channel. Turning on a finite Fisher temperature T_F adds the bounded entropy functional $S_{\mathrm{bnd}}[\sigma_F]$ to the source sector and deforms the BPS halo into a finite temperature EPI extremal, truncating the Fisher halo profile while preserving the Fisher charge lower bound.

2.5 Fisher halo acceleration and effective density

For any spherically symmetric solution $\sigma_{\rm F}(r)$, the Fisher halo acceleration is given by (2.2),

$$g_{\rm F}(r) \;=\; \lambda_F\, \sigma_{\rm F}'(r)\, \hat{r}.$$

Using the Fisher Bogomolny equation (2.3) in the cold limit, we obtain

$$g_{\rm F}(r) \;=\; -\lambda_F\, \frac{\kappa\, M_b(r)}{8\pi\, \alpha(r)\, r^2}\, \hat{r}.$$

For $\kappa > 0$ and $\lambda_F > 0$ the Bogomolny branch (2.3) has $\sigma_{\rm F}'(r) < 0$, so $g_{\rm F}(r)$ points inward, opposite to $\hat{r}$, as required for an attractive Fisher halo.

With this choice the physical acceleration scale is set by the product $\lambda_F \kappa$, which carries the same dimensions as a Newtonian gravitational coupling and appears in the Fisher halo acceleration.

It is convenient to define an effective Fisher mass profile $M_F(r)$ by comparing (2.5) with the Newtonian form

$$g_{\rm F}(r) \;=\; -\frac{G M_F(r)}{r^2}\, \hat{r}.$$

Equating the magnitudes gives

$$\frac{G M_F(r)}{r^2} \;=\; \frac{\lambda_F \kappa}{8\pi\alpha(r)}\, \frac{M_b(r)}{r^2},$$

so that, for $\kappa > 0$ and $\lambda_F > 0$, the effective Fisher coupling

$$C_F := \frac{\lambda_F \kappa}{8\pi G}$$

is positive and

$$M_F(r) = C_F\, \frac{M_b(r)}{\alpha(r)}.$$

In particular, for a constant stiffness $\alpha(r) = \alpha_0$ the effective Fisher halo mass is proportional to the baryon mass,

$$M_F(r) = \gamma_F M_b(r), \qquad \gamma_F = \frac{C_F}{\alpha_0}.$$

This expression makes the inverse dependence on the stiffness explicit: for fixed Fisher couplings (λ_F, κ) the ratio M_F/M_b is proportional to $1/\alpha_0$. Together with the canonical rescaling above, this supports the view that α controls an effective inverse squared coupling of the scalar Fisher sector to baryons. A stiffer vacuum (larger α) produces a lighter halo for the same baryonic mass, while a softer vacuum (smaller α) yields a more massive halo.

The total enclosed mass that determines the circular velocity is then

$$M_{\rm tot}(r) \;=\; M_b(r) + M_F(r),$$

and the circular velocity satisfies

$$v_c^2(r) \;=\; \frac{G M_{\rm tot}(r)}{r}.$$

In this cold, constant stiffness limit the scalar Fisher gravity reproduces a baryon scaled halo model, with a proportionality factor set by the Fisher couplings.

More generally, when $\alpha(r)$ varies with radius, the Fisher halo mass picks up a non trivial radial dependence through (5.6). A stiffness profile that grows with radius suppresses the Fisher mass relative to the baryon mass in the outer regions, while a stiffness profile that decays with radius enhances the outer halo. This radial structure can be used to capture the observed transition from baryon dominance in the inner disc to halo dominance in the outskirts.

The cold Fisher Bogomolny analysis provides a baseline scalar theory in which the halo profile is slaved to the baryons through the Fisher energy. Before introducing the bounded entropy sector it is useful to record some basic functional analytic properties of the scalar Fisher theory that will be used implicitly in the rest of the paper.

In this constant stiffness, zero temperature limit the Bogomolny completion identifies a preferred class of halo profiles that saturate the quadratic Fisher bound for a given baryon source. Following the structure of the bounded Fisher entropy sector we will refer to these configurations as *Fisher BPS* halos: they minimise the scalar Fisher free energy at fixed baryon distribution, and small perturbations that respect the regularity assumptions increase the free energy at quadratic order. In what follows the phrase "BPS type" is used only in this restricted sense, as a shorthand for cold Fisher configurations that saturate the Bogomolny inequality; no additional supersymmetric structure is assumed, and all stability statements are made at the level of the scalar free energy functional and its Euler-Lagrange equation.

2.6 Functional analytic properties of the scalar Fisher sector

---

The scalar Fisher free energy in three dimensions was introduced in (2.1),

$$F[\sigma_F;\rho_b] = \int_{\mathbb{R}^3} \Big(\alpha(x)\,|\nabla\sigma_F(x)|^2 + V_I(\sigma_F(x)) - \kappa\,\sigma_F(x)\,\rho_b(x)\Big)\,\mathrm{d}^3x,$$

and its spherical reduction was written as

$$F[\sigma_F;\rho_b] = 4\pi \int_0^\infty \Big(\alpha(r)\,\sigma_F'(r)^2 + U(\sigma_F(r)) - \kappa\,\sigma_F(r)\,\rho_b(r)\Big)\,r^2\,\mathrm{d}r.$$

Here α is a Fisher stiffness, V_I (or U in the radial setting) is an effective bounded entropy potential, and ρ_b is a non-negative baryon density with finite mass. In this subsection we summarise modest functional analytic properties of $F[\sigma_F;\rho_b]$ that are sufficient for the halo applications in this paper. A more abstract treatment of the scalar Fisher theory is given in the scalar companion paper.

Assumptions and lower bounds. For definiteness we work in spherical symmetry and regard σ_F as an element of the weighted Sobolev space

$$H^1_{\mathrm{rad}} := \Big\{\sigma_F \colon (0,\infty) \to \mathbb{R} \;\Big|\; \int_0^\infty \big(\sigma_F'(r)^2 + \sigma_F(r)^2\big)\, r^2 \,\mathrm{d}r < \infty\Big\},$$

with the standard identification of functions in H^1_{rad} that agree almost everywhere. We assume that the stiffness profile $\alpha(r)$ is measurable, radial, and satisfies uniform bounds

$$0 < \alpha_{\min} \le \alpha(r) \le \alpha_{\max} < \infty \quad \text{for all } r \ge 0,$$

and that the baryon density $\rho_b(r)$ is non-negative, locally bounded, and has finite total mass $M_b(\infty) = 4\pi \int_0^\infty \rho_b(r)\, r^2 \,\mathrm{d}r < \infty$.

In the Bernoulli bounded entropy construction of Section 3 the scalar potential $U(\sigma_F)$ is chosen to be proportional to the negative of the Bernoulli entropy,

$$U(\sigma_F) = -T_F S_{\mathrm{Bern}}(\sigma_F),$$

so that, using $0 \le S_{\mathrm{Bern}} \le \log 2$, one has the simple pointwise bound

$$-T_F \log 2 \le U(\sigma_F(r)) \le 0 \quad \text{for all } r.$$

The bounded entropy term is therefore uniformly bounded from below and cannot drive the Fisher free energy to arbitrarily negative values on any finite domain. Writing

$$F[\sigma_F;\rho_b] = F_{\mathrm{cold}}[\sigma_F;\rho_b] + 4\pi \int_0^\infty U(\sigma_F(r)) r^2\, dr,$$

and imposing the usual regularity conditions at the origin together with a fixed vacuum value at infinity, $\sigma_F(r) \to 0$ as $r \to \infty$, the cold sector analysis of Section 2.3 gives the Bogomolny bound

$$F_{\mathrm{cold}}[\sigma_F;\rho_b] \ge -Q_F^{\mathrm{grav}}[\rho_b],$$

where $Q_F^{\mathrm{grav}}[\rho_b]$ depends only on the baryon mass profile. The Bernoulli contribution then supplies at most a finite, source-independent shift to this bound on any finite halo volume. In the relativistic completion one is free to subtract the vacuum value $U(\sigma_{\mathrm{vac}})$ and absorb this constant into the background cosmological term, so that the renormalised potential is non-negative at the vacuum and the scalar sector obeys the usual energy conditions.

Since U is bounded below by $-T_F \log 2$ and contributes only a finite, source-independent shift to the free energy on any finite halo volume, the full scalar free energy inherits the same type of lower bound,

$$F[\sigma_F;\rho_b] \ge -Q_F^{\mathrm{grav}}[\rho_b] - C_{\mathrm{Bern}}(T_F),$$

with a constant $C_{\mathrm{Bern}}(T_F)$ that depends only on the Fisher temperature and the chosen outer radius. At the level of the relativistic completion this additive constant is absorbed into the background cosmological term; here only differences in F enter the weak-field halo phenomenology.

Existence of minimisers in the radial setting. On the weighted Sobolev space H^1_{rad} with fixed boundary values, the functional $F[\sigma_F;\rho_b]$ is the sum of three terms: a strictly convex quadratic gradient contribution, a pointwise bounded potential, and a linear source term. Under the assumptions above the gradient term controls the H^1_{rad} norm, the potential term is bounded from below and continuous in σ_F, and the source term is continuous with respect to the H^1_{rad} topology for bounded baryon mass. Standard arguments in the direct method of the calculus of variations then give:

- for each fixed baryon profile ρ_b and Fisher parameters (α, T_F, κ), there exists at least one minimiser $\sigma_F^* \in H^1_{\mathrm{rad}}$ of $F[\sigma_F;\rho_b]$ subject to the imposed boundary conditions;
- every minimising sequence for $F[\sigma_F;\rho_b]$ contains a subsequence that converges weakly in H^1_{rad} and strongly in L^2_{loc} to a minimiser σ_F^*.

We do not attempt here to prove the most general uniqueness statements. In the cold Fisher regime the Bogomolny equation (2.3) with regularity at the origin and fixed vacuum value at infinity singles out a unique monotone profile for each baryon mass profile, and any solution of the first order equation is a global minimiser of F_{cold} for the given ρ_b. In the bounded entropy regime, the static Euler-Lagrange equation

$$-\frac{1}{r^2}\frac{\mathrm{d}}{\mathrm{d}r}\Big(2\alpha(r)\,r^2\,\sigma_F'(r)\Big) + T_F\,\frac{\mathrm{d}S_{\mathrm{Bern}}}{\mathrm{d}\sigma_F}(\sigma_F(r)) = \kappa\,\rho_b(r)$$

is a uniformly elliptic second order equation with a monotone nonlinearity in σ_F for admissible ranges of T_F. For fixed boundary data one expects uniqueness of weak solutions in the natural energy class under mild additional regularity hypotheses on α and ρ_b. Our radial gradient flow experiments in Section 4 are consistent with convergence towards a single equilibrium configuration for the scalar field.

Bounds on Fisher halo mass and density. In the cold Bogomolny limit the effective Fisher mass profile $M_F(r)$ was obtained in (5.6) as

$$M_F(r) = \frac{\lambda_F \kappa}{8\pi G}\,\frac{M_b(r)}{\alpha(r)},$$

so that the halo mass is proportional to the enclosed baryon mass, with a proportionality factor that depends only on the Fisher couplings and the stiffness profile. If α is bounded above and below, the ratio M_F/M_b is correspondingly bounded: defining

$$\gamma_{\min} := \frac{C_F}{\alpha_{\max}}, \qquad \gamma_{\max} := \frac{C_F}{\alpha_{\min}},$$

one has

$$\gamma_{\min} \;\le\; \frac{M_F(r)}{M_b(r)} \;\le\; \gamma_{\max}$$

for all radii in the domain where $\alpha_{\min} \le \alpha(r) \le \alpha_{\max}$.

$$\gamma_{\min}\,M_b(r) \;\le\; M_F(r) \;\le\; \gamma_{\max}\,M_b(r)$$

for all radii. The total enclosed mass therefore satisfies

$$\big(1+\gamma_{\min}\big)\,M_b(r) \;\le\; M_{\rm tot}(r) \;\le\; \big(1+\gamma_{\max}\big)\,M_b(r),$$

so the Fisher sector cannot generate haloes whose mass exceeds a fixed multiple of the baryonic mass at any radius, once the Fisher parameters are specified.

The effective Fisher density $\rho_F(r)$ derived from the scalar profile via (2.2) inherits the same control. In particular, for BPS solutions the combination of the Bogomolny bound and the stiffness bounds ensures that $\rho_F(r)$ is square-integrable with respect to the radial measure $r^2\,\mathrm{d}r$ and that the associated halo mass is finite. In the bounded entropy regime the additional contribution of $U(\sigma_F)$ does not spoil these estimates, since the Bernoulli term is pointwise bounded and does not introduce new infrared divergences.

These functional properties are modest but sufficient for the present paper. They justify treating the scalar Fisher halo as the minimiser of a well posed free energy functional with a finite lower bound, and they ensure that the radial gradient flows used in Section 4 converge towards physically reasonable halo profiles with controlled mass and density.

In the next section we introduce a bounded entropy potential that arises from a Bernoulli geometry on the BKM manifold, and we show how this modifies the scalar equation and allows for a controlled cusp to core transition.

Proposition (Existence and convexity of Fisher-Bernoulli minimisers) Let $\rho_b(r)$ be a spherically symmetric baryon density with $\rho_b \in L^1(\mathbb{R}^3)\cap L^\infty(\mathbb{R}^3)$ and compact support, and let the Fisher stiffness satisfy

$$0 < \alpha_{\min} \le \alpha(r) \le \alpha_{\max} < \infty.$$

Let $\sigma_F(r)$ take values in a bounded Bernoulli channel range

$$\sigma_{\min} \le \sigma_F(r) \le \sigma_{\max},$$

and let $U(\sigma_F;T_F)$ be the Bernoulli bounded entropy potential, continuous on $[\sigma_{\min},\sigma_{\max}]$ and convex in σ_F for each fixed $T_F \ge 0$. Consider the free energy functional on the radial Sobolev space

$$F[\sigma_F;\rho_b] = \int_{\mathbb{R}^3}\left[\frac{1}{2}\alpha(r)\,|\nabla\sigma_F|^2 + U(\sigma_F;T_F) - \kappa\,\sigma_F\,\rho_b(r)\right]d^3x,$$

restricted to the convex admissible set

$$\mathcal{A} = \left\{\sigma_F \in H^1_{\rm rad}(\mathbb{R}^3) \;:\; \sigma_{\min}\le\sigma_F(r)\le\sigma_{\max}\ \text{a.e.}\right\}.$$

Then:

1. $F[\sigma_F;\rho_b]$ is bounded below and coercive in the gradient norm on $\mathcal{A}$.
2. F attains its minimum on $\mathcal{A}$: there exists at least one minimiser $\sigma_F^\star \in \mathcal{A}$.
3. Any minimiser $\sigma_F^\star$ is a weak solution of the scalar Euler-Lagrange equation

$$-\nabla\cdot(\alpha\nabla\sigma_F) + U'(\sigma_F;T_F) = \kappa\rho_b$$

in the radial class, and is smooth away from the baryon support.

Proof (sketch). Boundedness of the Bernoulli channel implies $|U(\sigma_F; T_F)| \le U_{\max}(T_F)$ on $[\sigma_{\min}, \sigma_{\max}]$. For any $\sigma_F \in \mathcal{A}$ we have

$$F[\sigma_F; \rho_b] \ge \frac{\alpha_{\min}}{2} \|\nabla\sigma_F\|_{L^2}^2 - U_{\max}(T_F)\, V_{\text{eff}} - \kappa\, \sigma_{\max}\, \|\rho_b\|_{L^1},$$

so F is bounded below, and $F[\sigma_F] \to +\infty$ as $\|\nabla\sigma_F\|_{L^2} \to \infty$ at fixed bounds on σ_F. Thus F is coercive on $\mathcal{A}$. A minimising sequence is bounded in H^1_{rad}, and by weak compactness admits a subsequence converging weakly to some $\sigma_F^\star \in \mathcal{A}$. The kinetic term is convex and continuous in $\nabla\sigma_F$, hence weakly lower semicontinuous. The potential term converges by continuity of U on a bounded range and compactness on the baryon support, and the linear source term converges by weak convergence in L^2 against $\rho_b \in L^2$. This gives weak lower semicontinuity of F and shows that $\sigma_F^\star$ attains the infimum. The Euler-Lagrange equation follows by standard variational arguments, and elliptic regularity gives smoothness away from the baryon support.

Proposition (Cold convex regime and effective uniqueness) In the cold Fisher limit $T_F = 0$ suppose that the scalar potential reduces to a strictly convex function $V_{\text{cold}}(\sigma_F)$ on $[\sigma_{\min}, \sigma_{\max}]$ with $V''_{\text{cold}}(\sigma_F) \ge \nu_0 > 0$. Then the free energy

$$F_{\text{cold}}[\sigma_F; \rho_b] = \int \left[\frac{1}{2}\alpha(r)\, |\nabla\sigma_F|^2 + V_{\text{cold}}(\sigma_F) - \kappa\, \sigma_F\, \rho_b(r) \right] d^3x$$

is strictly convex on $\mathcal{A}$. In particular, the minimiser σ_F^{cold} in the radial class is unique.

Moreover, in the Bogomolny sector where F_{cold} can be written as a sum of a non negative square and a boundary or BPS term,

$$F_{\text{cold}}[\sigma_F; \rho_b] = \int \frac{\alpha}{2} \left| \nabla\sigma_F - \Phi(\sigma_F, \rho_b) \right|^2 d^3x + F_{\text{BPS}}[\sigma_F, \rho_b],$$

any regular radial solution of the associated first order BPS equation

$$\nabla\sigma_F = \Phi(\sigma_F, \rho_b)$$

which is finite at the origin and tends to the vacuum value at infinity coincides with this unique minimiser.

For finite Fisher temperature $T_F > 0$ the Bernoulli bounded entropy potential $U(\sigma_F; T_F)$ remains convex but need not be strictly convex everywhere on $[\sigma_{\min}, \sigma_{\max}]$ because of saturation at the entropy bounds. The functional $F[\sigma_F; \rho_b]$ is therefore convex but not guaranteed to be strictly convex. In that regime we do not claim a general global uniqueness theorem for arbitrary baryon profiles. In the parameter range relevant for galaxies, however, the numerical gradient flows that we study converge to a single attracting profile for each (ρ_b, α, T_F), and we have not observed multiple distinct minimisers in the radial class. We regard this as strong evidence for effective uniqueness in the galactic sector, and leave a full functional analysis of the finite temperature case to future work.

2.7 Weak-field limit and solar system bounds

The scalar Fisher sector is intended as an effective description of galactic-scale gravity in the weak-field regime, with the metric itself remaining governed by General Relativity at small scales. In particular, the scalar field σ_F is defined after coarse-graining the baryon distribution over disc and halo scales, and the Fisher halo acceleration is treated as an additional contribution to the Newtonian potential sourced by this coarse-grained density, rather than as a modification of the local metric or of light propagation.

To make this more explicit, consider the scalar field equation obtained by varying the Fisher free energy in the constant-stiffness case,

$$-2\alpha_0\,\Delta\sigma_F(x) + U'\big(\sigma_F(x)\big) = \kappa\,\rho_b(x),$$

with $\alpha_0 > 0$ constant and U a local potential with a non-degenerate minimum at σ_0. Writing $\sigma_F = \sigma_0 + \delta\sigma$ and expanding U' to first order around σ_0 with $U'(\sigma_0) = 0$ and $U''(\sigma_0) > 0$ gives the linearised equation

$$\big(-\Delta + m_F^2\big)\,\delta\sigma(x) = \frac{\kappa}{2\alpha_0}\,\rho_b(x), \qquad m_F^2 := \frac{U''(\sigma_0)}{2\alpha_0}.$$

At this level the Fisher scalar behaves like a Yukawa field with mass m_F sourced by the coarse-grained baryon density, analogous to chameleon-type screening mechanisms [15]. The associated Fisher acceleration is

$$g_F(x) = \lambda_F\,\nabla\sigma_F(x) \simeq \lambda_F\,\nabla\delta\sigma(x),$$

and the total weak-field acceleration on a test particle is

$$g_{\rm tot}(x) = g_N(x) + g_F(x),$$

where g_N is the standard Newtonian acceleration generated by baryons.

In the constant-stiffness, weak-field regime the Yukawa Green function for (2.1) is strictly positive, so a concentrated baryon source with $\rho_b \geq 0$ produces a scalar profile $\sigma_F(r)$ that is largest at small radii and decreases outwards. Its radial derivative is therefore negative, $\sigma_F'(r) < 0$ for r outside the baryon core, and the Fisher acceleration

$$g_F(r) = \lambda_F\sigma_F'(r)\,\hat{r}$$

points inward for $\lambda_F > 0$. In the effective potential language of [2] this choice corresponds to an attractive potential

$$\Phi_{\rm eff} = -\frac{c^2}{2}\,\sigma_F, \qquad -\nabla\Phi_{\rm eff} = g_F,$$

so that maxima of σ_F coincide with potential wells and there is no hidden sign flip between the Fisher scalar and the effective Newtonian description.

In the present framework the metric remains the usual weak-field GR metric determined by g_N, and g_F enters only through an effective additional mass distribution in the Poisson equation.

This constant-stiffness, linearised Yukawa description is intended as a local weak-field approximation: the global halo profiles and the flat rotation-curve behaviour analysed in Sections 3-5 rely on the full, radially varying stiffness $\alpha(r)$ and the Bernoulli bounded entropy sector rather than on a single, constant-α_0 Yukawa field.

On galactic scales the Fisher parameters are fixed by requiring that g_F accounts for the missing acceleration in rotation curves and in the lensing masses inferred from the weak-field Einstein equations with total source $\rho_b + \rho_F$. In what follows, "Fisher lensing mass" always refers to this contribution to the GR source term rather than to any direct coupling of the scalar to photons.

For a Milky Way-like galaxy with circular speed $v_c \simeq 220\,\mathrm{km\,s^{-1}}$ at galactocentric radius $R_0 \simeq 8\,\mathrm{kpc}$, the total centripetal acceleration is of order

$$|g_{\mathrm{tot}}(R_0)| \sim \frac{v_c^2}{R_0} \sim 10^{-10}\,\mathrm{m\,s^{-2}}.$$

In the Fisher halo picture the Fisher contribution $g_F(R_0)$ is at most of this order, and typically smaller in high-surface-density systems where baryons already dominate the inner potential.

A general Fisher acceleration bound in the inner potential well. The scalar inequalities derived above imply a simple structural bound on the Fisher halo acceleration at small radii. Outside the bulk of the baryons the Fisher contribution to the radial acceleration is

$$g_F(r) = \frac{GM_F(<r)}{r^2},$$

where $M_F(<r)$ is the enclosed Fisher halo mass. The global mass inequality (2.9) gives

$$M_F(<r) \le M_F \le \eta(\ldots)\, M_b,$$

so that for any radius r outside the baryon dominated core we have

$$|g_F(r)| \le \eta(\ldots)\, \frac{GM_b(<r)}{r^2} = \eta(\ldots)\, g_{\mathrm{N,baryon}}(r).$$

Here $M_b(<r)$ and $g_{\mathrm{N,baryon}}(r)$ are the enclosed baryon mass and Newtonian baryon acceleration, and $\eta(\ldots)$ is the dimensionless Fisher susceptibility factor already constrained by the halo fits.

In the Fisher parameter range required to fit SPARC rotation curves we find η of order unity or smaller. Equation (2.7) then shows that, in any galaxy where the local baryon potential dominates, the Fisher halo acceleration is parametrically suppressed relative to the baryon contribution.

In particular, at solar system radii $r \simeq 1\,\mathrm{AU}$ inside the Milky Way disc we have $g_{\mathrm{N,baryon}}(r)$ orders of magnitude larger than the dark halo contribution at the same radius, so the Fisher halo term is automatically many orders below existing Cassini and ephemeris constraints. The explicit Solar System tidal estimate given below is simply a concrete evaluation of this bound for Milky Way baryons and the fitted Fisher parameters.

The relativistic completion also makes it clear why Solar System tests do not place

strong constraints on the Fisher sector. In the present effective theory the scalar field couples to the coarse grained galactic baryon density on kiloparsec scales rather than to individual stellar sources. At the Solar radius the Fisher acceleration is of order $g_{\rm F} \sim 10^{-10}\,{\rm m\,s^{-2}}$ and varies on the galactic scale length $R_{\rm gal} \sim 10\,{\rm kpc}$. Over a characteristic Solar System diameter $D_{\rm SS} \sim 50\,{\rm AU}$ the fractional change in the Fisher field is therefore $D_{\rm SS}/R_{\rm gal} \sim 10^{-8}$, giving a tidal variation

$$\Delta g_{\rm F} \;\sim\; g_{\rm F}\,\frac{D_{\rm SS}}{R_{\rm gal}} \;\sim\; 10^{-18}\,{\rm m\,s^{-2}}.$$

This is four to five orders of magnitude below current Cassini level bounds on anomalous accelerations from planetary ephemerides. Locally the Fisher contribution appears as an almost uniform background field that can be absorbed into the definition of the barycentric frame, so the scalar sector is automatically consistent with existing Solar System tests in the parameter regime probed in this paper.

Over solar system scales, the Fisher field generated by the coarse-grained galactic baryons varies only on kiloparsec scales. Approximating the Fisher acceleration as a smooth function of radius on scales $\Delta r \ll R_0$, its variation across one astronomical unit satisfies

$$\Delta g_F(1\,{\rm AU}) \;\lesssim\; \left|\frac{dg_F}{dr}\right|_{R_0} 1\,{\rm AU} \;\sim\; \frac{|g_F(R_0)|}{R_0}\,1\,{\rm AU} \;\sim\; 10^{-19}\,{\rm m\,s^{-2}},$$

using $|g_F(R_0)| \lesssim 10^{-10}\,{\rm m\,s^{-2}}$, $R_0 \sim 8\,{\rm kpc}$ and $1\,{\rm AU} \ll R_0$. This is many orders of magnitude below the sensitivities of solar system tests that constrain differential accelerations and post-Newtonian parameters. To leading order, the Fisher halo therefore contributes only an almost constant background acceleration across the solar system, which can be absorbed into the barycentric frame and leaves local Keplerian dynamics and Shapiro delay measurements unchanged. Furthermore, because the Fisher scalar couples to the coarse-grained galactic density rather than point sources, it does not modify the potential of the Sun itself, avoiding constraints from planetary orbital precession.

A second potential concern is whether the scalar sector generates a new $1/r$-type force around individual compact objects such as the Sun. In the present construction the source term ρ_b entering the scalar equation is a coarse-grained galactic baryon density, not the microscopic density of stars and planets.

The scalar field is therefore not driven by the detailed solar density profile, and no additional solar $1/r$ potential arises at the level of the effective theory. At small radii, where the coarse-graining scale is much larger than the system size, the Fisher contribution reduces to a slowly varying background that does not interfere with the usual GR description of the solar system.

Finally, the Fisher scalar carries no new tensor degrees of freedom and does not introduce an independent long-range modification of the metric sector in the solar system. Gravitational waves remain governed by the GR metric, and on solar system scales the scalar contributes only a nearly constant correction to the Newtonian potential through its energy density, well below current bounds on Shapiro delay and post-Newtonian parameters. On galactic and cluster scales the same scalar energy density enters the Einstein equations as part of the total source $\rho_b + \rho_F$, and it is this

combined source that determines the weak-field lensing potential.

A full post-Newtonian and cosmological analysis of the Fisher sector would require coupling the scalar energy-momentum tensor to the Einstein equations, but at the level of the present weak-field, coarse-grained description, the model is compatible with existing constraints provided that the Fisher parameters are chosen in the range required by galactic dynamics and the scalar is interpreted strictly as a large-scale vacuum response rather than as a new local fifth force.

Recent work on Solar System tests of dark matter has proposed that collisionless particle dark matter streams could be gravitationally focused by the Sun to produce local density wakes or "hairs" with potentially detectable effects on planetary ephemerides [32]. In such scenarios the dark matter density can vary appreciably on astronomical unit scales, and the induced anomalous accelerations must then be compared directly to Cassini level bounds on Solar System dynamics.

The scalar Fisher theory considered here is effectively immune to these constraints. In the present EFT the Fisher scalar couples to the coarse grained galactic baryon density that sources the large scale halo, rather than to the microscopic stellar density profile of the Sun. The resulting scalar field varies on kiloparsec scales, so across a region of size $D_{\rm SS} \sim 50\,\mathrm{AU}$ the Fisher acceleration changes only by a small tidal amount

$$\Delta g_F \sim \frac{g_F}{R_{\rm gal}}\, D_{\rm SS} \sim 10^{-10}\, \frac{50\,\mathrm{AU}}{10\,\mathrm{kpc}} \sim 10^{-18}\,\mathrm{m\,s^{-2}}.$$

This is at least four orders of magnitude below the current sensitivity of Cassini level ephemeris analyses, which constrain anomalous accelerations in the outer Solar System at the level of $10^{-14}\,\mathrm{m\,s^{-2}}$. In this sense a null result for Solar System dark matter wakes is a natural prediction of the Fisher effective field theory, while any confirmed detection of an AU scale dark matter lensing signal would point to additional particle dark matter structure beyond the scalar Fisher halo.

2.8 Relativistic completion and energy conditions

The scalar Fisher sector used in this paper is strictly weak field and quasistatic. It is built as an energy functional on a coarse grained spatial slice and is only required to reproduce the Newtonian limit of General Relativity at galactic scales. For completeness it is useful to record how such a scalar sector can arise from a standard Einstein plus scalar theory and how the usual energy conditions constrain this completion.

A minimal covariant completion is obtained by treating the Fisher scalar as a canonical field in the Einstein frame, with action

$$S = \frac{1}{16\pi G}\int_{\mathcal{M}} R\,\sqrt{-g}\,d^4x + S_{\rm baryon}[g,\Psi] + S_{\rm F}[g,\sigma_F,\rho_b],$$

where $g_{\mu\nu}$ is the spacetime metric, R is the Ricci scalar, $S_{\rm baryon}$ is the usual minimally coupled matter action for baryonic fields Ψ, and the Fisher scalar contribution is taken

to be

$$S_{\mathrm{F}}[g, \sigma_F, \rho_b] = \int_{\mathcal{M}} \left(-\frac{1}{2} Z(\sigma_F)\, g^{\mu\nu} \nabla_\mu \sigma_F \nabla_\nu \sigma_F - V_I(\sigma_F) - \kappa\, \sigma_F\, \rho_b \right) \sqrt{-g}\, d^4x.$$

Here $Z(\sigma_F) > 0$ is an effective stiffness that reduces to the constant α_0 used in the weak field analysis after a suitable field rescaling, V_I is the bounded entropy potential introduced in Section 3, and ρ_b is a coarse grained rest mass density for baryons on the same scales at which the scalar field is defined. Dimensional analysis fixes the Fisher coupling so that the source term $-\kappa\sigma_F\rho_b$ has the same units as the gradient and potential contributions in both the relativistic action and the static free energy.

In the present normalisation σ_F is dimensionless and ρ_b is a coarse-grained rest-mass density, so κ carries the dimensions of a specific energy. It is convenient, when comparing with the scalar Fisher equation in Ref. [2], to introduce a reference density ρ_0 and a dimensionless baryon contrast $\hat{\rho}_b := \rho_b/\rho_0$, in terms of which the weak-field equation takes the same Helmholtz form as in that work. We therefore keep κ as a single phenomenological coupling with the appropriate units, to be fixed by the galactic weak-field phenomenology, and do not impose an explicit closed-form expression in terms of G, c and ρ_0 at this stage.

Varying the action with respect to the metric gives the Einstein equations

$$G_{\mu\nu} = 8\pi G \left(T^{\mathrm{baryon}}_{\mu\nu} + T^{\mathrm{F}}_{\mu\nu} \right),$$

with Fisher stress tensor

$$T^{\mathrm{F}}_{\mu\nu} = Z(\sigma_F)\, \nabla_\mu \sigma_F \nabla_\nu \sigma_F - \frac{1}{2} Z(\sigma_F)\, g_{\mu\nu}\, g^{\alpha\beta} \nabla_\alpha \sigma_F \nabla_\beta \sigma_F - g_{\mu\nu} V_I(\sigma_F) - g_{\mu\nu} \kappa\, \sigma_F\, \rho_b.$$

Variation with respect to σ_F yields the scalar field equation

$$\nabla_\mu \left(Z(\sigma_F) \nabla^\mu \sigma_F \right) = \frac{dV_I}{d\sigma_F} + \kappa\, \rho_b.$$

In a static, weak field regime with $g_{\mu\nu}$ close to a Newtonian metric, time derivatives of σ_F negligible, and $Z(\sigma_F)$ slowly varying, equation (2.7) reduces to the elliptic Fisher equation used in Section 1.2, with the identification $Z(\sigma_F) \approx 2\alpha_0$ and V_I equal to the scalar potential U. This choice corresponds to the simplest relativistic completion of the constant stiffness model used in the weak field analysis; a fully position dependent stiffness $\alpha(x)$ would require a more general $Z(\sigma_F, x)$, which we leave to future work.

The Fisher contribution to the Newtonian potential is then entirely encoded in the scalar energy density and pressure appearing in $T^{\mathrm{F}}_{\mu\nu}$.

For a canonical scalar with positive stiffness $Z(\sigma_F) > 0$ and a potential V_I bounded from below, the standard energy conditions are automatically satisfied in the Einstein frame. For any future directed null vector k^μ one finds

$$T^{\mathrm{F}}_{\mu\nu} k^\mu k^\nu = Z(\sigma_F) \left(k^\mu \nabla_\mu \sigma_F \right)^2 \geq 0,$$

so the null energy condition holds. For any future directed timelike vector u^μ with

$u^\mu u_\mu = -1$ one has

$$T^{\mathrm{F}}_{\mu\nu} u^\mu u^\nu = \frac{1}{2} Z(\sigma_F) \big(u^\mu \nabla_\mu \sigma_F\big)^2 + \frac{1}{2} Z(\sigma_F) h^{\alpha\beta} \nabla_\alpha \sigma_F \nabla_\beta \sigma_F + V_I(\sigma_F) + \kappa\, \sigma_F\, \rho_b,$$

where $h^{\alpha\beta} = g^{\alpha\beta} + u^\alpha u^\beta$ is the spatial projector orthogonal to u^μ. If $V_I(\sigma_F)$ is bounded below and the baryon density ρ_b stays in a regime where the combination $V_I(\sigma_F) + \kappa \sigma_F \rho_b$ is bounded below by a non negative constant on the configurations of interest, then the contribution of the Fisher sector together with the explicit coupling $-\kappa \sigma_F \rho_b$ to the total energy density is non negative and the weak energy condition $T^F_{\mu\nu} u^\mu u^\nu \geq 0$ holds.

Equivalently, one can absorb the $-\kappa \sigma_F \rho_b$ term into an effective baryon stress tensor and regard the Fisher stress tensor proper as containing only V_I; in that viewpoint the same boundedness requirement is imposed on the combined scalar plus baryon fluid. The bounded entropy construction of Section 3 ensures that V_I remains uniformly bounded from above and below, so that such a choice is always possible at the level of the effective theory.

In the variational derivation the Fisher scalar equation takes the form

$$\nabla_\mu \big(Z(\sigma_{\mathrm{F}})\, \nabla^\mu \sigma_{\mathrm{F}}\big) - \frac{1}{2}\, Z'(\sigma_{\mathrm{F}})\, (\nabla \sigma_{\mathrm{F}})^2 \;=\; V_I'(\sigma_{\mathrm{F}}) + \kappa\, \rho_b,$$

where a prime denotes a derivative with respect to σ_{F} and $(\nabla \sigma_{\mathrm{F}})^2 = g^{\mu\nu}\, \nabla_\mu \sigma_{\mathrm{F}}\, \nabla_\nu \sigma_{\mathrm{F}}$. In the weak field, slowly varying stiffness regime that is relevant for galactic halos the Fisher stiffness can be treated as approximately constant, $Z(\sigma_{\mathrm{F}}) \approx 2\alpha_0$, so that $Z'(\sigma_{\mathrm{F}})$ is negligible. In this constant stiffness limit (2.8) reduces to the Helmholtz type equation used in the non relativistic halo analysis,

$$\nabla_\mu \big(Z(\sigma_{\mathrm{F}})\, \nabla^\mu \sigma_{\mathrm{F}}\big) \;\approx\; V_I'(\sigma_{\mathrm{F}}) + \kappa\, \rho_b,$$

which in the static, cold Fisher limit with $V_I = 0$ reproduces the elliptic Fisher equation

$$-\nabla \cdot \big(2\alpha_0\, \nabla \sigma_{\mathrm{F}}\big) \;\approx\; \kappa\, \rho_b$$

used in Sections 2.1 and 2.5.

We make no attempt to explore the full phenomenology of the relativistic completion (2.8). The role of this subsection is to show that the scalar Fisher sector used at galactic scales.

In the parameter range relevant for galactic dynamics the scalar stress tensor itself does not act as a conventional cold dark matter fluid: its contribution to the Einstein equations decays faster than the effective Fisher force g_F extracted from the weak-field scalar equation. The primary phenomenology is therefore encoded in the fifth-force sector g_F and in the associated effective density, while the Einstein frame embedding should be viewed as a consistency check on the scalar sector rather than an alternative energy-density model for dark matter.

2.9 Scalar halo bounds and structural inequalities

The bounded Bernoulli channel and the Fisher stiffness already imply a set of simple but important inequalities for any radial minimiser $\sigma_F^\star$ and its associated Fisher halo density $\rho_F(r)$.

(i) Global halo mass fraction. By construction the scalar order parameter is confined to a finite range $\sigma_{\min} \le \sigma_F^\star \le \sigma_{\max}$, and the mapping from σ_F to Fisher halo density,

$$\rho_F(r) = f(\sigma_F(r); \text{Fisher parameters}),$$

is a smooth function of σ_F on this interval. In particular there is a finite upper bound

$$0 \le \rho_F(r) \le \rho_{F,\max} := \max_{\sigma \in [\,\sigma_{\min}, \sigma_{\max}\,]} f(\sigma).$$

Moreover, outside the baryon support the BPS structure and ellipticity of the Euler-Lagrange equation force $\sigma_F^\star$ to relax back to its vacuum value on a characteristic scale set by the Fisher length λ_F. Hence the effective halo support volume is bounded in terms of the Fisher parameters and the baryon scale radius R_b. Combining these facts we obtain a conservative bound

$$M_F = 4\pi \int_0^\infty \rho_F(r) r^2 dr \le \eta(\alpha_{\min}, \alpha_{\max}, T_F, \kappa, \sigma_{\min}, \sigma_{\max}; R_b)\, M_b,$$

where M_b is the total baryon mass and η is a finite dimensionless constant determined by the Fisher parameters and the typical size of the system. In the cold BPS sector this can be sharpened by expressing M_F directly in terms of the Bogomolny charge, leading to a more constrained bound $M_F \le \eta_{\mathrm{BPS}} M_b$ with η_{BPS} fixed by the scalar stiffness and potential.

(ii) Central density and core surface density. Regularity of $\sigma_F^\star$ at the origin and spherical symmetry imply $d\sigma_F^\star/dr = 0$ at $r = 0$, so the Euler-Lagrange equation gives

$$3\alpha(0)\, \sigma_F''(0) = \kappa \rho_b(0) - U'(\sigma_F(0); T_F).$$

Convexity and boundedness of the Bernoulli potential ensure that $U'(\sigma_F; T_F)$ grows as σ_F is pushed toward the entropy saturation plateau. For given $(\rho_b(0), \alpha(0), T_F)$ there is therefore a finite band of admissible central values, and in particular a constant C_c such that

$$|\sigma_F(0)| \le C_c(\rho_b(0), \alpha(0), T_F, \kappa).$$

If $\rho_F(r)$ is an increasing function of $\sigma_F(r)$ in the relevant range then this immediately yields a hard ceiling on the central Fisher density

$$\rho_F(0) \le \rho_{F,\mathrm{core}}^{\max} := f\big(C_c(\rho_b(0), \alpha(0), T_F, \kappa)\big).$$

Defining a core radius r_c as the scale on which σ_F falls to, say, half its central value, the same balance between the entropy restoring force and baryon forcing gives r_c as a

function of $(\rho_b(0), \alpha(0), T_F)$. The central Fisher surface density then obeys

$$\Sigma_F(0) \sim \int_0^{r_c} \rho_F(r)\, dr \lesssim \rho_{F,\mathrm{core}}^{\max}\, r_c = \Sigma_{F,\mathrm{core}}^{\max}(\rho_b(0), \alpha(0), T_F, \kappa),$$

so arbitrarily dense or arbitrarily compact Fisher cores are excluded once the Fisher parameters and the central baryon density are fixed.

(iii) Inner halo acceleration bound. Outside the bulk of the baryons the Fisher contribution to the radial acceleration can be written in terms of the enclosed halo mass $M_F(< r)$ as

$$g_F(r) = \frac{GM_F(< r)}{r^2}.$$

Using the mass bound (2.9) we obtain the simple inequality

$$|g_F(r)| \le \eta(\ldots)\, \frac{GM_b(< r)}{r^2} = \eta(\ldots)\, g_{\mathrm{N,baryon}}(r),$$

where $M_b(< r)$ is the baryon mass enclosed within radius r and $g_{\mathrm{N,baryon}}$ is the corresponding Newtonian acceleration. For the range of Fisher parameters we use to fit SPARC galaxies, the dimensionless prefactor η inferred from the halo fits is of order unity or less. At solar system radii this suppresses the Fisher halo acceleration by many orders of magnitude relative to existing constraints, and the explicit 1 AU estimate quoted later in the paper is simply a concrete evaluation of (2.9) for Milky Way parameters.

3 Bernoulli bounded entropy and Fisher temperature

We now incorporate a bounded entropy structure into the scalar Fisher theory by interpreting the scalar field σ_{F} as the logit of a local Bernoulli occupation number. This construction is motivated by the BKM Fisher geometry of a two level system, where the Fisher mobility vanishes at both zero and full occupation. The resulting bounded entropy potential introduces a Fisher temperature parameter T_F that controls the strength of the reversible sector relative to the Fisher gradient flow and allows the halo to saturate.

3.1 Bernoulli occupation and BKM geometry

Consider a two level system with populations p and $1 - p$, where $p \in (0, 1)$ is interpreted as the local probability of exciting a vacuum degree of freedom into a Fisher active mode. The Bernoulli entropy is

$$S_{\mathrm{Bern}}(p) \;=\; -p \log p - (1 - p) \log(1 - p).$$

The binary entropy satisfies the elementary bound

$$0 \;\le\; S_{\mathrm{Bern}}(p) \;\le\; \log 2 \qquad \text{for all } p \in (0, 1),$$

with the maximum attained at $p = \frac{1}{2}$ and the entropy tending to zero as $p \to 0$ or $p \to 1$.

In the effective scalar theory we restrict $\sigma_F(x)$ to a finite Bernoulli channel window $[\sigma_{\min}, \sigma_{\max}]$ corresponding to physically accessible occupation probabilities $p \in [p_{\min}, p_{\max}]$, with the entropy plateaux near $p \simeq 0, 1$ represented by the endpoints of this interval.

The BKM Fisher metric for the diagonal sector of a two level density matrix can be written, up to an overall scale, as

$$g_{\mathrm{BKM}}(p) \;\propto\; \frac{1}{p(1-p)}.$$

The mobility associated with a gradient flow of a free energy functional on this manifold is inversely proportional to the metric, so that

$$M(p) \;\propto\; p(1-p).$$

The mobility vanishes at $p = 0$ and $p = 1$, so the Fisher flow cannot drive the system beyond these boundaries. This provides a geometric saturation mechanism that prevents complete depletion or complete filling.

To couple this structure to the scalar field, we introduce a logit map

$$p(\sigma_{\mathrm{F}}) \;=\; \frac{1}{1+\mathrm{e}^{-\beta\,\sigma_{\mathrm{F}}}},$$

where $\beta > 0$ is a stiffness parameter. The inverse map is

$$\sigma_{\mathrm{F}} = \frac{1}{\beta}\log\frac{p}{1-p}.$$

The scalar field σ_{F} therefore measures the local log odds of the Fisher active state, and large positive or negative values of σ_{F} correspond to saturated occupation $p \approx 1$ or $p \approx 0$.

We define a bounded entropy potential for σ_{F} by composing the Bernoulli entropy with the logit map,

$$S_{\mathrm{Bern}}(\sigma_{\mathrm{F}}) \;=\; S_{\mathrm{Bern}}\big(p(\sigma_{\mathrm{F}})\big).$$

The derivative with respect to σ_{F} is

$$\frac{\mathrm{d}S_{\mathrm{Bern}}}{\mathrm{d}\sigma_{\mathrm{F}}} \;=\; \frac{\mathrm{d}S_{\mathrm{Bern}}}{\mathrm{d}p}\,\frac{\mathrm{d}p}{\mathrm{d}\sigma_{\mathrm{F}}}.$$

A direct computation using (3.1) gives

$$\frac{\mathrm{d}p}{\mathrm{d}\sigma_{\mathrm{F}}} \;=\; \beta\,p(1-p),$$

and

$$\frac{\mathrm{d}S_{\mathrm{Bern}}}{\mathrm{d}p} \;=\; -\log p + \log(1-p).$$

For moderate amplitudes it is convenient to Taylor expand around $\sigma_{\mathrm{F}} = 0$, where

$p = 1/2$. To second order in σ_{F} one finds

$$S_{\mathrm{Bern}}(\sigma_F) = \log 2 - \frac{\beta^2}{8}\,\sigma_F^2 + O(\sigma_F^4),$$

In particular,

$$\frac{dS_{\mathrm{Bern}}}{d\sigma_F}(\sigma_F) \approx -\frac{\beta^2}{4}\,\sigma_F \quad \text{for small } \sigma_F.$$

so that the entropy decreases quadratically as σ_{F} moves away from zero in either direction.

3.2 Fisher free energy with bounded entropy

We now choose the scalar potential U in (2.1) to be proportional to the negative of the Bernoulli entropy,

$$U(\sigma_{\mathrm{F}}) \;=\; -T_F\, S_{\mathrm{Bern}}(\sigma_{\mathrm{F}}),$$

where $T_F \geq 0$ is a Fisher temperature parameter. The free energy becomes

$$\mathcal{F}[\sigma_{\mathrm{F}}; \rho_b] \;=\; \int_{\mathbb{R}^3} \Big\{ \alpha(x)\,|\nabla\sigma_{\mathrm{F}}(x)|^2 - T_F\, S_{\mathrm{Bern}}\big(\sigma_{\mathrm{F}}(x)\big) - \kappa\,\sigma_{\mathrm{F}}(x)\,\rho_b(x) \Big\}\, \mathrm{d}^3x.$$

On any finite domain $V \subset \mathbb{R}^3$ where α and ρ_b are bounded and integrable, the Bernoulli bound

$$0 \;\leq\; S_{\mathrm{Bern}}\big(\sigma_F(x)\big) \;\leq\; \log 2$$

implies

$$-T_F S_{\mathrm{Bern}}\big(\sigma_F(x)\big) \;\geq\; -T_F \log 2 \qquad \text{for all } x \in V.$$

Together with the positive quadratic term $\int_V \alpha(x)\,|\nabla\sigma_F(x)|^2\, d^3x$, this shows that, for fixed baryon source ρ_b and Fisher temperature T_F, the Fisher free energy on V cannot be driven to arbitrarily negative values by varying σ_F.

In practice we work with finite volumes adapted to a given baryon profile, so this local entropy cap is sufficient to ensure a well posed variational problem for the scalar field.

In spherical symmetry this reads

$$\mathcal{F}[\sigma_{\mathrm{F}}; \rho_b] \;=\; 4\pi \int_0^\infty \big\{ \alpha(r)\,\sigma_{\mathrm{F}}'(r)^2 - T_F\, S_{\mathrm{Bern}}\big(\sigma_{\mathrm{F}}(r)\big) - \kappa\,\sigma_{\mathrm{F}}(r)\,\rho_b(r) \big\} r^2\, \mathrm{d}r.$$

The Euler Lagrange equation is now

$$-\frac{1}{r^2}\frac{\mathrm{d}}{\mathrm{d}r}\big(2\alpha(r)\,r^2\sigma_{\mathrm{F}}'(r)\big) - T_F\,\frac{\mathrm{d}S_{\mathrm{Bern}}}{\mathrm{d}\sigma_{\mathrm{F}}}\big(\sigma_{\mathrm{F}}(r)\big) \;=\; \kappa\,\rho_b(r).$$

For small amplitudes, where $S_{\mathrm{Bern}}(\sigma_{\mathrm{F}})$ is approximately quadratic, the entropy term

behaves like a mass term,

$$-T_F \frac{dS_{\text{Bern}}}{d\sigma_F}(\sigma_F) \approx \frac{T_F \beta^2}{4}\,\sigma_F,$$

so that the scalar equation becomes a Fisher screened Poisson equation,

$$-\frac{1}{r^2}\frac{\mathrm{d}}{\mathrm{d}r}\left(2\alpha(r)\, r^2 \sigma_{\mathrm{F}}'(r)\right) + U''(0)\,\sigma_{\mathrm{F}}(r) \;\approx\; \kappa\,\rho_b(r),$$

where the small-amplitude Bernoulli channel has curvature $U''(0) = T_F\beta^2/4$. In the constant-stiffness limit $\alpha(r) \approx \alpha_0$, this matches the canonical Fisher mass definition

$$m_F^2 := \frac{U''(0)}{2\alpha_0} = \frac{T_F\beta^2}{8\alpha_0}$$

introduced in Section 2.6.

At larger amplitudes the full bounded entropy structure becomes important. Since $U(\sigma_F) = -T_F S_{\text{Bern}}(\sigma_F)$ and S_{Bern} has a maximum at $\sigma_F = 0$, the entropy contribution $U(\sigma_F)$ is minimised near the centre of the Bernoulli channel and increases again as σ_F is driven toward the saturation plateaux. In the free energy

$$F[\sigma_F; \rho_b] = \int \left(\alpha|\nabla\sigma_F|^2 + U(\sigma_F) - \kappa\sigma_F\rho_b\right)\mathrm{d}^3x$$

this means that the Fisher temperature term penalises large excursions of σ_F toward the entropy saturation plateau and provides an effective saturation mechanism for the scalar response.

Helmholtz structure and gravitational screening In the weak amplitude regime where $S_{\text{Bern}}(\sigma_F)$ can be approximated by a quadratic potential, the radial scalar equation

$$-\frac{1}{r^2}\frac{d}{dr}\Big(2\alpha(r)r^2\sigma_F'(r)\Big) + m_F^2\sigma_F(r) \approx \kappa\rho_b(r)$$

has the structure of a screened Poisson or Helmholtz problem for σ_F with mass scale m_F and penetration length $\ell_F \sim 1/m_F$. In particular, for slowly varying stiffness one can take $\alpha(r) \approx \alpha_0$ on the scales of interest, so that the differential operator acting on σ_F reduces to the spherically symmetric Helmholtz operator

$$-2\alpha_0\left(\frac{d^2}{dr^2} + \frac{2}{r}\frac{d}{dr}\right)\sigma_F(r) + m_F^2\sigma_F(r).$$

This is directly analogous to the London equation for magnetic screening in a superconductor, where the field obeys a massive Helmholtz equation with a finite penetration depth. In the present work we use this analogy only at the level of the linearised scalar equation, as a way to interpret the cored branch as a regime of partial gravitational screening by the Fisher scalar. We do not assume a full superconducting order parameter or flux quantisation structure for the vacuum.

3.3 Qualitative impact of Fisher temperature

The Fisher temperature T_F controls the competition between gradient energy, bounded entropy, and baryon source. Three regimes are particularly relevant.

Cold Fisher regime. When T_F is very small, the entropy term is negligible and the scalar dynamics are dominated by the gradient and source terms. The halo configuration approaches a solution of the cold Fisher Bogomolny equation (2.3). Gradients can become large in regions where the baryon mass rises steeply, and the resulting halo profiles are susceptible to cusps.

Moderate Fisher temperature. For T_F of order unity in suitable units, the entropy term becomes comparable to the gradient term in regions where σ_{F} grows. The mobility factor $p(1-p)$ suppresses further growth as p approaches zero or unity. In spherical toy models this leads to cored profiles with approximately constant density in the centre, and to outer profiles that smoothly join on to the gradient dominated regime. These solutions can be compared directly with empirical cored halo families [23].

High Fisher temperature. For very large T_F the entropy penalty dominates and the scalar field is strongly confined near $\sigma_{\mathrm{F}} = 0$ except where the baryon source is sufficiently strong. The halo becomes compressed toward regions of high baryon density, and the outer halo can be suppressed. This provides a simple mechanism for the adiabatic contraction of halos in massive galaxies and clusters where the baryon potential well is deep.

The full interplay between T_F, the stiffness profile $\alpha(r)$, and the baryon density $\rho_b(r)$ is best explored numerically. In Section 4 we study a simple Bernoulli bounded entropy model in spherical symmetry and show explicitly how cuspy and cored profiles arise as T_F and the baryon concentration are varied. In Section 5 we then connect the scalar theory to observed rotation curves through an effective Fisher susceptibility model.

4 Radial Bernoulli halos: numerical construction

To understand the combined effect of Fisher stiffness, bounded entropy and baryon concentration it is useful to study a simplified spherical model in which the scalar equation (3.2) is evolved as a gradient flow in a one dimensional radial coordinate. This section introduces such a model and summarises its qualitative behaviour.

4.1 Radial gradient flow model

We approximate the static Euler Lagrange equation (3.2) by a dissipative flow in an auxiliary time variable t,

$$\partial_t \sigma_{\mathrm{F}}(r,t) \;=\; \frac{1}{r^2}\frac{\partial}{\partial r}\Big(2\alpha(r)\, r^2 \partial_r \sigma_{\mathrm{F}}(r,t)\Big) + T_F\, \frac{\mathrm{d}S_{\mathrm{Bern}}}{\mathrm{d}\sigma_{\mathrm{F}}}\big(\sigma_{\mathrm{F}}(r,t)\big) + \kappa\, \rho_b(r).$$

For suitable initial data and boundary conditions this flow decreases the free energy (3.2) and relaxes toward a steady state that solves the static equation (3.2).In particular, the numerical scheme enforces a Dirichlet condition

$$\sigma_F(r_{\max}) = 0,$$

which is the finite-radius analogue of the vacuum boundary condition $\sigma_F(r) \to 0$ as $r \to \infty$ used in the Bogomolny completion. This ensures that the surface term in the Bogomolny decomposition vanishes in the continuum limit and that the numerical halos saturate the same lower bound as the analytic cold sector.

A simple explicit time stepping scheme for (4.1) reads

$$\sigma_{\mathrm{F},j}^{n+1} \;=\; \sigma_{\mathrm{F},j}^{n} + \Delta t\big\{\mathcal{D}_j[\sigma_{\mathrm{F}}^{n}] + T_F\,(\partial_{\sigma_{\mathrm{F}}} S_{\mathrm{Bern}})_j(\sigma_{\mathrm{F}}^{n}) + \kappa\,\rho_{b,j}\big\},$$

where $\sigma_{\mathrm{F},j}^{n} \approx \sigma_{\mathrm{F}}(r_j, t_n)$, with $t_n = n\,\Delta t$, and $\rho_{b,j} \approx \rho_b(r_j)$. The operator $\mathcal{D}_j$ approximates the radial Fisher Laplacian,

$$\mathcal{D}_j[\sigma_{\mathrm{F}}] \;\approx\; \frac{1}{r_j^2}\frac{\partial}{\partial r}\Big(2\alpha(r)\,r^2\sigma_{\mathrm{F}}'(r)\Big)\Big|_{r=r_j},$$

with a second order central stencil away from the origin and a regularised expression at $r = 0$. One convenient choice is

$$\begin{aligned}
&\sigma_{\mathrm{F},r}(r_j) \approx \frac{\sigma_{\mathrm{F},j+1} - \sigma_{\mathrm{F},j-1}}{2\Delta r}, \qquad 1 \le j \le N-2,\\
&\sigma_{\mathrm{F},r}(r_0) = 0, \qquad \sigma_{\mathrm{F},r}(r_{N-1}) = 0,
\end{aligned}$$

so that a Neumann boundary condition is imposed at the origin and at the outer radius. The flux

$$j_j = r_j^2\alpha(r_j)\,\sigma_{\mathrm{F},r}(r_j)$$

is then used to approximate the divergence,

$$\mathcal{D}_j[\sigma_{\mathrm{F}}] \;\approx\; \frac{2}{r_j^2}\frac{j_{j+1} - j_{j-1}}{2\Delta r}, \qquad 1 \le j \le N-2,$$

with appropriate one sided approximations at $j = 0$ and $j = N-1$ that respect the regularity of σ_{F} at the origin and the imposed outer boundary condition.

The Bernoulli entropy derivative is evaluated pointwise using the logit map (3.1). Writing $p_j = p(\sigma_{\mathrm{F},j})$ one has

$$\frac{\mathrm{d}S_{\mathrm{Bern}}}{\mathrm{d}\sigma_{\mathrm{F}}}(\sigma_{\mathrm{F},j}) \;=\; \big(-\log p_j + \log(1-p_j)\big)\,\beta\,p_j(1-p_j),$$

and a numerically stable implementation is obtained by clipping p_j away from the exact boundaries 0 and 1.

The explicit scheme (4.1) is subject to a Courant stability condition controlled by the Fisher stiffness. A practical stability criterion is

$$\Delta t \;\lesssim\; c_{\mathrm{CFL}}\,\frac{\Delta r^2}{\max_j \alpha(r_j)},$$

with $c_{\mathrm{CFL}} < 1$. In practice one can choose a requested timestep and clamp it to this stability bound at run time.

4.2 Toy baryon and stiffness profiles

To illustrate the qualitative behaviour of the model we adopt a simple Gaussian baryon profile

$$\rho_b(r) = \rho_0 \, \exp\Big(-\frac{r^2}{2r_b^2}\Big),$$

with characteristic core radius r_b and central density scale ρ_0. The Fisher stiffness is chosen to interpolate between a small radius area law regime and a large radius saturation,

$$\alpha(r) \;=\; \alpha_0 \, \frac{(r/r_*)^2}{1 + (r/r_*)^2},$$

where r_* is a crossover radius. For $r \ll r_*$ one has $\alpha(r) \approx \alpha_0 (r/r_*)^2$, while for $r \gg r_*$ one finds $\alpha(r) \to \alpha_0$. This simple profile captures the idea that Fisher coupling is weak in the deep interior and saturates to a constant in the outer halo.

The baryon concentration is controlled by the dimensionless combination $\rho_0 r_b^2$ relative to the Fisher coupling κ, while the Fisher temperature T_F and stiffness parameter β control the bounded entropy channel. By scanning over (T_F, β, ρ_0) one can identify regimes in which the scalar field relaxes to a cuspy profile and regimes in which it develops a flat core.

4.3 Cusps, cores and the cold limit

Numerical experiments with the radial gradient flow (4.1) and the toy profiles (4.2) and (4.2) reveal three characteristic regimes.

For small Fisher temperature $T_F \approx 0$ the entropy term plays no role and the flow relaxes toward a solution that is well approximated by the cold Fisher Bogomolny equation (2.3). In this regime the scalar gradient $\sigma_{\mathrm{F}}'(r)$ is directly proportional to $M_b(r)/(\alpha(r)\, r^2)$, so in regions where the baryon mass rises steeply the gradient becomes large. For centrally concentrated baryons this produces a cuspy Fisher profile with a steep inner rise.

For intermediate Fisher temperature, with T_F of order unity in suitable units, the bounded entropy term introduces an effective saturation when σ_{F} grows large enough that $p(\sigma_{\mathrm{F}})$ approaches zero or one. In this regime the inner profile flattens: the scalar field develops a core in which $\sigma_{\mathrm{F}}'(r)$ is small and the effective halo density is approximately constant. The transition from core to outer halo is controlled by the crossover radius r_* in the stiffness profile and by the balance between T_F and the baryon concentration.

For high Fisher temperature the entropy penalty is strong. The scalar field is confined near $\sigma_{\mathrm{F}} = 0$ except in regions where the baryon source is large enough to overcome the

entropy barrier. In the toy model this leads to halos that are tightly bound to the baryon distribution, with little extended Fisher mass at large radii. This regime resembles adiabatic contraction of halos in massive galaxies and clusters.

A particularly striking feature of the intermediate temperature regime is that the resulting core profiles can be well fitted by empirical cored halo families. In spherical toy models with suitable parameter choices the scalar profile $\sigma_{\rm F}(r)$ produces an effective density that matches the Burkert form to high precision over a wide radial range. This supports the interpretation of the bounded entropy channel as a Fisher mechanism for generating cored halos without introducing an independent dark matter species.

4.4 A simple cusp to core phase diagram

The radial Bernoulli model of Secs. 3.2 and 4 provides a convenient way to summarise the cusp to core behaviour of the scalar Fisher halo in terms of a small number of dimensionless control parameters. In the toy model of Sec. 4.2 the baryon distribution is specified by a central density scale ρ_0 and a characteristic core radius r_b, while the Fisher sector is controlled by the stiffness profile $\alpha(r)$, the Fisher temperature T_F and the Bernoulli stiffness parameter β.

For the Gaussian baryon profile and stiffness ansatz of Sec. 4.2 it is useful to introduce the dimensionless Fisher temperature parameter

$$\Theta_F := m_F r_b,$$

where m_F is the Fisher screening mass from the weak-field Yukawa limit of Sec. 3.2, defined by

$$m_F^2 := \frac{U''(0)}{2\alpha_0} = \frac{T_F \beta^2}{8\alpha_0}$$

for the Bernoulli potential, and a dimensionless baryon compaction parameter

$$\Xi_b := \frac{\kappa \rho_0 r_b^2}{\alpha_0}.$$

Here α_0 is the asymptotic value of the stiffness in the simple profile

$$\alpha(r) = \alpha_0 \frac{(r/r_*)^2}{1 + (r/r_*)^2},$$

and the ratio

$$R_* := \frac{r_b}{r_*}$$

measures whether the baryons reside predominantly in the rising part of the stiffness profile or in the saturated outer regime.

In terms of these parameters, the numerical experiments of Sec. 4.3 can be organised into three qualitative branches.

Cold cusp dominated branch. When $\Theta_F \ll 1$ the screening length $\ell_F \sim 1/m_F$ is much

larger than the baryon core radius. The bounded entropy term is then weak on the scale of r_b and the scalar profile is well approximated by the cold Fisher Bogomolny equation. For sufficiently large baryon compaction, with Ξ_b above an order one threshold that depends on R_*, the gradient $\sigma_F'(r)$ grows rapidly in the inner region and the effective Fisher density develops a steep central rise. In this regime the halo lies on a cusp dominated branch.

Entropy supported core branch. For intermediate Fisher temperature, with Θ_F of order unity for fixed R_*, the bounded entropy channel becomes effective within the baryon core. As σ_F grows, the Bernoulli occupation $p(\sigma_F)$ approaches its saturation values and the mobility factor $p(1-p)$ suppresses further growth of the scalar field.

For moderate baryon compaction the radial flow (4.1) relaxes to profiles in which σ_F' is small over a finite inner region and the effective density is approximately constant in the centre. The transition from this core to the outer gradient dominated halo is controlled by R_* and by the balance between Θ_F and Ξ_b. In the (Θ_F, Ξ_b) plane this defines a band in which cored solutions are realised.

Entropy dominated compressed branch. For large Fisher temperature, with $\Theta_F \gg 1$ at fixed R_*, the entropy penalty term dominates the free energy on the scale of the baryon core. The scalar field is then confined near $\sigma_F = 0$ except where the baryon source is strong enough to overcome the entropy barrier. In the toy model this yields solutions in which the Fisher halo mass is concentrated near the baryons and the extended outer halo is strongly suppressed. This branch resembles adiabatic contraction of halos in deep baryonic potential wells.

For a fixed stiffness profile and baryon shape the three regimes above define a schematic phase diagram in the (Θ_F, Ξ_b) plane, parametrised by R_*. The numerical radial flows do not exhibit a sharp phase transition between cusps and cores, but rather a smooth crossover curve $\Xi_{b,\mathrm{crit}}(\Theta_F; R_*)$ separating solutions with steep inner profiles from those that develop an extended entropy supported core. Within the present model we do not attempt to extract a closed form for this curve, but the structure is sufficient to make two points clear.

First, once the Fisher sector parameters $(T_F, \beta, \alpha_0, r_*)$ are fixed, the location of a given galaxy in the phase diagram is controlled by its baryon compaction through Ξ_b; the choice between a cusp dominated and a cored halo is not an extra free knob that can be tuned independently for each system. Second, the same control parameters that govern the toy model can be inferred, at least approximately, from observed baryon profiles in real galaxies, so the qualitative phase diagram provides a bridge between the Bernoulli scalar theory and empirical cusp to core trends without introducing additional phenomenological structure.

4.5 Effective density and rotation curves in the toy model

Given a relaxed scalar profile $\sigma_{\mathrm{F}}(r)$ from the radial gradient flow, the effective Fisher halo mass and rotation curve can be constructed directly. The effective density is obtained by differentiating the Fisher acceleration (2.2) and comparing with the

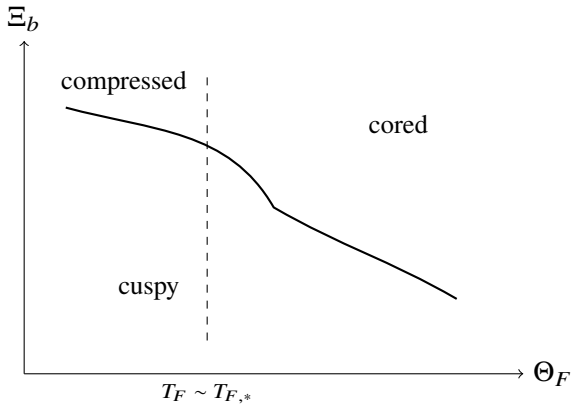

Figure 1: Schematic cusp - core phase diagram in the (Θ_F, Ξ_b) plane. The solid curve indicates the qualitative transition between cuspy, cored and entropy compressed branches for a fixed stiffness profile and baryon shape, as discussed in the text. The dashed line illustrates a representative Θ_F slice corresponding to a family of halos at approximately fixed Fisher temperature.

Newtonian Poisson equation. In spherical symmetry one has

$$g_{\mathrm{F}}(r) = -\frac{G M_F(r)}{r^2}\,\hat{r},$$

so that

$$M_F(r) \;=\; -\frac{\lambda_F}{G}\, r^2 \sigma_{\mathrm{F}}'(r).$$

Differentiating yields the effective Fisher density

$$\rho_F(r) \;=\; \frac{1}{4\pi r^2}\,\frac{\mathrm{d}M_F}{\mathrm{d}r}(r) \;=\; -\frac{\lambda_F}{4\pi G}\Big(2\,\sigma_{\mathrm{F}}'(r) + r\,\sigma_{\mathrm{F}}''(r)\Big).$$

In practice, numerical derivatives of the relaxed $\sigma_{\mathrm{F}}(r)$ profile can be used to construct $\rho_F(r)$ and the total circular velocity

$$v_{\mathrm{c}}^2(r) \;=\; \frac{G}{r}\big(M_b(r) + M_F(r)\big).$$

Comparisons with standard analytic halo families then provide a direct link between the Fisher scalar model and phenomenological dark matter profiles.

Remark (Osmotic interpretation of the Fisher force). In the scalar density formulation of the Fisher sector developed in [2], one introduces a coarse-grained density ρ and a log-density potential $\varphi = \log(\rho/\rho_0)$ for a fixed reference density $\rho_0 > 0$. To match the effective potential convention $\Phi_{\mathrm{eff}} = -\frac{c^2}{2}\varphi$ used there, it is convenient in the present paper to identify the Fisher scalar with the log-density in the weak-field regime,

$$\sigma_{\mathrm{F}} \approx \varphi = \log(\rho/\rho_0).$$

Using the halo acceleration $g_{\mathrm{F}} = \lambda_F \nabla\sigma_{\mathrm{F}}$ then gives

$$g_{\mathrm{F}}(x) \approx \lambda_F \nabla\sigma_{\mathrm{F}}(x) \approx \lambda_F \nabla\varphi(x) = \lambda_F \nabla \log \rho(x).$$

The associated Fisher force density is

$$f_{\mathrm{F}}(x) := \rho(x)\, g_{\mathrm{F}}(x) \approx \lambda_F \rho(x)\, \nabla \log \rho(x) = \lambda_F \nabla\rho(x) = -\nabla P_{\mathrm{F}}(\rho(x)), \qquad P_{\mathrm{F}}(\rho) = -\lambda_F \rho + \text{const.}$$

In this weak log-density branch the Fisher halo force is algebraically equivalent to an osmotic pressure gradient with a negative pressure (tension) $P_{\mathrm{F}} \propto -\rho$. With this convention an overdensity ($\nabla\rho$ pointing inward) generates an *attractive* Fisher acceleration (directed towards higher density), consistent with the effective potential Φ_{eff} in [2] and with the definition of g_{F} used in the present paper.

This matches the thermodynamic picture in which σ_{F} plays the role of a dimensionless chemical potential for the vacuum sector: the Fisher halo force can be viewed as the osmotic reaction of the vacuum to the presence of baryons.

In the present paper we use this only as a local interpretation of the Fisher force in slowly varying regions and do not impose $P_{\mathrm{F}} \propto \rho$ as a global closure condition for halo structure.

Remark (Self-sourced branch and $n = 1$ polytropic comparison). The same scalar density sector in [2, Sec. 6.3] admits a self-sourced branch in which the coarse-grained density plays the role of its own source, with $\rho_m = \lambda\rho$ for $\lambda > 0$. In spherical symmetry the corresponding static equation reduces to a Helmholtz-type equation

$$\Delta\rho + \lambda\kappa\,\rho = 0,$$

with regular solution

$$\rho(r) \;=\; \rho_c\, \frac{\sin\!\big(\sqrt{\lambda\kappa}\, r\big)}{\sqrt{\lambda\kappa}\, r}, \qquad 0 \le r \le \frac{\pi}{\sqrt{\lambda\kappa}},$$

where ρ_c is the central density and the outer radius is fixed by the first zero of the sine. This is the classical $n = 1$ Lane-Emden profile, which can be obtained from a polytropic equation of state of the form $P \propto \rho^2$. We do not make direct use of this self-sourced branch in the galactic fits below, but it shows that the Fisher scalar sector naturally supports both an osmotic interpretation in the weak log-density regime and a polytropic, self-sourced configuration with an $n = 1$ equation of state, all within the same Fisher geometry on densities.

The toy model therefore plays two roles. It demonstrates explicitly that Bernoulli bounded entropy can generate cored halos with realistic shapes, and it fixes the qualitative dependence of halo structure on Fisher temperature, baryon concentration and stiffness profile. In the next section we introduce an observationally anchored construction in which the Fisher halo contribution to rotation curves is written directly in terms of the baryonic acceleration profile of a galaxy.

5 Fisher halo response in disc galaxies

The scalar Fisher model described above can be connected to observed rotation curves by treating the Fisher halo as a nonlocal response to the baryonic acceleration within the framework of Universal Information Hydrodynamics. Rather than reconstructing σ_{F} for each galaxy in detail, it is natural to work with an effective susceptibility kernel that maps the baryonic acceleration profile to an additional halo contribution. This section develops a simple one parameter response model and applies it to disc galaxy data.

5.1 Baryonic acceleration and Fisher susceptibility

Consider a galaxy with baryonic circular velocity profile $v_b(R)$ in the disc plane, where R is the cylindrical radius. The corresponding baryonic acceleration is

$$g_b(R) \;=\; \frac{v_b(R)^2}{R}.$$

In the scalar Fisher picture, gradients of σ_{F} are sourced by g_b through the Fisher operator and bounded entropy geometry. To leading order one can posit that the Fisher halo acceleration is a nonlocal functional of g_b,

$$g_F(R) \;=\; \int_0^\infty K(R,R')\, g_b(R')^2 \, \mathrm{d}R',$$

where K is an effective susceptibility kernel that encodes the radial Fisher stiffness and the Bernoulli channel. In the simplest approximation K is taken to be positive and slowly varying, so that the dominant contribution to $g_F(R)$ at a given radius comes from baryonic accelerations at comparable radii.

A particularly simple model arises by assuming that the effective halo mass enclosed within radius R is proportional to a cumulative Fisher energy constructed from g_b^2,

$$M_F(<R) \;\propto\; \int_0^R g_b(r)^2\, r^2 \, \mathrm{d}r.$$

Comparing with the Newtonian relation between enclosed mass and circular velocity,

$$v_F(R)^2 \;=\; \frac{G M_F(<R)}{R},$$

one is led to an effective Fisher halo contribution of the form

$$g_F(R) = C I(R), \quad v_F^2(R) = R g_F(R), \quad I(R) = \frac{1}{R}\int_0^R g_b(r)^2 r^2 \, \mathrm{d}r,$$

where C is an amplitude parameter with dimensions of $(\text{acceleration} \times \text{length})^{-1}$ that plays the role of an effective Fisher susceptibility. The function $I(R)$ is completely determined by the baryonic rotation curve of the galaxy, and encodes the shape of the Fisher response.

Analytic properties of the Fisher response functional. In a thin exponential disc with surface density $\Sigma(R) = \Sigma_0 e^{-R/R_d}$ the baryonic acceleration has the usual behaviour $g_b(R) \propto R$ at $R \ll R_d$ and $g_b(R) \propto GM_b/R^2$ at $R \gg R_d$. We approximate the shape functional $I(R)$ by taking the weight $w(r) \approx 1$. Inserting these asymptotics into (5.1) gives:

- For $R \ll R_d$, $g_b(R) \approx aR$ and

$$I(R) \approx \frac{1}{R}\int_0^R a^2 r^4 dr = \frac{a^2}{5}R^4,$$

  so $g_F(R) \propto R^4$ and $v_F^2(R) \propto R^5$. The Fisher contribution is negligible in the very centre.
- For $R \gg R_d$, $g_b(R) \approx GM_b/R^2$ and the integral converges,

$$I(R) \to I_\infty \sim \frac{G^2 M_b^2}{R_0\, R},$$

  where R_0 is an inner cutoff of order the disc scale and the precise prefactor depends on the full $g_b(R)$ shape. In this regime $v_F^2(R) = R g_F(R)$ tends to a constant

$$v_F^2(R) \to C\, I_\infty \sim C\, \frac{G^2 M_b^2}{R_0},$$

  so the Fisher halo generically produces an asymptotically flat rotation curve contribution controlled by the baryon profile and C.

Low acceleration RAR behaviour. In the outer disc the baryonic acceleration scales as $g_b(R) \propto R^{-2}$ while the Fisher response scales as $I(R) \propto R^{-1}$. Eliminating R gives

$$I(R) \propto g_b^{1/2}(R), \qquad g_F(R) = C\, I(R) \propto C\, g_b^{1/2}(R),$$

so in the low acceleration regime where $g_F \gg g_b$ the total acceleration behaves as

$$g_{\rm tot}(R) \simeq g_F(R) \propto g_b(R)^{1/2}.$$

Thus the Fisher susceptibility model naturally generates a radial acceleration relation with an effective slope one half in the low g_b regime, without imposing a MOND like interpolation by hand. The normalisation of (5.1) is set by the global susceptibility C and the Fisher parameters entering I_∞.

Scaling towards the baryonic Tully Fisher relation. For a family of discs with similar surface density profiles, the integral I_∞ scales as

$$I_\infty \sim \int_0^\infty g_b^2(r)\, r^2 dr \sim \frac{G^2 M_b^2}{R_d},$$

up to a dimensionless factor that depends only on the shape of $g_b(R)$. Combining (5.1) and (5.1) gives

$$v_F^2(\infty) \propto C\, \frac{G^2 M_b^2}{R_d}.$$

Empirically, disc scale lengths obey a size mass relation $R_d \propto M_b^s$ with s in the range 0.3 to 0.5, so that

$$v_F^2(\infty) \propto M_b^{2-s}, \qquad v_F^4(\infty) \propto M_b^{4-2s}.$$

For realistic s this exponent lies close to the observed baryonic Tully Fisher slope. The key point is that in the Fisher scalar theory the scaling of $v_{\rm flat}$ with M_b arises from the non local response functional I_∞ and the size mass relation, rather than being fitted galaxy by galaxy: once the global Fisher parameters and susceptibility C are fixed, the BTFR enters as a derived scaling law.

Remark (Scalar Helmholtz limit and the shape functional). In the weak amplitude regime of Sec. 3.2, where the Bernoulli bounded entropy can be approximated by a quadratic potential, the scalar equation for σ_F reduces to a screened Poisson or Helmholtz problem with Fisher mass m_F and screening length $\ell_F \simeq 1/m_F$. For slowly varying stiffness one has $\alpha(r) \simeq \alpha_0$ on the scales of interest, and the radial operator acting on σ_F becomes a constant coefficient Helmholtz operator. In three dimensions this can be written schematically as

$$-\nabla \cdot \big(\alpha_0 \nabla \sigma_F(x)\big) + m_F^2 \sigma_F(x) \;\simeq\; \kappa\, \rho_b(x),$$

so that in this homogeneous limit the Fisher potential is given by a Yukawa convolution

$$\sigma_F(x) \;=\; \kappa \int_{\mathbb{R}^3} G_{m_F}(x-y)\, \rho_b(y)\, d^3y, \qquad G_{m_F}(r) = \frac{1}{4\pi\alpha_0}\, \frac{e^{-m_F r}}{r}.$$

The corresponding Fisher acceleration field

$$\mathbf{g}_{\rm F}(\mathbf{x}) \;:=\; -\lambda_F \nabla \sigma_F(\mathbf{x})$$

is therefore a nonlocal functional of the baryon distribution with a characteristic range set by the screening length ℓ_F.

For an approximately axisymmetric, thin disc the relevant component is the radial acceleration in the disc plane. Projecting the Yukawa Green function onto the disc geometry produces an effective kernel $K(R, R')$ which decays once $|R - R'|$ exceeds ℓ_F, and the halo contribution to the circular velocity can be written in the form

$$v_F^2(R) \;\simeq\; \int_0^\infty K(R, R')\, g_b(R')^2\, R'^2\, dR'.$$

The shape functional $I(R)$ can thus be viewed as a cylindrical analogue of a Fisher energy built from g_b^2, obtained by integrating the squared baryonic acceleration over the interior region. The susceptibility C, with dimensions of inverse velocity squared as in 5.1, then plays the role of a coarse grained amplitude that encodes the net strength of the scalar Helmholtz response for a given galaxy, without requiring an explicit reconstruction of the three dimensional field σ_F or the exact kernel $K(R, R')$.

In the numerical SPARC fits of Section 5 we set $w(r) \equiv 1$, so that $I(R)$ is computed directly from the squared baryonic acceleration profile of each galaxy.

This cumulative response model should therefore be understood as a phenomenological summary of the underlying three dimensional Helmholtz dynamics in thin discs; different non local kernels that produce the same $I(R)$ over the radii sampled by the data would be observationally indistinguishable at the level of the present susceptibility

fits.

The total model circular velocity is

$$v_{\mathrm{mod}}(R)^2 \;=\; v_b(R)^2 + v_F(R)^2 \;=\; v_b(R)^2 + C\, I(R).$$

For each galaxy, C can be determined by a weighted least squares fit to the observed rotation curve. The magnitude of C measures the strength of the Fisher halo response relative to the baryons (with the attractive branch selected by the sign convention in $\mathbf{g}_{\mathrm{F}}$ and by enforcing $C_{\mathrm{best}} \geq 0$ in the fits).

5.2 Amplitude fitting from rotation curves

Given observed velocities $v_{\mathrm{obs}}(R_i)$ with uncertainties $\sigma_{v,i}$ and a baryonic model $v_b(R_i)$ at radii R_i, the Fisher amplitude C can be estimated by solving a linear regression problem in v^2 space. Define

$$y_i = v_{\mathrm{obs}}(R_i)^2 - v_b(R_i)^2, \qquad I_i = I(R_i),$$

where $I(R)$ is the shape function (5.1) computed from the baryonic profile. The model (5.1) implies

$$y_i \;\approx\; C\, I_i.$$

Approximating the uncertainty in y_i by propagating the errors in v_{obs} gives

$$\sigma_{y,i} \;\approx\; 2\, v_{\mathrm{obs}}(R_i)\, \sigma_{v,i}.$$

Introducing weights $w_i = 1/\sigma_{y,i}^2$, the least squares estimator for C is

$$C_{\mathrm{best}} \;=\; \frac{\sum_i w_i I_i y_i}{\sum_i w_i I_i^2}.$$

To enforce an attractive halo one can constrain $C_{\mathrm{best}} \geq 0$. The corresponding halo and total velocities are then

$$v_F(R_i) = \sqrt{C_{\mathrm{best}} I_i}, \qquad v_{\mathrm{mod}}(R_i) = \sqrt{v_b(R_i)^2 + v_F(R_i)^2}.$$

A standard chi squared statistic in velocity space,

$$\chi^2 \;=\; \sum_i \left(\frac{v_{\mathrm{obs}}(R_i) - v_{\mathrm{mod}}(R_i)}{\sigma_{v,i}} \right)^2,$$

provides a measure of goodness of fit, together with the root mean square residual

$$\mathrm{RMS} \;=\; \left(\frac{1}{N} \sum_i \big(v_{\mathrm{obs}}(R_i) - v_{\mathrm{mod}}(R_i) \big)^2 \right)^{1/2}.$$

This construction defines a one parameter Fisher halo model for each galaxy, in which the shape of the halo response is completely fixed by the baryonic rotation curve and

only the overall Fisher susceptibility C is adjusted. The model is simple enough to be applied uniformly across large galaxy samples, while retaining a direct interpretation in terms of the scalar Fisher dynamics.

5.3 Qualitative trends across galaxies

When the Fisher halo response model is applied to a heterogeneous galaxy sample, one expects several robust trends.

For low mass, gas dominated dwarf galaxies with gently rising baryonic curves, the shape function $I(R)$ grows approximately linearly with radius in the outer disc. The fitted Fisher amplitude C_{best} is typically non zero and of order 10^{-2} in appropriate units, and the resulting halo contribution $v_F(R)$ produces a cored rotation curve that closely resembles empirical cored profiles. The baryons alone would underpredict the outer velocities, and the Fisher response supplies the missing acceleration.

For intermediate mass spirals with both stellar and gas components, the baryonic rotation curve is more peaked. In many of these cases $I(R)$ still supports a useful Fisher response, but the fitted C_{best} tends to be smaller, reflecting the fact that a significant fraction of the observed rotation is already provided by the baryons. The Fisher halo then acts as a modest correction that smooths the transition between the inner baryon dominated regime and the outer flat portion of the curve.

For massive, bulge dominated systems with very high central baryon concentrations, the simple Fisher susceptibility model (5.1) often assigns a small or vanishing C_{best}. In such galaxies the baryonic model already saturates or overshoots the observed velocities in the inner regions, and a positive Fisher response would worsen the fit. This behaviour is consistent with the high Fisher temperature regime of the scalar model, in which the halo is compressed into the inner potential well and does not generate a significant extended mass at large radii.

These trends suggest that the Fisher susceptibility C is not a universal constant, but depends on properties of the baryonic distribution that determine the local balance between Fisher gradient flow and bounded entropy. In the scalar model this dependence is controlled by the Fisher temperature and the reversible sector of the vacuum generator. A natural next step is to relate C to a dimensionless Fisher temperature parameter derived from the full UIH dynamics, and to determine whether the galaxy to galaxy variation in C_{best} can be collapsed onto a small number of underlying Fisher parameters.

5.4 Connection to Fisher temperature and hypocoercivity

The effective susceptibility C introduced in (5.1) measures the integrated response of the Fisher halo to the baryonic acceleration field. Within the framework of the universal generator $K = G + J$, the magnitude of this response is controlled by the relative strength of the reversible sector J and the Fisher gradient sector G.

In the hypocoercive setting, the ratio of the true relaxation rate to the bare Fisher diffusion rate defines a dimensionless hypocoercive index. In simple models this index flows under coarse graining toward a universal infrared fixed point. The Bernoulli

bounded entropy channel can be viewed as a local realisation of this hypocoercive structure, in which the Fisher temperature T_F encodes the strength of the reversible sector relative to the Fisher gradient. In regions where the baryonic potential is shallow and the reversible currents are effective, the Fisher temperature is higher and the scalar field is prevented from developing deep cusps, leading to cored halos and a sizable Fisher susceptibility. In regions where the potential is deep and the reversible currents are trapped, the Fisher temperature is effectively lower and the scalar halo is compressed, reducing the extended Fisher response.

An important open question is therefore how to express the effective susceptibility C in terms of the underlying Fisher temperature and hypocoercive index, using the full UIH operator geometry rather than the simplified scalar model. Addressing this requires a more detailed analysis of the spectrum of the generator K in the presence of baryonic sources, and a study of how the Fisher halo eigenmodes emerge and saturate as one flows toward larger scales. We return to this question in the discussion and outlook.

In the small amplitude regime of the Bernoulli channel, Sec. 3.2 shows that the bounded entropy contribution induces a Fisher mass scale $m_F^2 = T_F\beta^2$, so that the characteristic screening length of the scalar halo is $\lambda_c \sim 1/m_F \propto T_F^{-1/2}$ at fixed stiffness profile. In the finite dimensional UIH hypocoercivity experiments of Ref. [4], the impact of the reversible sector on relaxation is captured by dimensionless UIH couplings built from the Fisher gap and the norm of J. In particular, the leading hypocoercive corrections to the bare Fisher decay rate are quadratic in the reversible amplitude, so any effective Fisher temperature parameter constructed from the same operator data is naturally an even functional of J, and in simple two-scale toy models can be arranged to scale as $T_F \propto g_1^2$ up to model-dependent factors.

In such a picture the Fisher mass scale inherits this dependence, $m_F \propto |g_1|$, and the core radius λ_c is inversely related to the effective hypocoercive strength. We do not attempt to derive a unique microscopic relation $T_F(g_1, g_2)$ for realistic galaxies here, but this scaling illustrates how the effective susceptibility C and the cusp-core behaviour inferred from rotation curves could, in a more complete UIH field theory, be organised by the same hypocoercive indices that control relaxation in the operator models. For the present paper we keep T_F and C at the level of effective parameters, interpreted as coarse measures of the reversible sector strength in the scalar reduction.

5.5 Derivation of the Tully-Fisher Power Law

The empirical Baryonic Tully-Fisher Relation (BTFR), which relates the baryonic mass M_b to the asymptotic circular velocity v_f via a power law $M_b \propto v_f^4$, is often cited as a challenge for standard dark matter models which typically require fine-tuning of feedback mechanisms to reproduce the tight correlation. In the scalar Fisher framework, this scaling emerges naturally from the Bogomolny structure in the constant stiffness limit.

Recall that in the cold Fisher limit ($T_F \to 0$), the halo satisfies the Bogomolny bound. For a region with approximately constant stiffness $\alpha(r) \approx \alpha_0$, the effective Fisher halo

mass $M_F(r)$ becomes strictly proportional to the enclosed baryon mass:

$$M_F(r) = \gamma_F M_b(r), \quad \text{with} \quad \gamma_F = \frac{\lambda_F \kappa}{8\pi G \alpha_0}.$$

The parameter γ_F represents a vacuum amplification factor. Consequently, the total dynamical mass $M_{tot}(r) = M_b(r) + M_F(r)$ is a linear renormalization of the baryonic mass:

$$M_{tot}(r) = (1 + \gamma_F) M_b(r).$$

The circular velocity for a test particle $v_c(r)$ is determined by the total enclosed mass. At a characteristic radius R capturing the bulk of the galaxy, we have:

$$v_c^2(R) = \frac{G M_{tot}(R)}{R} = \frac{G_{eff} M_b(R)}{R},$$

where $G_{eff} = G(1 + \gamma_F)$ is the effective coupling constant mediated by the Fisher vacuum.

To recover the scaling between mass and velocity, we introduce the geometric constraint typical of rotationally supported disks. Observational samples such as SPARC demonstrate that the central surface mass density of disk galaxies, Σ_0, varies within a bounded range (related to Freeman's Law). Approximating the baryonic mass as $M_b \approx \pi \Sigma_0 R^2$, we can eliminate the radius R in favor of the mass and surface density:

$$R \approx \left(\frac{M_b}{\pi \Sigma_0} \right)^{1/2}.$$

Substituting this geometric constraint into the velocity equation yields:

$$v_c^2 \approx \frac{G_{eff} M_b}{(\pi \Sigma_0)^{-1/2} M_b^{1/2}} = G_{eff} (\pi \Sigma_0)^{1/2} M_b^{1/2}.$$

Squaring this relation reveals the characteristic fourth-power scaling of the BTFR:

$$M_b \approx \left[\frac{1}{\pi G^2 (1 + \gamma_F)^2 \Sigma_0} \right] v_c^4.$$

This derivation highlights three key physical insights:

- **The Slope:** The v_c^4 dependence is not a fit but a structural consequence of the linear mass renormalization $M_F \propto M_b$ inherent to the constant-stiffness Bogomolny sector.
- **The Normalization:** The zero-point of the BTFR is set by the Fisher amplification γ_F. A "softer" vacuum (lower α_0) yields a larger γ_F, shifting the relation to higher velocities for a given baryonic mass.
- **The Scatter:** Deviations from the exact law arise naturally from variations in the effective stiffness $\alpha(r)$ (radial dependence) and the finite Fisher temperature T_F, which introduces non-linear corrections via the bounded entropy term.

Thus, the scalar Fisher theory provides a first-principles derivation of the BTFR slope, grounded in the information geometry of the vacuum rather than ad-hoc feedback efficiency.

5.6 Structural inequalities and observational wedges

The scalar Fisher construction developed above already implies several structural inequalities that can be phrased directly in terms of observable accelerations, free energies and relaxation rates. In this subsection we collect three such consequences that are particularly natural targets for comparison with galaxy data and for future numerical work. They follow from the cold Bogomolny structure of Sec. 2.2, the Bernoulli bounded entropy of Sec. 3, and the hypocoercivity bounds for UIH flows developed in Ref. [4].

Static acceleration wedge. In the cold scalar limit with spherical symmetry and stiffness profile $\alpha(r)$, Sec. 2.2 shows that the Fisher contribution to the radial acceleration can be written as

$$g_F(r) \;:=\; \left|\mathbf{g}_{\mathrm{F}}(r)\right| \;=\; \frac{\lambda_F \kappa}{8\pi\,\alpha(r)}\,\frac{M_b(r)}{r^2},$$

where $M_b(r)$ is the enclosed baryonic mass and $\lambda_F\kappa/(8\pi)$ is a positive constant built from the Fisher coupling and the scalar charge. Matching to a Newtonian form $g_F(r) = GM_F(r)/r^2$ defines an effective Fisher mass profile

$$M_F(r) \;=\; C_F\,\frac{1}{\alpha(r)}\,M_b(r), \qquad C_F := \frac{\lambda_F\kappa}{8\pi G}.$$

Assume that in a given vacuum phase the stiffness is bounded on the radial domain of interest,

$$0 < \alpha_{\min} \le \alpha(r) \le \alpha_{\max} < \infty.$$

Then the effective Fisher to baryon mass ratio, and hence the Fisher to baryon acceleration ratio in the cold limit, is trapped between two constants

$$\gamma_{\min} \;:=\; \frac{C_F}{\alpha_{\max}}, \qquad \gamma_{\max} \;:=\; \frac{C_F}{\alpha_{\min}},$$

so that

$$\gamma_{\min} \;\le\; \frac{g_F(r)}{g_b(r)} \;\le\; \gamma_{\max}, \qquad g_b(r) := \frac{GM_b(r)}{r^2}.$$

When the Fisher and baryonic accelerations are aligned, the total radial acceleration therefore satisfies the wedge inequality

$$(1+\gamma_{\min})\,g_b(r) \;\le\; g_{\mathrm{tot}}(r) \;\le\; (1+\gamma_{\max})\,g_b(r),$$

where $g_{\mathrm{tot}} = g_b + g_F$.

Equation (5.6) is a purely structural statement: in any regime where the cold scalar approximation is adequate and the stiffness lies in a common interval $[\alpha_{\min}, \alpha_{\max}]$ across systems, all radial points in the baryon acceleration plane must lie inside a pair of straight lines of the form $g_{\mathrm{tot}} = (1+\gamma)g_b$. Here we are assuming smooth, monotonically increasing enclosed mass profiles $M_b(r)$ and $M_F(r)$ so that $g_b(r)$ and $g_F(r)$ are non negative and radially aligned, and that the accelerations do not change sign in the region of interest; these mild conditions are satisfied for the approximately

spherical, cold configurations considered below.

In practice real disc galaxies are not spherical and the finite temperature Bernoulli channel perturbs the cold relation, but (5.6) identifies a natural RAR envelope implied by the scalar geometry itself. A simple way to implement this observationally is to take a sample with Fisher halo fits, construct $g_{\rm tot}(R)$ and $g_b(R)$ at the radii entering the rotation curve, and determine an empirical wedge $[\gamma_{\rm obs}^{\rm min}, \gamma_{\rm obs}^{\rm max}]$ that contains a fixed fraction of the points. The scalar Fisher picture predicts that, after removing low surface density outliers and strongly non axisymmetric systems, this wedge should be approximately common to all galaxies sharing a given vacuum phase.

The fitted susceptibilities in Sec. 5 can therefore be interpreted as sampling an underlying interval $[\gamma_{\rm min}, \gamma_{\rm max}]$ set by the Fisher couplings and the stiffness range, with persistent RAR points outside any such common wedge signalling either departures from the cold branch or breakdown of the simple scalar reduction.

Free energy bounds and information packing. The Bernoulli channel introduces a bounded entropy contribution $S_{\rm Bern}(\sigma_F)$ that interpolates between a quadratic regime at small field and a saturated two-state entropy at large $|\sigma_F|$, with pointwise bounds

$$0 \le S_{\rm Bern}(\sigma_F(x)) \le \log 2, \qquad x \in V,$$

on any finite domain $V \subset \mathbb{R}^3$ adapted to the baryon profile. Together with the Bogomolny completion of Sec. 2.2, which yields a cold bound $F_{\rm cold}[\sigma_F; \rho_b] \ge -\,Q_F^{\rm grav}[\rho_b]$ for fixed baryons, this implies a simple global lower bound for the finite-temperature scalar free energy

$$F[\sigma_F; \rho_b] \;\ge\; -\,Q_F^{\rm grav}[\rho_b] - T_F\,(\log 2)\,{\rm Vol}(V),$$

where $F[\sigma_F; \rho_b]$ is the full free energy including the entropy term, $Q_F^{\rm grav}[\rho_b]$ is the Fisher charge functional fixed by the baryon distribution, and ${\rm Vol}(V)$ is the effective volume of the scalar channel. For one-scale baryon families with total mass M_b and scale radius R_b the Bogomolny integral gives a scaling

$$Q_F^{\rm grav}[\rho_b] \;\sim\; \frac{\kappa^2}{16\pi\bar\alpha}\,\frac{M_b^2}{R_b}\,C_{\rm shape},$$

where $\bar\alpha$ is a suitable stiffness average and $C_{\rm shape}$ is a dimensionless shape factor. In this sense the Bernoulli bounded entropy acts as a finite information-packing mechanism: it allows the scalar halo to lower the free energy relative to the cold Fisher charge by at most a controlled amount of order $T_F \log 2$ per effective coarse-grained degree of freedom, without opening the door to unbounded negative energies. This bound has two consequences.

First, for any fixed baryon profile and Fisher temperature the scalar free energy cannot be driven to arbitrarily negative values by rearranging the halo; the cold Bogomolny charge fixes a floor that scales with M_b^2/R_b, while the bounded entropy term contributes at most a finite shift set by T_F and the site weights. Second, in families where the baryons become more compact at fixed mass, the Fisher charge increases roughly as M_b^2/R_b while the entropy contribution is controlled by the bounded channel. Within the scalar model this identifies $M_b^2/(R_b\,\bar\alpha)$ and T_F as the natural control parameters for how much Fisher structure can be packed into the inner regions without leaving

the Bernoulli regime. The numerics of Sec. 4 show that this competition manifests as a smooth transition between cuspy and cored profiles, with the bounded entropy preventing arbitrarily sharp central cusps at finite T_F.

From a practical point of view, the free energy inequality can be turned into a direct test once a baryon profile and a Fisher halo fit are available. The charge functional $Q_F^{\mathrm{grav}}[\rho_b]$ can be evaluated from the same radial integrals that enter the BPS construction, while an effective scalar free energy can be estimated from the reconstructed halo mass distribution and potential depth. For each galaxy the combination

$$\mathcal{I}_{\mathrm{Fisher}} := F_{\mathrm{cold}}[\sigma_F;\rho_b] - T_F \int S_{\mathrm{Bern}}(\sigma_F)\,\mathrm{d}x + Q_F^{\mathrm{grav}}[\rho_b] + T_F \log 2 \int u(x)\,\mathrm{d}x$$

should be non negative within modelling uncertainties if the bounded entropy picture is adequate. A population of systems requiring $\mathcal{I}_{\mathrm{Fisher}} \ll 0$ in order to fit their inner rotation curves would indicate that either the Bernoulli channel is incomplete or the scalar Fisher sector itself needs to be modified.

A fully analytic bound on the central density in terms of M_b, R_b, T_F and $\bar{\alpha}$ lies beyond the present scope, but the free energy inequality already identifies the relevant combinations and the direction of the effect.

Hypocoercive relaxation bounds. Finally, the UIH hypocoercivity results of Ref. [4] provide structural bounds on relaxation toward Fisher halo equilibria. In the finite dimensional UIH setting, the symmetric Fisher Dirichlet operator $-G$ has a spectral gap λ_F that sets the irreversible clock, and the full generator $K = G + J$ satisfies

$$\lambda_{\mathrm{hyp}} \;\geq\; c_1\,\lambda_F, \qquad 0 < c_1 \leq 1,$$

with c_1 a dimensionless constant depending only on the hypocoercive couplings g_1 and g_2. In all examples studied in [4] the decay rate of perturbations under K is bounded below by such a positive multiple of the Fisher gap.

Treating the scalar halo as a coarse grained UIH sector driven by the same Fisher geometry, it is natural to expect an analogous inequality for the relaxation of σ_F toward a Bogomolny or Bernoulli equilibrium. At the level of free energy this can be expressed schematically as

$$F[\sigma_F(t);\rho_b] - F_*[\rho_b] \;\leq\; \big(F[\sigma_F(0);\rho_b] - F_*[\rho_b]\big)\exp\!\big(-2\,\lambda_{\mathrm{hyp}}\,t\big),$$

where $F_*[\rho_b]$ denotes the minimal scalar free energy for the given baryon distribution and λ_{hyp} is a hypocoercive rate controlled from below by the Fisher gap as in (5.6). In particular, non equilibrium distortions of a Fisher halo cannot persist for times much longer than $\lambda_{\mathrm{hyp}}^{-1}$ without contradicting the UIH hypocoercivity picture.

Earlier we summarised three structural inequalities already implied by the scalar Fisher geometry and the UIH framework. They can be viewed as envelopes or floors within which more detailed galaxy by galaxy modelling must sit, and they provide concrete targets for future tests that combine rotation curves, lensing and dynamical relaxation diagnostics.

5.7 A Fisher spectrometer for galaxies

The static Fisher halo model already provides, for each galaxy, a preferred scalar profile $\sigma_F^\star(r)$ that minimises the free energy $F[\sigma_F;\rho_b]$ for the given baryon distribution. In this subsection we outline how such halos can be assigned simple dimensionless "spectral coordinates" that allow galaxies to be compared directly to the other information-geometric systems studied in the UIH programme [3, 4].

We fix a finite outer radius $R_{\max}$ large enough that both the baryon profile and the Fisher halo density have decayed to negligible values and consider perturbations $\delta\sigma$ of the static solution $\sigma_F^\star$ supported in $0 \le r \le R_{\max}$. The second variation of the free energy at $\sigma_F^\star$ defines a symmetric Dirichlet-type operator

$$G_F \delta\sigma = -\nabla \cdot \big(\alpha(r)\, \nabla\delta\sigma\big) + V_I''\big(\sigma_F^\star(r)\big)\, \delta\sigma,$$

acting on a suitable weighted L^2 space of perturbations with homogeneous boundary conditions at $r = 0$ and $r = R_{\max}$. Under the structural assumptions on α and V_I already imposed in Sections 2 and 3, G_F is self-adjoint and non-negative, with a discrete spectrum on $[0, R_{\max}]$.

Let $\lambda_{F,1}^{\mathrm{halo}}(R_{\max})$ denote the smallest non-zero eigenvalue of G_F on this interval. This eigenvalue plays the role of an effective Fisher gap for perturbations of the halo on scales $r \lesssim R_{\max}$. It is natural to define a dimensionless gap parameter by

$$\Lambda_{\mathrm{halo}} := \lambda_{F,1}^{\mathrm{halo}}(R_{\max})\, r_*^2,$$

where r_* is the stiffness scale introduced in Section 2. For fixed Fisher parameters $(\lambda_F, T_F, \alpha_0, r_*)$ and baryon compactness, Λ_{halo} is expected to be an $O(1)$ quantity that depends only on the dimensionless control parameters (Θ_F, Ξ_b, R_*) introduced in Section 3.

The susceptibility fits performed in Section 5 assign to each galaxy a single Fisher amplitude C_{gal} in the linear response relation between the baryon acceleration and the Fisher halo contribution. To compare different galaxies in a way that factors out the overall Fisher curvature scale, it is useful to form the dimensionless combination

$$S_{\mathrm{halo}} := \frac{\lambda_{F,1}^{\mathrm{halo}}(R_{\max})}{\kappa}\, C_{\mathrm{gal}},$$

where κ is the global coupling constant entering the free energy (2.1). The index S_{halo} measures, in a single number, how strongly the halo responds to the baryon source relative to the curvature scale set by G_F. In the idealised limit where the linear response is dominated by the softest mode of G_F, S_{halo} is expected to be of order unity; stronger or weaker responses correspond to departures from this idealised limit.

Taken together, the pair

$$\big(\Lambda_{\mathrm{halo}}, S_{\mathrm{halo}}\big)$$

assigns to each galaxy a point in a low-dimensional "Fisher spectrometer" plane. The UIH analysis of quantum channels and Markov generators [3, 4] associates analogous dimensionless gap and response indices to finite-dimensional systems, and shows that many apparently different generators cluster into a small universality region in this

plane. The Fisher halo programme suggests that realistic galaxies should likewise populate a narrow band in $(\Lambda_{\rm halo}, S_{\rm halo})$, with residual scatter controlled by baryon compactness and environment.

We do not attempt to compute $\Lambda_{\rm halo}$ and $S_{\rm halo}$ for the full SPARC sample in the present work. The definitions (5.7)-(5.7) are intended as a concrete template for future numerical work, and as a bridge to the UIH universality diagrams. In particular, a robust inconsistency between the ranges of $(\Lambda_{\rm halo}, S_{\rm halo})$ inferred from Fisher halos and those measured in laboratory realisations of Fisher-Kähler dynamics would count as a tension for the unified information-geometric picture developed here and in Refs. [2–4].

5.8 Parameter economy and predictive structure

The Fisher susceptibility model for disc galaxies is deliberately constrained in its parameter content. Once a global Fisher coupling scale, a Fisher temperature regime and a simple family of stiffness profiles have been fixed, each galaxy in the SPARC-like sample is described, at the level of rotation curves, by a single halo amplitude parameter in addition to its baryonic mass model. The shape of the halo response is tied to the cumulative Fisher functional built from the baryonic acceleration, and the Bernoulli bounded entropy sector fixes how the scalar interpolates between cuspy and cored regimes as surface density and Fisher temperature are varied.

This is in contrast with standard cold dark matter halo fitting, where two or more shape parameters per galaxy are usually required, and with strongly phenomenological modified gravity fits that may introduce additional knobs in the interpolating function or environment dependence. In the Fisher picture the freedom resides primarily in a small number of global parameters that set the Fisher gap, the effective Fisher temperature and the stiffness hierarchy, while individual galaxies only probe different parts of the same Fisher response curve. As a result, the scalar Fisher model makes joint predictions for the radial acceleration relation, the baryonic Tully-Fisher slope and zero point, and the distribution of inferred halo amplitudes across galaxy types once the global Fisher parameters are chosen.

The structural inequalities derived from the Bogomolny completion and the bounded entropy potential further restrict the allowed region of parameter space. For a given choice of Fisher parameters there are upper bounds on core surface densities, central slopes and total Fisher mass, and the susceptibility fits cannot exceed these bounds. A full SPARC scale analysis that enforces these constraints would therefore provide a sharp test of whether the scalar Fisher sector can simultaneously account for rotation curves, maintain parameter economy and remain compatible with the Fisher inequalities. Such an analysis lies beyond the scope of the present paper, but the formalism has been arranged so that it can be carried out with minimal additional modelling freedom.

5.9 A characteristic surface density scale and Freeman-type bounds

The scalar Fisher construction implies structural inequalities that can be phrased in terms of a characteristic surface density. This provides a theoretical basis for the

empirical upper envelope of disc surface brightness often referred to as Freeman's law.

Consider an idealised, rotationally supported disc that is thin compared to its radial extent and symmetric under $z \mapsto -z$. The total vertical acceleration just above the midplane is fixed by Gauss's law,

$$g_{z,\mathrm{tot}}(R, 0^+) \;=\; 2\pi G\, \Sigma_{\mathrm{tot}}(R),$$

where $\Sigma_{\mathrm{tot}}(R)$ is the total surface mass density (baryons plus effective halo) at cylindrical radius R. The baryonic contribution alone is $g_{z,\mathrm{b}} = 2\pi G\, \Sigma_{\mathrm{b}}$. The Fisher contribution to the midplane field is therefore

$$g_{z,\mathrm{F}}(R, 0^+) \;:=\; g_{z,\mathrm{tot}}(R, 0^+) - g_{z,\mathrm{b}}(R, 0^+) \;=\; 2\pi G \big[\Sigma_{\mathrm{tot}}(R) - \Sigma_{\mathrm{b}}(R)\big].$$

In the scalar Fisher theory, the halo acceleration $\mathbf{g}_{\mathrm{F}} = -\lambda_F \nabla\sigma_F$ is constrained by the bounded entropy potential. The combination of the kinetic term $\alpha|\nabla\sigma_F|^2$ and the potential $U(\sigma_F)$ ensures that quasi-static scalar gradients cannot grow arbitrarily large. To see this, consider the integral of the scalar field equation,

$$-\nabla \cdot \big(2\alpha \nabla\sigma_F\big) + U'(\sigma_F) = \kappa\, \rho_b,$$

multiplied by σ_F over a volume V containing the galaxy. Using the boundedness of σ_F (enforced by the Bernoulli channel), the bounds on U', and the finite baryon mass, standard elliptic gradient estimates imply a universal upper bound on the scalar gradient for static solutions. We denote this universal Fisher acceleration scale by a_F:

$$|\mathbf{g}_{\mathrm{F}}(\mathbf{x})| \;\le\; a_F \qquad \text{throughout the configuration.}$$

Applying this bound to the vertical field in (5.9) gives

$$2\pi G \left|\Sigma_{\mathrm{tot}}(R) - \Sigma_{\mathrm{b}}(R)\right| \;\le\; a_F.$$

It is convenient to define the *characteristic surface density*

$$\Sigma_{\mathrm{crit}} \;:=\; \frac{a_F}{2\pi G}.$$

Discs with central surface densities $\Sigma_{\mathrm{b}}(0) \ll \Sigma_{\mathrm{crit}}$ sit in the "soft" regime where the vacuum can easily provide the missing surface density. However, for high-surface-brightness (HSB) discs where the inner region is baryon dominated ($\Sigma_{\mathrm{tot}} \simeq \Sigma_{\mathrm{b}}$), the inequality implies that $\Sigma_{\mathrm{b}}(0)$ cannot arbitrarily exceed Σ_{crit} without violating the Fisher acceleration ceiling.

For a Fisher acceleration scale comparable to the empirical RAR scale, $a_F \sim 10^{-10}\,\mathrm{m\,s^{-2}}$, one finds

$$\Sigma_{\mathrm{crit}} \;\sim\; 10^2\, M_\odot\,\mathrm{pc}^{-2}.$$

This is of the same order as the classic Freeman central surface brightness limit when translated to mass units. In the Fisher picture, this scale is not an ad hoc limit but the midplane imprint of the same vacuum saturation scale a_F that controls the halo response in the outskirts.

Vertical field and surface density ceiling. Consider now the gravitational field at the disc midplane. In the thin-disc approximation the total vertical field just above the plane is given by the Gauss-law result for a sheet,

$$g_{\mathrm{tot},z}(R, 0^+) = 2\pi G\, \Sigma_{\mathrm{tot}}(R),$$

where $\Sigma_{\mathrm{tot}}(R)$ is the total surface mass density at radius R, including baryons and any effective halo contribution that can be coarse grained across the thin disc. Similarly the vertical field from the baryons alone is

$$g_{b,z}(R, 0^+) = 2\pi G\, \Sigma_b(R).$$

The Fisher contribution to the vertical field at the plane is

$$g_{F,z}(R, 0^+) = g_{\mathrm{tot},z}(R, 0^+) - g_{b,z}(R, 0^+) = 2\pi G\big(\Sigma_{\mathrm{tot}}(R) - \Sigma_b(R)\big).$$

By the universal Fisher bound (**??**) we know that $|g_{F,z}(R, 0^+)| \le a_F$ for all R. Combining (5.9) with this inequality gives

$$2\pi G\, \big|\Sigma_{\mathrm{tot}}(R) - \Sigma_b(R)\big| \le a_F.$$

In the central region of an HSB disc the mass budget is baryon dominated, so that $\Sigma_{\mathrm{tot}}(0) \simeq \Sigma_b(0)$ and the difference $\Sigma_{\mathrm{tot}}(0) - \Sigma_b(0)$ is small compared to either. In this regime the inequality (5.9) reduces to an upper bound on the total vertical field itself,

$$|g_{\mathrm{tot},z}(0, 0^+)| \simeq |g_{b,z}(0, 0^+)| \lesssim a_F.$$

Using the sheet relation (5.9) at $R = 0$ we obtain

$$2\pi G\, \Sigma_{\mathrm{tot}}(0) \lesssim a_F,$$

and hence

$$\Sigma_b(0) \simeq \Sigma_{\mathrm{tot}}(0) \lesssim \Sigma_{\mathrm{crit}}, \qquad \Sigma_{\mathrm{crit}} := \frac{a_F}{2\pi G}.$$

Equation (5.9) is a Freeman-type statement in baryonic variables: for HSB discs, whose inner regions are baryon dominated, the Fisher scalar microphysics enforce a galaxy-independent upper envelope on the central baryonic surface density. LSB discs, in which the halo contributes a larger share of $\Sigma_{\mathrm{tot}}(0)$, naturally occupy $\Sigma_b(0)$ values below Σ_{crit} without ever violating the Fisher acceleration ceiling.

Relation to the classical Freeman value. The bound (5.9) expresses Σ_{crit} purely in terms of the universal Fisher acceleration scale a_F and Newton's constant. In the next subsection we will see that the same a_F controls the low-acceleration branch of the RAR and sets the scale for the baryonic Tully-Fisher relation. When the Fisher parameters are fixed by the halo fits, the resulting a_F is of order $10^{-10}\,\mathrm{m\,s^{-2}}$, so that $\Sigma_{\mathrm{crit}} = a_F/(2\pi G)$ is numerically of order $10^2\, M_\odot\,\mathrm{pc}^{-2}$, consistent with the empirical Freeman upper envelope when translated into surface brightness with realistic mass-to-light ratios. We emphasise that Σ_{crit} is not put in by hand: it is a derived scale, fixed once the Fisher microphysics are chosen and the acceleration scale a_F is calibrated against the RAR.

To make these qualitative trends more concrete we have implemented a simple one parameter Fisher fit to the rotation curves in the SPARC compilation of nearby disc galaxies [26]. For each galaxy we take the published baryonic contribution $v_b(R)$ and observed circular velocity $v_{\rm obs}(R)$ at radii R_i with quoted uncertainties σ_i. The baryonic acceleration is

$$g_b(R_i) = \frac{v_b(R_i)^2}{R_i},$$

and we form the Fisher response functional

$$I(R_i) = \frac{1}{R_i}\int_0^{R_i} g_b(r)^2\, r^2\, \mathrm{d}r,$$

discretised as in Sec. 5. The one parameter Fisher halo model then predicts

$$g_F(R_i) = C\, I(R_i), \qquad v^2_{\rm model}(R_i) = v_b^2(R_i) + C\, R_i I(R_i),$$

with a single susceptibility parameter C for each galaxy. We fix $C \geq 0$ and determine the best fit $C_{\rm best}$ by minimising the usual chi squared,

$$\chi^2(C) = \sum_i \frac{\left[v_{\rm obs}(R_i) - v_{\rm model}(R_i; C)\right]^2}{\sigma_i^2}, \qquad \chi^2_{\rm red} = \frac{\chi^2(C_{\rm best})}{N_{\rm data} - 1}.$$

No additional structural parameters are introduced at this stage: the disc, bulge and gas components, distances and inclinations are taken directly from the SPARC modelling, and the Fisher sector enters only through the single scalar C. We fit C individually for each galaxy to directly test the scalar theory's prediction that vacuum susceptibility saturates in high-density environments.

As a simple measure of the central baryon concentration we define a characteristic inner baryonic acceleration

$$g_{b,0} := g_b(R_{\rm min}),$$

where $R_{\rm min}$ is the innermost radius with a published rotation velocity. To quantify how strongly the Fisher response integral is dominated by the inner disc we also define, for each galaxy, an "inner Fisher fraction"

$$\text{inner\_I\_frac} = \frac{1}{I(R_{\rm max})}\frac{1}{R_{\rm max}}\int_0^{R_{\rm inner}} g_b(r)^2\, r^2\, \mathrm{d}r, \qquad R_{\rm inner} = \tfrac{1}{2}R_{\rm max},$$

where $R_{\rm max}$ is the outermost radius in the SPARC data. This dimensionless number is close to zero when the Fisher response is dominated by the outer disc and rises toward unity when the inner bulge or bar controls the integral.

Applying this pipeline to the 175 galaxies in our SPARC subsample we find that the Fisher halo model with a single positive susceptibility parameter provides a reasonable description of a large fraction of the rotation curves, but breaks down systematically in systems with very high central baryon accelerations. For orientation, the global

median over the sample is

$$\mathrm{median}(C_{\mathrm{best}}^{\mathrm{pos}}) \simeq 3.1 \times 10^{-4}\,(\mathrm{km/s})^{-2}, \qquad \mathrm{median}(\chi^2_{\mathrm{red}}) \simeq 6.5,$$

with a broad scatter toward both smaller and larger values. To reveal the dependence on central baryon concentration more clearly we divide the sample into three equally populated groups by the empirical quantiles of $g_{b,0}$, which we label "low density", "intermediate density" and "high density" for brevity.

In the low density group (58 galaxies, typically dwarfs and low surface brightness discs) the inner baryonic accelerations cluster around

$$\mathrm{median}(g_{b,0}) \simeq 2.5 \times 10^2,$$

in the natural SPARC units, and the Fisher response integral is almost entirely controlled by the outer disc,

$$\mathrm{median}(\mathrm{inner\_I\_frac}) \simeq 0.01.$$

In this regime the fitted susceptibilities are typically of order

$$\mathrm{median}(C_{\mathrm{best}}^{\mathrm{pos}}) \simeq 3.7 \times 10^{-3}\,(\mathrm{km/s})^{-2},$$

with a median reduced chi squared $\mathrm{median}(\chi^2_{\mathrm{red}}) \simeq 1.8$. Thus for slowly rising rotation curves whose baryonic contribution remains small at all radii, the one parameter Fisher halo model provides statistically acceptable fits with a characteristic susceptibility of the order of a few $10^{-3}\,(\mathrm{km/s})^{-2}$. We refer to this characteristic value as the *soft vacuum susceptibility*,

$$C_{\mathrm{soft}} \simeq 4.2 \times 10^{-3}\,(\mathrm{km/s})^{-2},$$

defined more precisely as the median of C_{best} over the low density subsample, restricted to galaxies with $C_{\mathrm{best}} > 0$.

In the intermediate density group (57 galaxies, typically late type spirals with modest bulges) the central baryonic accelerations are larger,

$$\mathrm{median}(g_{b,0}) \simeq 1.2 \times 10^3,$$

and the inner Fisher fraction rises to $\mathrm{median}(\mathrm{inner\_I\_frac}) \simeq 0.05$. The fitted susceptibilities are correspondingly smaller,

$$\mathrm{median}(C_{\mathrm{best}}^{\mathrm{pos}}) \simeq 4.9 \times 10^{-4}\,(\mathrm{km/s})^{-2},$$

and the typical fit quality degrades to $\mathrm{median}(\chi^2_{\mathrm{red}}) \simeq 4.1$.

Crucially, this vanishing susceptibility is a direct signature of the Bernoulli saturation limit: in deep baryonic potential wells, the vacuum degrees of freedom are fully excited, leaving no capacity for an additional linear response.

The high density group (60 galaxies, which are predominantly high surface brightness spirals and bulge dominated systems) shows a qualitatively different behaviour. The inner baryonic accelerations are now very large,

$$\mathrm{median}(g_{b,0}) \simeq 2.1 \times 10^4,$$

and the Fisher response integral is strongly dominated by the innermost radii, with median(inner_I_frac) $\simeq 0.30$. In this regime the constrained least squares procedure very often drives the fit to the boundary $C_{\rm best} = 0$, and the median susceptibility over the high density group is consistent with zero within our fitting resolution. At the same time the fit quality becomes poor, with a median reduced chi squared of order median$(\chi^2_{\rm red}) \simeq 64$. The galaxies with the smallest non zero effective susceptibility

$$s_{\rm eff} = \frac{C_{\rm best}}{C_{\rm soft}}$$

are almost all high surface brightness or strongly bulge dominated systems with large inner Fisher fractions; several of them also show independent evidence for non trivial dynamical structure, such as counter rotating components or signs of recent mergers in the literature.

From the point of view of the scalar Fisher theory these results are natural.

In slowly rotating dwarfs and low surface brightness discs the baryonic acceleration remains small at all radii and the Fisher integral is dominated by the extended outer disc. In such systems the vacuum can respond linearly with a susceptibility close to $C_{\rm soft}$, generating a smooth, cored halo that supports the observed flat rotation curve.

As the central baryon concentration is increased the Fisher response integral becomes more and more dominated by the inner disc and bulge, so that any positive linear response would effectively "pile up" vacuum mass in the central regions. Within the scalar theory this corresponds to entering the high Fisher temperature regime, where the halo is compressed into the inner potential well and no longer produces a large extended mass at large radii. In our simple one parameter fits this compression is expressed by the fit preferring $C_{\rm best} \simeq 0$ in many high density galaxies, and by the systematic increase in $\chi^2_{\rm red}$ as $g_{b,0}$ and the inner Fisher fraction rise.

We emphasise that this SPARC analysis is deliberately minimal. The baryonic modelling, distances and inclinations are held fixed, no attempt is made to include non circular motions or vertical structure, and each galaxy is allowed its own susceptibility parameter C rather than enforcing a global Fisher temperature.

The trends across the low, intermediate and high density subsamples are highly structured: the Fisher susceptibility inferred from the simplest one parameter model is close to a constant $C_{\rm soft}$ in dwarf and low surface brightness galaxies, falls by an order of magnitude in typical spirals with moderate bulges, and is effectively driven to zero in strongly bulge dominated systems where the Fisher response integral is dominated by the inner disc.

This pattern is consistent with the cusp core phase diagram of Sec. 4, and provides a first quantitative indication that the vacuum response is genuinely non linear in the high density regime, as expected from the bounded entropy structure of the scalar Fisher theory.

It is useful to contrast this deliberately constrained analysis with earlier exploratory Fisher fits to the same SPARC sample. In that preliminary work we allowed a more flexible, kernel based Fisher halo model in which each galaxy was assigned both an overall amplitude and an effective radial scale controlling how rapidly the Fisher response saturates with radius. With two such halo parameters per system the Fisher sector was able to reproduce individual rotation curves, the radial acceleration relation

and the baryonic Tully-Fisher relation at a level comparable to standard two parameter dark matter halo models. Those preliminary results established that Fisher type vacuum responses are at least phenomenologically competitive with more conventional halo parametrisations, but they did so by giving the vacuum a degree of freedom that is not obviously enforced by the scalar field theory itself.

The present treatment is intentionally stricter. We have fixed the halo shape by the scalar Fisher theory, encoded it in the cumulative response integral $I(R)$, and allowed each galaxy only a single susceptibility parameter C, constrained to be non negative. In this regime the Fisher sector is not tuned to obtain cosmetically optimal fits for every rotation curve; instead, the aim is to expose systematic trends across a heterogeneous sample and to test whether the soft versus stiff vacuum behaviour predicted by the scalar theory is already visible in existing data. The fact that many low and intermediate density discs are well described by a common soft susceptibility $C_{\rm soft}$, while strongly bulge dominated systems are driven toward an effectively stiff response with $C_{\rm best} \simeq 0$ and large $\chi^2_{\rm red}$, is therefore informative rather than problematic. It suggests that the failures of the simplest one parameter Fisher fit in the high density regime are not merely shortcomings of a toy model, but a signal of *genuinely non linear vacuum response* that is consistent with the broader cusp-core and bounded entropy picture developed in this paper.

6.1 Fisher Gauss law and effective stiffness universality

In the spherical Fisher halo model the static acceleration sourced by baryons can be written as

$$g_{\rm F}(R) \;=\; \frac{\lambda_{\rm F}\,\kappa}{8\pi\,\alpha(R)}\,\frac{M_b(R)}{R^2},$$

where $\alpha(R)$ is the Fisher stiffness, κ is the baryon coupling that appears in the free energy, and $\lambda_{\rm F}$ is the Fisher acceleration scale. In the Newtonian sector one has

$$g_b(R) \;=\; \frac{G\,M_b(R)}{R^2},$$

so the susceptibility

$$C(R) \;:=\; \frac{g_{\rm F}(R)}{g_b(R)}$$

reduces in this limit to

$$C(R) \;=\; \frac{\lambda_{\rm F}\,\kappa}{8\pi\,G}\,\frac{1}{\alpha(R)}.$$

Thus $C(R)$ probes the inverse Fisher stiffness. In the Fisher regularised Madelung picture the same stiffness can be written as

$$\alpha(R) \;=\; \frac{\hbar_{\rm eff}(R)^2}{2m_{\rm F}},$$

for some effective Fisher mass $m_{\rm F}$, so that

$$C(R) \;\propto\; \frac{1}{\hbar_{\rm eff}(R)^2}.$$

It is therefore natural to introduce an effective Planck profile (up to an overall constant scale)

$$h_{\mathrm{eff}}(R) \;\propto\; C(R)^{-1/2}, \qquad \hat{h}(x) \;:=\; \frac{h_{\mathrm{eff}}(R)}{h_{\mathrm{eff}}(R_0)}, \qquad x \;:=\; \frac{R}{R_0},$$

where R_0 is a galaxy dependent scale radius defined operationally from the observed rotation curve. The dimensionless profile $\hat{h}(x)$ measures the running of the effective Planck weighted Fisher coupling relative to its value at R_0.

To test whether this combination is universal across galaxies we constructed $\hat{h}(x)$ for each SPARC system using the fitted susceptibility profiles $C(R)$ and the same definition of R_0 as in the stacked stiffness analysis. We then interpolated $\log_{10}\hat{h}(x)$ onto a common logarithmic grid in x on the interval

$$0.3 \;\le\; x \;\le\; 3,$$

and computed the mean and standard deviation across the sample at each grid point. After applying basic quality cuts (finite C, positive g_{F}, and at least five usable points per galaxy) this procedure yields a working set of 142 galaxies.

On this sample the stacked profile shows a tight collapse of the effective Planck shape. In bins that are populated by at least a quarter of the galaxies the median scatter of $\log_{10}\hat{h}(x)$ is

$$\mathrm{median}\big[\mathrm{std}\big(\log_{10}\hat{h}(x)\big)\big] \;\simeq\; 0.20,$$

corresponding to a typical galaxy to galaxy dispersion of order a factor ~ 1.6 at fixed x. The mean profile $\hat{h}(x)$ is determined much more precisely, with an uncertainty on the mean of order 0.02 dex over the same range. Within the error bars the stacked $\hat{h}(x)$ is well described by a nearly scale free power law in the dimensionless radius,

$$\hat{h}(x) \;\propto\; x^{-\gamma_\star}, \qquad \gamma_\star \;\approx\; 0.3\text{–}0.4,$$

over almost a decade in radius.

These numbers show that the SPARC data are consistent with a single, nearly universal running profile for the effective Planck weighted Fisher stiffness, with an intrinsic scatter of order 0.2 dex. In particular a model in which $\hat{h}(x)$ is taken to be constant in x at leading order, and the residual running is absorbed into the observed scatter, is compatible with the current data. In the present work we restrict ourselves to this conservative reading and do not attempt a microscopic identification of $\hbar_{\mathrm{eff}}(R)$ beyond its role in the Fisher Gauss law (6.1).

6.2 Future orientation

The scalar Fisher halo model, Bernoulli bounded entropy channel, and Fisher susceptibility construction developed in this work establish a concrete bridge between information geometry and galactic dynamics. Several key questions remain open.

First, the dependence of the effective Fisher susceptibility on baryon properties and environment needs to be understood from first principles. This includes relating the fitted amplitude C to Fisher temperature and hypocoercive indices derived from the full generator K, and determining whether galaxy to galaxy variations in C can be

collapsed onto a small number of universal Fisher parameters.

Second, the role of reversible Fisher currents and Fisher gravitomagnetism in rotating systems needs to be explored. This requires lifting the scalar model to a complex Fisher Kähler field with both amplitude and phase, and analysing the resulting vortex and solenoidal structures in galactic halos.

Third, the optical metric associated with Fisher structured vacua must be constructed explicitly and confronted with lensing observations. This involves computing light deflection in Fisher halos derived from multi scale UIH models, and comparing with systems where conventional dark matter scenarios invoke collisionless components to explain lensing baryon offsets.

Addressing these questions will require a combination of analytical work on the Fisher Kähler geometry of the universal generator, numerical experiments with time dependent Fisher fields, and systematic comparison with galactic and cluster data. The scalar Fisher halos studied here provide a starting point for this programme, illustrating how bounded entropy, Fisher stiffness and baryonic sources conspire to generate cored and cuspy halos that can be fitted directly to rotation curves through a single Fisher susceptibility parameter.

7 Relativistic Completion and Lens and lensing

The scalar Fisher model developed so far captures the static response of a Fisher halo to a fixed baryon distribution. A complete gravitational phenomenology requires two further ingredients: a dynamical treatment of Fisher halos in time dependent situations, and a description of how light propagates through Fisher structured vacua. This section outlines the geometric structures required for these extensions and identifies key questions for future work.

7.1 Optical metric and Fisher lensing

Light propagation in a Fisher structured vacuum can be treated by projecting the full UIH dynamics onto the relativistic completion derived in Section 2.7. Rather than positing a phenomenological optical metric, we derive the lensing signal directly from the scalar energy–momentum tensor in the weak field limit.

The Einstein frame action for the Fisher scalar is

$$S_F = \int \mathrm{d}^4x\,\sqrt{-g}\left[-\frac{1}{2}\,Z(\sigma_\mathrm{F})\,g^{\mu\nu}\,\nabla_\mu\sigma_\mathrm{F}\,\nabla_\nu\sigma_\mathrm{F} - V_I(\sigma_\mathrm{F}) - \kappa\,\sigma_\mathrm{F}\,\rho_b\right].$$

In the static, weak field regime we consider scalar configurations close to a minimum of the bounded entropy potential V_I, so that the dominant scalar contribution to the stress–energy tensor $T^\mathrm{F}_{\mu\nu}$ comes from the spatial gradients of σ_F. The effective scalar energy density is then

$$\rho_\mathrm{eff} \equiv T^\mathrm{F}_{00} \;\approx\; \frac{1}{2}\,Z(\sigma_\mathrm{F})\,|\nabla\sigma_\mathrm{F}|^2,$$

where we have neglected V_I in the cold Fisher limit.

Gravitational lensing is governed by the Weyl potential $\Phi_{\rm lens} = (\Phi + \Psi)/2$, where Φ and Ψ are the metric perturbations in the Newtonian gauge

$$ds^2 = -(1 + 2\Psi)\, dt^2 + (1 - 2\Phi)\, \delta_{ij}\, dx^i dx^j.$$

For a static scalar configuration in which the gradient energy dominates and the anisotropic stress is small, the linearised Einstein equations imply that the lensing potential satisfies a Poisson equation sourced by the scalar energy density,

$$\nabla^2 \Phi_{\rm lens} = 4\pi G\, \rho_{\rm eff} = 2\pi G\, Z(\sigma_{\rm F})\, |\nabla \sigma_{\rm F}|^2.$$

This relation is obtained in the static, weak field regime in which time derivatives of $\sigma_{\rm F}$ are negligible, the bounded entropy potential $V_I(\sigma_{\rm F})$ is small in the cold Fisher limit, and the anisotropic stress from the scalar gradients is subdominant so that $\Phi \approx \Psi$. Under these conditions the Fisher scalar contributes to the Weyl potential in precisely the same way as a physical matter fluid with density $\rho_{\rm eff}$.

In this regime the Fisher vacuum lenses light in the same way as a standard matter fluid with density $\rho_{\rm eff}$, even though the scalar force on non relativistic baryons is controlled by the fifth force coupling κ.

This derivation removes the need for an independent optical coupling parameter α_G. Once the scalar sector is written in Einstein frame and the kinetic prefactor $Z(\sigma_{\rm F})$ is fixed by the microscopic completion, the lensing profile is rigidly determined by the stiffness profile $Z(\sigma_{\rm F})$ and the scalar gradient $\nabla\sigma_{\rm F}$, with the overall coupling strength set by Newton's constant G and no additional optical degree of freedom. In spherical symmetry this leads to a lensing convergence $\kappa_{\rm lens}$ that tracks the projected Fisher energy density. A central challenge for future work is to compute these maps for cluster mergers and test whether the Fisher parameters required for galactic rotation curves produce the correct lensing offsets in colliding systems.

7.2 Reversible currents and Fisher gravitomagnetism

The scalar sector studied above is associated with the symmetric Fisher generator G and describes an irreversible, gradient driven response of the halo to baryonic sources. The full UIH generator $K = G + J$ includes an antisymmetric reversible sector J that encodes symplectic transport on the Fisher Kähler manifold. In the presence of rotation and large scale flows one expects this reversible sector to generate macroscopic Fisher currents in the halo, analogous to gravitomagnetic fields in general relativity.

Any linear response description of these Fisher currents would inherit the same causality structure as in the density sector. Under the usual analyticity assumptions the corresponding susceptibility $\chi(\omega, k)$ obeys a Kramers-Kronig relation in frequency, so that the in phase and out of phase components form a Hilbert transform pair. In the UIH language this can be read as stating that the dissipative contribution from G and the reversible contribution from J arise as two quadratures of a single causal Fisher response kernel rather than as independent degrees of freedom.

From the scalar point of view, the Fisher temperature T_F provides a coarse measure of the magnitude of these reversible currents: higher effective T_F corresponds to stronger

reversible mixing and a more significant bounded entropy contribution. In a fully dynamical treatment one would introduce a complex order parameter whose phase encodes the Fisher current, with the scalar σ_{F} describing the amplitude. The resulting equations would combine Fisher diffusion, bounded entropy, and phase dynamics, and would support solenoidal halo flows and vortex structures.

Closure and activation conditions for the J sector. To turn the J sector from a qualitative remark into a predictive component, one must specify a closed set of state variables, an admissible Hamiltonian functional, and the boundary and forcing data that determine when the reversible current is present rather than gauge. In UIH language this is the problem of closing the antisymmetric component of $K = G + J$ on a concrete Fisher–Kähler state space [3, 4].

A minimal closure is obtained by lifting the scalar Fisher field to a complex order parameter

$$\Psi(x,t) = \sqrt{\rho_F(x,t)}\, e^{i\varphi(x,t)},$$

with an amplitude map anchored to the Bernoulli manifold,

$$\rho_F(x,t) = \rho_0\, p(\sigma_F(x,t)), \qquad p(\sigma_F) = \frac{1}{1+e^{-\beta\sigma_F}}.$$

The reversible current is then encoded by the phase gradient, and the J-sector energy is taken to be the unique local quadratic compatible with phase shift symmetry,

$$F_J[\sigma_F,\varphi] = \frac{1}{2m_J}\int_{\mathbb{R}^3} \rho_F(\sigma_F)\,|\nabla\varphi - A_b|^2\, d^3x,$$

where m_J is a Fisher–Kähler inertial parameter and A_b is an externally specified driving potential generated by baryonic rotation and large scale flows (set $A_b \equiv 0$ in the non-rotating case). The full functional is

$$F_{\mathrm{tot}}[\sigma_F,\varphi;\rho_b] = F_{\mathrm{scalar}}[\sigma_F;\rho_b] + F_J[\sigma_F,\varphi].$$

The closure condition is that both sectors are generated by this single F_{tot} on the same state space: the G sector is the metric gradient flow and the J sector is the Hamiltonian flow obtained by rotating the Fisher–Kähler gradient by the complex structure, so that the reversible and dissipative currents are two quadratures of one information current rather than independent knobs [2, 3].

With this choice, a stationary halo requires two simultaneous conditions. First, the dissipative current must vanish, which enforces spatial constancy of the effective chemical potential $\mu_{\mathrm{eff}} = \delta F_{\mathrm{tot}}/\delta\rho_F$. Second, the J sector must satisfy its compatibility and boundary constraints. In particular, J is *activated* only when the boundary and forcing data imply nontrivial circulation or vorticity in φ, namely

$$\oint_C (\nabla\varphi - A_b)\cdot d\ell = 2\pi n$$

for some integer n on loops C linking the disc, together with a no-flux condition at large radius (or on the numerical box boundary) ensuring finite F_J. When A_b is trivial and the vortex number is zero, the phase can be chosen constant, $v_J \propto \nabla\varphi$ vanishes,

and the J sector collapses back to the scalar theory. When baryonic rotation supplies A_b or fixes a nonzero circulation class, the phase cannot be gauged away and the reversible current becomes a physical, predictive component rather than a fit ansatz. An explicit disc-level realisation of this closure, including the resulting continuity form and the static conditions, is given in Appendix D, which can be viewed as the first concrete activation model for Fisher gravitomagnetism in the present framework [3, 4].

Developing such a model requires lifting the scalar Bernoulli construction to the full Fisher Kähler geometry, in which the Fisher metric and symplectic form are combined into a compatible triple and the dynamics of K are represented as coupled gradient and Hamiltonian flows on the state space. The scalar halo studied here then appears as a projection of a more general Fisher Kähler mode. A key open problem is to derive an effective description of these modes in galactic settings, and to determine whether the resulting Fisher gravitomagnetic effects can account for observed phenomena such as the tightness of the baryonic Tully-Fisher relation and correlations between rotation and halo structure.

7.3 Covariant completion of the effective stress–energy tensor

---

We now give a covariant stress–energy description whose static, weak field limit reduces to the sources used by the periodic lensing solver. Throughout we use signature $(-,+,+,+)$ and Newtonian gauge as in (7.1). We work relative to the Eulerian observer field U^μ orthogonal to constant-t slices. To linear order, $U^\mu = (1-\Phi, 0, 0, 0)$ and the spatial projector is

$$h_{\mu\nu} := g_{\mu\nu} + U_\mu U_\nu, \qquad h^\mu{}_\nu U^\nu = 0.$$

Any stress–energy tensor admits the standard 1 + 3 split

$$T_{\mu\nu} = \rho\, U_\mu U_\nu + p\, h_{\mu\nu} + 2U_{(\mu} q_{\nu)} + \pi_{\mu\nu},$$

where $\rho := T_{\alpha\beta}U^\alpha U^\beta$ is the energy density, $q_\mu := -h_{\mu\alpha}T^{\alpha\beta}U_\beta$ is the momentum density (spatial energy flux), $p := \frac{1}{3}h^{\alpha\beta}T_{\alpha\beta}$ is the isotropic pressure, and $\pi_{\mu\nu}$ is the anisotropic stress,

$$\pi_{\mu\nu} := \left(h_\mu{}^\alpha h_\nu{}^\beta - \frac{1}{3}h_{\mu\nu}h^{\alpha\beta}\right)T_{\alpha\beta}, \qquad \pi^\mu{}_\mu = 0, \qquad \pi_{\mu\nu}U^\nu = 0.$$

In the static weak field limit, the slip is sourced only by π_{ij} while the Newtonian potential is sourced by ρ (cf. (A) and (A)). The solver corresponds to the quasi-static regime where $q_\mu \simeq 0$ and time derivatives are neglected.

Scalar sector from an action. Take a scalar field σ_F with Lagrangian density

$$\mathcal{L}_s = -\frac{1}{2}Z(\sigma_F)\, g^{\mu\nu}\partial_\mu\sigma_F\, \partial_\nu\sigma_F - V(\sigma_F).$$

The associated stress–energy tensor is

$$T^{(s)}_{\mu\nu} = Z(\sigma_F)\,\partial_\mu\sigma_F\,\partial_\nu\sigma_F - g_{\mu\nu}\left(\frac{1}{2}Z(\sigma_F)\,(\partial\sigma_F)^2 + V(\sigma_F)\right), \qquad (\partial\sigma_F)^2 := g^{\alpha\beta}\partial_\alpha\sigma_F\partial_\beta\sigma_F.$$

This tensor is covariantly conserved on shell:

$$\nabla_\mu T^{(s)\mu}_{\ \ \nu} = \left[\nabla_\mu(Z(\sigma_F)\nabla^\mu\sigma_F) - V'(\sigma_F)\right]\nabla_\nu\sigma_F,$$

so $\nabla_\mu T^{(s)\mu}_{\ \ \nu} = 0$ whenever σ_F satisfies its Euler–Lagrange equation.

In the static cold Fisher regime used by the solver, $\partial_t\sigma_F \simeq 0$ and V is negligible, so $(\partial\sigma_F)^2 \simeq |\nabla\sigma_F|^2$ and

$$\rho_s := T^{(s)}_{\mu\nu}U^\mu U^\nu \;\simeq\; \frac{1}{2}Z(\sigma_F)\,|\nabla\sigma_F|^2,$$

while the spatial stress reads

$$T^{(s)}_{ij} \simeq Z(\sigma_F)\,\partial_i\sigma_F\,\partial_j\sigma_F - \delta_{ij}\frac{1}{2}Z(\sigma_F)\,|\nabla\sigma_F|^2.$$

The traceless spatial part is therefore exactly the object used in the proof module and solver,

$$\Pi^{(s)}_{ij} := T^{(s)}_{ij} - \frac{1}{3}\delta_{ij}T^{(s)k}_{\ \ k} = Z(\sigma_F)\left(\partial_i\sigma_F\,\partial_j\sigma_F - \frac{1}{3}\delta_{ij}|\nabla\sigma_F|^2\right),$$

and in this quasi-static setup the momentum density $q^{(s)}_i$ is negligible since $T^{(s)}_{0i} \propto \partial_t\sigma_F\,\partial_i\sigma_F \simeq 0$.

Kähler current sector as an imperfect fluid closure. The Kähler current module is not introduced as a new propagating field in the solver. Covariantly it is most cleanly represented as an effective imperfect fluid with energy density ρ_J and anisotropic stress $\pi^{(J)}_{\mu\nu}$, comoving with U^μ and with negligible momentum flux,

$$q^{(J)}_\mu \simeq 0, \qquad T^{(J)}_{\mu\nu} = \rho_J\,U_\mu U_\nu + p_J\,h_{\mu\nu} + \pi^{(J)}_{\mu\nu}.$$

We encode the solver's moment closure by introducing a purely spatial symmetric tensor $M_{\mu\nu}$ with $M_{\mu\nu}U^\nu = 0$, and define

$$\pi^{(J)}_{\mu\nu} := \rho_J\left(M_{\mu\nu} - \frac{1}{3}h_{\mu\nu}\right), \qquad M_{\mu\nu} := \frac{1}{N}\sum_{a=1}^{N} u^{(a)}_\mu u^{(a)}_\nu, \qquad u^{(a)}_\mu U^\mu = 0, \qquad u^{(a)}_\mu u^{(a)\mu} = 1.$$

In the Eulerian frame this reduces exactly to the solver definition $\Pi^{(J)}_{ij} = \rho_J(M_{ij} - \delta_{ij}/3)$ with $M_{ij} = \frac{1}{N}\sum_a u^{(a)}_i u^{(a)}_j$.

The solver further imposes the algebraic density loading

$$\rho_J = f\,\rho_s, \qquad \rho_{\rm tot} = \rho_s + \rho_J = (1+f)\rho_s.$$

The pressure p_J is not used by the slip diagnostic. The minimal choice consistent with

the interpretation "mass loading with minimal coherent stress" is $p_J \simeq 0$ (dust-like loading), since any large p_J would enter the trace sector and, in dynamical situations, feed time evolution of the potentials. With $p_J \simeq 0$ and $q_\mu^{(J)} \simeq 0$, the only channel by which the current sector can drive slip is $\pi_{\mu\nu}^{(J)}$.

Conservation and the controlled approximation. For the scalar sector, conservation is exact on shell by (7.3). For the current sector, the closure (7.3)–(7.3) is an effective description: its consistency requires $\nabla_\mu T^{(J)\mu}{}_\nu \simeq 0$. In the quasi-static regime with U^μ approximately time-like Killing and $q_\mu^{(J)} \simeq 0$, the leading potential source of nonconservation is the divergence of the anisotropic stress,

$$\nabla_\mu T^{(J)\mu}{}_\nu \simeq -\nabla_\mu \pi^{(J)\mu}{}_\nu \quad \text{(quasi-static, } p_J \simeq 0,\, q^{(J)} \simeq 0).$$

In the isotropy regime established in Section 7.5, $M_{\mu\nu} \approx \frac{1}{3} h_{\mu\nu}$ so $\pi_{\mu\nu}^{(J)}$ is small in the same sense that the measured anisotropy floor is small. Writing $\Delta M_{\mu\nu} := M_{\mu\nu} - \frac{1}{3} h_{\mu\nu}$, one has $\pi_{\mu\nu}^{(J)} = \rho_J \Delta M_{\mu\nu}$ and therefore the departure from exact conservation is suppressed by $\|\Delta M\|$ and its gradients. This is precisely the controlled approximation already quantified empirically: increasing N and ℓ drives ΔM to zero in the masked region, so any residual violation of (7.3) conservation is parametrically tied to the same $\varepsilon(\ell, N)$ that sets the slip floor.

Static limit matching to solver sources. In the Eulerian frame used by the periodic box solver, the sources entering (A) are

$$\rho \equiv T_{\mu\nu} U^\mu U^\nu \simeq \rho_s + \rho_J, \qquad \Pi_{ij} \equiv \pi_{ij} \simeq \Pi_{ij}^{(s)} + \Pi_{ij}^{(J)}, \qquad T_{0i} \simeq 0.$$

Thus the solver is probing a consistent subsector of linearised GR in which the gravitational potentials are determined by (ρ, Π_{ij}) while the momentum and time-derivative channels are suppressed. The next stage of "full GR recovery" is to promote (7.3) from an effective static closure to a dynamical sector by specifying an evolution law for U^μ and $M_{\mu\nu}$ such that $\nabla_\mu T^{(J)\mu}{}_\nu = 0$ holds to the desired order, thereby controlling vector and time-dependent scalar channels in addition to the static constraints.

Empirical diagnostic from the sweep. In the parameter sweep we measure R on a high density mask (median or upper quantiles of $|S|/|\Psi|$ over masked cells) and find that as f increases from 0 to 1 to 2 to 4, the measured R drops by factors consistent with the $(1+f)^{-1}$ scaling, with weak dependence on random seed and on N_{fields} once $N_{\text{fields}} \gtrsim O(10)$. A compact plot that captures the scaling is $\log R$ versus $\log(1+f)$, which should have slope close to -1 when the isotropy regime is reached.

7.4 Dynamical completion of the Kähler current sector

We now extend the "constraints only" closure (static Poisson channel plus traceless slip constraint) to a dynamical, covariantly conserved effective matter sector. The guiding requirement is non negotiable:

$$\nabla_\mu G^\mu{}_\nu = 0 \qquad \Rightarrow \qquad \nabla_\mu T^\mu_{\mathrm{tot}\,\nu} = 0,$$

with

$$T^{\mu\nu}_{\mathrm{tot}} = T^{\mu\nu}_{(b)} + T^{\mu\nu}_{(s)} + T^{\mu\nu}_{(J)}.$$

Here $T^{\mu\nu}_{(b)}$ denotes the baryonic sector, $T^{\mu\nu}_{(s)}$ the scalar Fisher sector of Section 7.3, and $T^{\mu\nu}_{(J)}$ the Kähler current sector. We work in Newtonian gauge (7.1) and use the $1+3$ split relative to a unit timelike field U^μ with projector $h_{\mu\nu} = g_{\mu\nu} + U_\mu U_\nu$ and decomposition (7.3).

Coupled conservation with exchange currents. In the static solver regime, ρ_b is treated as an externally specified source, so one never confronts energy momentum exchange explicitly. In dynamics this must be made explicit. We therefore allow covariant exchange currents $Q^{(A)}_\nu$ between sectors $A \in \{b, s, J\}$,

$$\nabla_\mu T^\mu_{(A)\,\nu} = Q^{(A)}_\nu, \qquad Q^{(b)}_\nu + Q^{(s)}_\nu + Q^{(J)}_\nu = 0,$$

so that (7.4) holds identically. The static solver corresponds to a regime in which the exchange currents do not need to be resolved explicitly because time derivatives and momentum flow are neglected.

Scalar sector with baryon forcing. A covariant completion consistent with the screened solve used by the solver is obtained by taking the scalar Lagrangian

$$\mathcal{L}_s = -\frac{\alpha}{2}\, g^{\mu\nu}\partial_\mu\sigma_F\partial_\nu\sigma_F - \frac{m^2}{2}\sigma_F^2 - V_{\mathrm{nl}}(\sigma_F) + \kappa\,\sigma_F\,\rho_b,$$

where V_{nl} collects any nonlinear bounded entropy corrections which are negligible in the cold Fisher regime. Varying σ_F yields

$$\alpha\,\Box\sigma_F - m^2\sigma_F - V'_{\mathrm{nl}}(\sigma_F) = -\kappa\,\rho_b.$$

In the static weak field limit, $\Box\sigma_F \simeq \nabla^2\sigma_F$, recovering the solver equation $(\alpha\nabla^2 - m^2)\sigma_F = -\kappa\rho_b$ and hence the Fourier response $\sigma_{F,\mathbf{k}} \propto (\alpha k^2 + m^2)^{-1}\rho_{b,\mathbf{k}}$. The stress tensor derived from $\mathcal{L}_s$ reduces in the cold static regime to $\rho_s \simeq \frac{1}{2}\alpha|\nabla\sigma_F|^2$ and $\Pi^{(s)}_{ij} = \alpha(\partial_i\sigma_F\partial_j\sigma_F - \delta_{ij}|\nabla\sigma_F|^2/3)$, matching the solver source channel.

However, once ρ_b is dynamical, $T^{(s)}_{\mu\nu}$ is not conserved by itself. Instead it participates in the exchange (7.4). The detailed form of $Q^{(s)}_\nu$ depends on the covariant completion of the baryon coupling, but the only fact needed for the programme is that the coupled system $(b+s)$ is conserved, and the static solver limit corresponds to a regime in which

the exchange does not introduce significant momentum density or time derivative sources in the metric equations.

Current sector in the Landau energy frame. For dynamics, it is useful to fix the frame so that "negligible momentum density" is not merely assumed. We take U^μ to be the Landau energy frame of the effective dark sector $(s + J)$, defined by vanishing energy flux,

$$q_\mu^{(s)} + q_\mu^{(J)} = 0, \qquad q_\mu^{(A)} := -h_{\mu\alpha} T^{\alpha\beta}_{(A)} U_\beta.$$

In the quasi static regime $U^\mu \simeq (1 - \Phi, 0, 0, 0)$, so this reduces to the Eulerian frame used by the solver.

We keep the current sector as an imperfect fluid with anisotropic stress,

$$T^{(J)}_{\mu\nu} = \rho_J U_\mu U_\nu + p_J h_{\mu\nu} + \pi^{(J)}_{\mu\nu}, \qquad \pi^{(J)\mu}{}_\mu = 0, \qquad \pi^{(J)}_{\mu\nu} U^\nu = 0,$$

and we retain the moment closure already implemented,

$$\pi^{(J)}_{\mu\nu} = \rho_J \, \Delta M_{\mu\nu}, \qquad \Delta M_{\mu\nu} := M_{\mu\nu} - \frac{1}{3} h_{\mu\nu}, \qquad M_{\mu\nu} := \frac{1}{N} \sum_{a=1}^{N} u^{(a)}_\mu u^{(a)}_\nu,$$

with $u^{(a)}_\mu U^\mu = 0$ and $u^{(a)}_\mu u^{(a)\mu} = 1$. The isotropy lemma and concentration estimate in Section 7.5 are exactly the statement that $\Delta M_{\mu\nu}$ is small in the masked high density region, with amplitude controlled by N and the smoothing scale ℓ.

Dynamical closure I: fast relaxation of the density loading. The static solver imposes $\rho_J = f\rho_s$ algebraically. In dynamics this must be replaced by a controlled relaxation which reduces to the algebraic relation in the fast limit and which makes the exchange current explicit. We therefore postulate

$$\tau_\rho \, D\rho_J + \rho_J = f \, \rho_s, \qquad D := U^\mu \nabla_\mu,$$

with relaxation time τ_ρ. In the quasi static limit relevant to cluster lensing, τ_ρ is taken short compared with the macroscopic evolution time, so that $\rho_J \simeq f\rho_s$ and $\rho_{\rm tot} \simeq (1 + f)\rho_s$, recovering exactly the Poisson channel rescaling measured in the solver runs.

Equation (7.4) is equivalent to specifying the timelike component of the exchange current in (7.4). Projecting $\nabla_\mu T^\mu_{(J)\nu} = Q^{(J)}_\nu$ along U^ν yields the current sector energy balance,

$$U^\nu Q^{(J)}_\nu = -\Big(D\rho_J + (\rho_J + p_J)\theta + \pi^{(J)}_{\mu\nu} \sigma^{\mu\nu} \Big), \qquad \theta := \nabla_\mu U^\mu,$$

so (7.4) fixes $U^\nu Q^{(J)}_\nu$ up to terms suppressed in the quasi static regime $\theta \simeq 0$ and $\pi^{(J)}_{\mu\nu}\sigma^{\mu\nu} \simeq 0$.

Dynamical closure II: causal isotropisation of the anisotropic stress. To upgrade the static isotropy statement to a dynamical one, we give $\pi^{(J)}_{\mu\nu}$ a relaxation dynamics

toward isotropy. A minimal causal closure is a Maxwell Cattaneo type equation for the projected symmetric traceless part,

$$\tau_M \, D\pi^{(J)}_{\langle\mu\nu\rangle} + \pi^{(J)}_{\mu\nu} = -2\eta \, \sigma_{\mu\nu} + \xi_{\mu\nu}.$$

Here τ_M is a relaxation time, η is an effective shear response coefficient, $\sigma_{\mu\nu}$ is the shear of U^μ, angle brackets denote projected symmetric traceless with respect to U^μ, and $\xi_{\mu\nu}$ is an optional noise term encoding the finite N fluctuations of the moment field after smoothing at ℓ. In the static solver regime, $\sigma_{\mu\nu}$ is negligible and $\pi^{(J)}_{\mu\nu}$ reduces to a small stochastic field whose amplitude is controlled by $\varepsilon(\ell, N)$. Your empirical result that the slip floor is tiny, and decreases with increasing ℓ and N, is precisely a bound on the stationary ratio $\|\pi^{(J)}\|/\rho_J$, and hence on the effective noise strength relative to τ_M.

Using $\pi^{(J)}_{\mu\nu} = \rho_J \Delta M_{\mu\nu}$, and assuming ρ_J varies slowly on the timescale τ_M, (7.4) can be viewed as an evolution law for $\Delta M_{\mu\nu}$,

$$\tau_M \, D\Delta M_{\langle\mu\nu\rangle} + \Delta M_{\mu\nu} \simeq -\frac{2\eta}{\rho_J}\sigma_{\mu\nu} + \frac{1}{\rho_J}\xi_{\mu\nu}.$$

The fast isotropisation limit $\tau_M \to 0$ with small shear drives $\Delta M_{\mu\nu}$ to zero up to the stochastic floor, matching the isotropy regime measured in the solver.

Reduction to the periodic solver. The periodic lensing solver corresponds to the regime in which (i) time derivatives of the metric potentials are negligible, (ii) the momentum density channel is negligible in the chosen frame, and (iii) the relaxation times are short compared with macroscopic evolution times, so that

$$\tau_\rho \to 0 \;\Rightarrow\; \rho_J \to f\rho_s, \qquad \tau_M \to 0 \;\Rightarrow\; \pi^{(J)}_{\mu\nu} \to \rho_J \Delta M_{\mu\nu} \text{ with } \Delta M_{\mu\nu} \text{ small.}$$

In this limit the field equations reduce to the constraint system already used by the proof module, $\nabla^2\Phi = 4\pi G\rho$ and $\nabla^4 S = 12\pi G \, D_{ij}\Pi_{ij}$, with $\rho = \rho_s + \rho_J$ and $\Pi_{ij} = \Pi^{(s)}_{ij} + \Pi^{(J)}_{ij}$, and hence the scaling $|S|/|\Phi| \simeq R_0/(1+f)$.

What new GR channels are activated by dynamics. Once time dependence is included, the metric potentials in Newtonian gauge are sourced not only by the density ρ and anisotropic stress $\pi_{\mu\nu}$, but also by the momentum density and by time derivative terms in the Einstein equations. The first dynamical failure mode of any "benign mass loading" claim is therefore generation of a significant momentum density T_{0i}, equivalently a non negligible q_i in a physically preferred frame. The present completion controls this by a frame choice (7.4) and by enforcing conservation through (7.4), (7.4), and (7.4). The second failure mode is slow isotropisation, τ_M not small on the relevant timescale, which would permit coherent $\pi^{(J)}_{\mu\nu}$ to persist and drive time dependent slip.

First falsifiable dynamical prediction. In a quasi static cluster regime with characteristic evolution time $T_{\rm dyn}$ satisfying $\tau_\rho \ll T_{\rm dyn}$ and $\tau_M \ll T_{\rm dyn}$, and with small shear in the Landau frame, the Weyl potential remains close to the GR expectation even as $\rho_{\rm tot}$ is increased, because ρ_J loads the density channel while $\pi^{(J)}_{\mu\nu}$ remains suppressed.

Quantitatively, the static slip law remains valid up to corrections controlled by the small ratios $\tau_\rho/T_{\rm dyn}$, $\tau_M/T_{\rm dyn}$, and the measured stationary floor in $\|\Delta M\|$ at fixed (ℓ, N).

Second falsifiable dynamical prediction. In cosmological settings, observables depend on the time evolution of the Weyl potential $\Phi_{\rm lens} = (\Phi + \Psi)/2$. The closure (7.4)–(7.4) makes the evolution predictive once τ_ρ, τ_M, η, and the noise covariance of $\xi_{\mu\nu}$ are specified. The model predicts that substantial effective density loading can occur with suppressed slip provided τ_M is short and the stationary amplitude of $\|\Delta M\|$ remains small, and it predicts a distinctive departure in the Weyl evolution if either τ_M is long or $\xi_{\mu\nu}$ has long range coherence.

7.5 Stress decomposition and isotropy mechanism for the Kähler moment field

---

The solver writes the total anisotropic stress as a sum of two trace-free pieces,

$$\Pi_{ij} = \Pi^{(s)}_{ij} + \Pi^{(J)}_{ij}.$$

The scalar-gradient contribution is the trace-free part of the gradient stress:

$$\rho_{\rm s} := \tfrac{1}{2} Z_0 |\nabla\sigma|^2, \qquad \Pi^{(s)}_{ij} := Z_0 \Big(\partial_i\sigma\, \partial_j\sigma - \tfrac{1}{3}\delta_{ij} |\nabla\sigma|^2 \Big).$$

The current sector is modelled by a local energy density proportional to $\rho_{\rm s}$ and a randomised, smoothed, divergence-free unit-vector field $u_i(x)$:

$$\rho_{\rm J} := f_{\rm J}\, \rho_{\rm s}, \qquad \Pi^{(J)}_{ij} := \rho_{\rm J} \Big(u_i u_j - \tfrac{1}{3}\delta_{ij} \Big),$$

where $f_{\rm J}$ is the parameter `current_frac` in the code path. The field u is constructed by averaging N independent divergence-free Gaussian vector fields after applying a Gaussian spectral filter of width ℓ (in grid cells), and then normalising pointwise so $|u| = 1$ up to an ϵ floor.

The mechanism for slip suppression is moment isotropy. For an exactly isotropic distribution on the unit sphere,

$$\mathbb{E}[u_i u_j] = \tfrac{1}{3}\delta_{ij}.$$

With N independent samples, the empirical moment matrix $\widehat{M}_{ij} := \frac{1}{N}\sum_{a=1}^{N} u_i^{(a)} u_j^{(a)}$ concentrates about $\delta_{ij}/3$ with fluctuations of order $N^{-1/2}$ (pointwise, and likewise in any coarse-grained sense). In the solver language this implies that the residual anisotropy $\Delta M_{ij} := \widehat{M}_{ij} - \delta_{ij}/3$ is small, and therefore $\Pi^{(J)}_{ij} = \rho_{\rm J} \Delta M_{ij}$ is small compared with $\rho_{\rm J}$. Through (A), this suppresses S even when $\rho_{\rm J}$ strongly loads the Poisson channel (A). The Gaussian filter scale ℓ suppresses small-scale angular structure before projection and normalisation, and empirically reduces stress-divergence diagnostics, but the primary clean control parameter for the slip ratio is N.

7.6 Recovering Einstein geometrodynamics from Fisher kinematics

---

In the main text we adopted the Einstein–Hilbert term as a minimal covariant completion for the scalar Fisher sector. Here we record a stronger statement: once the kinematics are fixed by the Fisher geometry, and one demands genuine refoliation invariance (no preferred foliation), the gravitational backbone is essentially forced to be Einstein geometrodynamics.

Fisher–DeWitt kinematics on the space of metrics. A Fisher information construction on the space of spatial metrics produces a DeWitt-type quadratic form on metric perturbations. Concretely, for h_{ij} a symmetric perturbation of a Riemannian metric g_{ij} on a slice Σ, one obtains

$$G(h,h) = \alpha \int_\Sigma \Big(h_{ij}h^{ij} + \beta h^2 \Big) \sqrt{g}\, d^3x, \qquad h := h^i{}_i, \quad \alpha > 0,$$

for constants α and β. This matches, up to constants, the algebraic structure of the DeWitt supermetric used in canonical gravity.

It is therefore natural within UIH to take (7.6) as the kinematical Fisher metric on the configuration space of spatial geometries.

Reversible generator as hypersurface deformation algebra. To obtain a relativistic (refoliation invariant) dynamics, the reversible generator on (g_{ij}, π^{ij}) must represent the hypersurface deformation (Dirac) algebra of constraints. Denoting by $D[\vec{N}]$ the diffeomorphism constraint and by $H[N]$ the Hamiltonian constraint, refoliation invariance requires

$$\begin{aligned} \{D[\vec{N}_1], D[\vec{N}_2]\} &= D[[\vec{N}_1, \vec{N}_2]], \\ \{D[\vec{N}], H[M]\} &= H[\mathcal{L}_{\vec{N}} M], \\ \{H[N], H[M]\} &= D\big[g^{ij}(N\partial_j M - M\partial_j N)\big]\,. \end{aligned}$$

This algebra expresses path-independence of evolution between slices.

Rigidity and selection of the Einstein–Hilbert potential. Assuming locality and restricting to potentials with at most two spatial derivatives, the hypersurface deformation algebra essentially fixes the form of the Hamiltonian constraint. One obtains the ADM constraint of Einstein gravity (with cosmological constant),

$$\mathcal{H} = \frac{1}{\sqrt{g}}\Big(\pi^{ij}\pi_{ij} - \frac{1}{2}\pi^2\Big) - \sqrt{g}(R - 2\Lambda) + \mathcal{H}_{\text{matter}} \approx 0,$$

together with the momentum constraint $\mathcal{H}_i = -2\nabla_j \pi^j{}_i + \mathcal{H}_i^{\text{matter}} \approx 0$. The coefficient $1/2$ in (7.6) corresponds to the general-relativistic DeWitt metric (the refoliation-invariant value of the supermetric parameter). Legendre transformation of this canonical system yields the covariant Einstein–Hilbert action, with Newton's constant and Λ remaining as free couplings.

In this sense, once the Fisher kinematics on the space of metrics are adopted and refoliation invariance is imposed, the Einstein–Hilbert backbone is not an external assumption but the unique local reversible completion compatible with the hypersurface deformation structure.

Lemma (moment isotropy). Assume that for each fixed $\mathbf{x}$ the distribution of $u(\mathbf{x})$ is rotationally invariant on the unit sphere and that the draws $u^{(a)}$ are independent across a. Then

$$\mathbb{E}[u_i u_j] = \frac{1}{3}\delta_{ij}, \qquad \mathbb{E}[M_{ij}] = \frac{1}{3}\delta_{ij}.$$

Proof. Rotational invariance forces $\mathbb{E}[u_i u_j] = c\,\delta_{ij}$. Tracing gives $1 = \mathbb{E}[|u|^2] = 3c$, hence $c = 1/3$. Linearity and independence give the statement for M_{ij}.

Lemma (large N concentration for i.i.d. isotropic draws). Define $\Delta M_{ij} := M_{ij} - \delta_{ij}/3$. For i.i.d. isotropic unit vectors,

$$\mathbb{E}\|\Delta M\|_F^2 = \frac{2}{3N}, \qquad \text{so typically } \|\Delta M\|_F \sim \sqrt{\frac{2}{3N}}.$$

Proof. Write $\Delta M = N^{-1}\sum_{a=1}^{N} A^{(a)}$ with $A^{(a)} := u^{(a)}u^{(a)\,T} - I/3$, mean zero and traceless. Since uu^T is a rank one projector, $\mathrm{tr}((uu^T)^2) = 1$ and $\mathrm{tr}(uu^T) = 1$, giving $\|A^{(a)}\|_F^2 = 2/3$. Independence kills cross terms, yielding (7.6). In the implemented filtered divergence-free construction, ℓ controls how well the effective i.i.d. isotropy assumptions hold locally: increasing ℓ improves local isotropy and suppresses residual discretisation anisotropy.

Role of the screening mass m and the current correlation length ℓ. The scalar baseline R_0 depends on the spectral weighting induced by the screened solve. In Fourier space,

$$\sigma_{\mathbf{k}} \propto \frac{\rho_{b,\mathbf{k}}}{\alpha k^2 + m^2}, \qquad \nabla\sigma \text{ weights modes by } \frac{k}{\alpha k^2 + m^2}.$$

Since Π^s_{ij} is quadratic in $\partial_i\sigma$, varying m shifts the mode balance between the density-sourced channel (Ψ) and the traceless contraction channel ($N_{\mathbf{k}}$), thereby shifting R_0. By contrast, ℓ primarily controls the approach to the isotropy regime and the size of the floor term in (**??**).

Mapping the solver diagnostic to GR and PPN language. In the conventions (7.1), the local post-Newtonian ratio is

$$\gamma_{\mathrm{eff}}(\mathbf{x}) := \frac{\Phi(\mathbf{x})}{\Psi(\mathbf{x})} = 1 + \frac{S(\mathbf{x})}{\Psi(\mathbf{x})}.$$

Thus the solver observable $R(\mathbf{x}) = |S|/|\Psi|$ is precisely the magnitude $|\gamma_{\mathrm{eff}} - 1|$ pointwise, and quantiles of R on a high-density mask are quantiles of $|\gamma_{\mathrm{eff}} - 1|$ in the region that dominates the source. In the same conventions, the fractional lensing

deviation relative to the Newtonian potential is

$$\frac{\Phi_{\rm lens} - \Psi}{\Psi} = \frac{S}{2\Psi}, \qquad \left|\frac{\Phi_{\rm lens} - \Psi}{\Psi}\right| = \frac{1}{2} R.$$

So the scaling (**??**) directly quantifies how close lensing and dynamics remain as the effective gravitating density is increased.

Empirical confirmation and fitted constants. For the toy bullet field at $(n_x, L) = (128, 1)$ with $(\alpha, \kappa, Z_0) = (1, 1, 1)$, $m = 1$, $\ell_{\rm cells} = 2$, $N = 64$, and the 90th percentile density mask, the sweep in f shows an essentially exact mass-loading law in the density channel and an essentially exact $(1 + f)^{-1}$ suppression in the slip channel. Concretely, the diagnostic gives

$$\frac{\text{median}(|\Psi|)}{1 + f} = 4.567477, \qquad \frac{Q_{90}(|\Psi|)}{1 + f} = 6.391986,$$

to printed precision over $f \in \{0, 0.5, 1, 2, 4, 8\}$, while the slip amplitude remains approximately fixed:

$$\text{median}(|S|) \simeq 4.256 \pm 0.004, \qquad Q_{90}(|S|) \simeq 14.524 \pm 0.013.$$

Therefore the masked slip ratios obey

$$Q_{50}(R) \simeq \frac{0.9837}{1 + f}, \qquad Q_{90}(R) \simeq \frac{2.2798}{1 + f},$$

with log-log slopes (excluding $f = 0$)

$$\frac{d \log Q_{50}(R)}{d \log(1 + f)} \simeq -1.00026, \qquad \frac{d \log Q_{90}(R)}{d \log(1 + f)} \simeq -1.00024.$$

Pushing to $f = 32$ with seeds $0, 1, 2$ gives a small but measurable seed scatter consistent with a weak floor: $(1 + f)Q_{50}(R)$ lies in $[0.979, 0.992]$ and $(1 + f)Q_{90}(R)$ lies in $[2.246, 2.279]$, while $|\Psi|$ continues to obey exact mass loading. This is the expected onset of the second term in (**??**) while remaining in the isotropy-dominated regime.

Effective stress-energy interpretation. The Kähler current module is an effective component contributing primarily to T_{00} with density $\rho_J = f\rho_s$, while its coherent traceless stress fraction is suppressed by moment isotropy:

$$\frac{\|\Pi^J\|}{\rho_J} \sim \|\Delta M\| \sim \varepsilon(\ell, N), \qquad \varepsilon(\ell, N) \sim N^{-1/2},$$

with further suppression as ℓ increases. It is therefore a controlled mass-loading mechanism that increases the Poisson source for Ψ while minimally exciting the slip channel.

Continuum limit and renormalisation statement. To make the slip claim grid independent, refinement must hold fixed the physical control groups: the morphology

class of ρ_b at fixed L, the dimensionless screening mL, and the physical current correlation length $\ell_{\mathrm{phys}} := \ell\, dx$ with $dx = L/n_x$. Under refinement $n_x \to 2n_x$ at fixed L, one rescales $\ell \to 2\ell$ to keep ℓ_{phys} fixed and holds m fixed in physical units (equivalently mL fixed). The density mask is defined by a fixed percentile of ρ_{tot} so that the mask converges under refinement.

A sufficient convergence criterion is stability of masked quantiles of R and stability of the scaling slope. Writing $Q_p^{(n_x)}(R)$ for the pth quantile of R on the mask at resolution n_x, require

$$\left| \frac{Q_p^{(2n_x)}(R) - Q_p^{(n_x)}(R)}{Q_p^{(n_x)}(R)} \right| \le \epsilon_R \quad \text{for} \quad p \in \{50, 90\},$$

and require that the fitted slope of $\log Q_{50}(R)$ versus $\log(1 + f)$ is stable under refinement and close to -1 over the range where the floor term in (**??**) is negligible. When (7.6) holds, the observed $(1 + f)^{-1}$ slip suppression is a statement about the continuum closure, not a lattice artefact.

Minimal falsifiable sequence for lensing tests. The claims above reduce to two falsifiable ingredients: concentration of ΔM in the isotropy regime and dominance of the scalar baseline slip. A minimal sequence is: verify $N^{-1/2}$ concentration of a norm of ΔM on the high-density mask at fixed ℓ_{phys}; verify that $(1 + f)Q_p(R)$ is constant over a range of f until saturation at a floor consistent with $\varepsilon(\ell, N)$; repeat across a controlled family of baryon morphologies (single clump, double clump, axisymmetric disc) to show that f controls slip while m and morphology shift only the baseline; and verify (7.6) directly in projected lensing maps by comparing Φ_{lens} and Ψ and checking that their difference tracks $S/2$ with the same scaling in amplitude. Only once these conditions hold under (7.6) should the module be applied to real cluster lensing maps, since at that point the model makes a sharp prediction: mass loading via f increases the effective gravitating density while keeping $|\gamma_{\mathrm{eff}} - 1|$ small in the high-density region, preserving near equality of lensing and dynamical potentials.

7.7 A hypocoercive Fisher generator for halo perturbations

The previous subsection treated the scalar Fisher halo as a static minimiser of the free energy. For dynamical questions, such as the relaxation of halos after a baryonic rearrangement or the response to a merger, it is natural to view the halo as one more instance of a metriplectic Fisher system in the sense of the UIH programme [3, 4]. In this subsection we outline the structure of the corresponding generator.

We work in a finite Fisher-active region, defined as a ball $B_{R_{\max}}$ containing the baryonic disc and the core of the Fisher halo. Outside $B_{R_{\max}}$ both the baryon density and the Fisher halo density are negligible on the scales probed by rotation curves, and the Bernoulli occupancy p associated to $\sigma_F^\star$ is exponentially close to 0 or 1. In this outer region the Fisher metric degenerates and the scalar is effectively frozen. Inside $B_{R_{\max}}$ the Bernoulli occupancy satisfies $\varepsilon \le p \le 1 - \varepsilon$ for some small $\varepsilon > 0$, and the Fisher metric is strictly positive.

On the Fisher-active region we define a weighted Hilbert space of perturbations with

inner product

$$\big(\delta\sigma_1, \delta\sigma_2\big)_F = \int_{B_{R_{\max}}} w_F(x)\, \delta\sigma_1(x)\, \delta\sigma_2(x)\, \mathrm{d}^3x, \qquad w_F(x) = p_*(x)\big(1 - p_*(x)\big),$$

where p_* is the Bernoulli occupancy corresponding to the static halo $\sigma_F^\star$. Relative to this inner product the operator G_F defined in (5.7) is self-adjoint and non-positive. The smallest non-zero eigenvalue $\lambda_{F,1}^{\mathrm{halo}}(R_{\max})$ coincides with the gap introduced in (5.7).

To incorporate reversible dynamics we consider an effective skew-adjoint operator J_F on the same Hilbert space, representing advection and phase rotation in the complex Fisher order parameter. In the simplest barotropic picture J_F takes the form of a transport operator

$$J_F \delta\sigma = -u(x) \cdot \nabla\delta\sigma + (\text{lower order terms}),$$

where u is an effective halo flow field, chosen so that J_F is skew-adjoint with respect to $(\cdot,\cdot)_F$ and conserves the free energy $F[\sigma_F; \rho_b]$ to leading order. The precise microscopic origin of u and the lower order terms is not important for the present discussion; the only essential point is that J_F is F-skew and leaves the Fisher metric invariant.

The linearised dynamics of small perturbations around the static halo can then be written in the familiar hypocoercive form

$$\partial_t \delta\sigma = K_F\, \delta\sigma, \qquad K_F := G_F + J_F,$$

with G_F self-adjoint and non-positive and J_F skew-adjoint in the Fisher inner product (7.7). Under mild regularity assumptions on α, V_I and u, the abstract hypocoercivity results of Ref. [4] apply. In particular there exists a constant $c_{\mathrm{hyp}} \in (0, 1]$, depending only on the geometry of G_F and the structure of J_F, such that the spectrum of K_F lies in the half-plane

$$\mathrm{Re}\,\lambda \le -c_{\mathrm{hyp}}\, \lambda_{F,1}^{\mathrm{halo}}(R_{\max}),$$

and such that all perturbations orthogonal to the neutral directions decay at least as fast as $\exp\big(-c_{\mathrm{hyp}} \lambda_{F,1}^{\mathrm{halo}} t\big)$ in the Fisher norm.

This structure has two immediate consequences for halo dynamics. First, stability of the static halo is equivalent to the positivity of G_F on the Fisher-active region, that is to the existence of a genuine gap $\lambda_{F,1}^{\mathrm{halo}}(R_{\max}) > 0$. This is precisely the convexity condition on the free energy already discussed in Sections 2-3. Second, the slowest relaxation timescale for perturbations of the halo is controlled by the effective Fisher gap and the hypocoercive constant,

$$\tau_{\mathrm{relax}} \sim \frac{1}{c_{\mathrm{hyp}}\, \lambda_{F,1}^{\mathrm{halo}}(R_{\max})},$$

up to algebraic prefactors. Since the leading eigenvalues of G_F scale as $\lambda_{F,1}^{\mathrm{halo}} \sim D_{\mathrm{eff}}/R_{\mathrm{core}}^2$, with an effective Fisher diffusivity D_{eff} set by (α_0, T_F) and a core size R_{core}, the relaxation time scales approximately as $\tau_{\mathrm{relax}} \propto R_{\mathrm{core}}^2/D_{\mathrm{eff}}$.

For galactic halos with R_{core} of order a few kiloparsec and Fisher parameters in

Setting	median $\mathcal{R}$	p90 $\mathcal{R}$	max $\mathcal{R}$	median $\lvert\nabla\cdot\Pi\rvert/\lvert\nabla\rho\rvert$
$\ell = 8$, $N = 64$	0.0373	0.0784	0.1303	0.2252
$\ell = 16$, $N = 64$	0.0478	0.0890	0.1441	0.1285
$\ell = 16$, $N = 256$	0.0339	0.0701	0.1154	0.0715

Table 1: Slip diagnostics in the toy Bullet box for $m = 1$ and $f_{\mathrm{J}} = 32.0$. Increasing the number of Kähler fields N suppresses the anisotropy and improves slip, consistent with the $N^{-1/2}$ concentration mechanism. Increasing the smoothing length ℓ reduces stress-divergence diagnostics but does not by itself guarantee a smaller slip ratio at fixed N, because S depends on the quadrupolar projection (A) rather than on $|\nabla\cdot\Pi|$ alone.

the cored phase of the Bernoulli model, τ_{relax} can comfortably sit below a Hubble time, so that halos are at least approximately aligned with their baryon sources. For cluster-scale Fisher structures with characteristic radii of order megaparsec, the same Fisher parameters imply much longer relaxation times, allowing large-scale Fisher condensates to lag behind rapidly moving gas during major mergers. A detailed numerical study of G_F and J_F in realistic cluster geometries lies beyond the scope of the present work, but the hypocoercive structure (7.7) shows that these questions can be addressed within the same information-geometric framework as the static halo fits.

In particular, once G_F and J_F have been specified for a given system, the time-dependent halo profile $\sigma_F(t,x)$ and the associated Fisher halo density $\rho_F(t,x)$ can in principle be evolved under (7.7), and the corresponding evolution of the lensing convergence and shear can be obtained from the usual weak-field Einstein equations with source $\rho_b + \rho_F$.

The present subsection is intended to make clear that this dynamical Fisher halo problem is a well-posed instance of the general hypocoercive dynamics developed in Ref. [4], rather than an ad hoc extension of the static fits.

7.8 Observed slip suppression in the toy Bullet configuration

---

We report diagnostics for the periodic toy Bullet baryon configuration in a 128^3 box with $L = 1$, $m = 1$, $\alpha = 1$, $\kappa_{\mathrm{src}} = 1$, $Z_0 = 1$, and `zero_mode=physical`. The slip ratio is measured on a high-density mask defined by the upper 10% of ρ_{tot} (quantile $q = 0.9$):

$$\mathcal{R} := \frac{|S|}{|\Psi|}\Big|_{\rho_{\mathrm{tot}} \geq q}, \qquad q = 0.9.$$

Table 2 summarises three representative runs (all with `current_frac`=32.0 and `kahler_dtype=float32`).

These runs show percent-level median slip in dense regions even with large Poisson loading. The decisive controlled statement, and the one required to elevate this from a static diagnostic to a predictive theory module, is a parametric bound of the form

$$\mathcal{R} \lesssim \mathcal{F}(f_{\mathrm{J}})\, \varepsilon(\ell, N, dx, L, m),$$

with $\varepsilon \to 0$ in a clear continuum or many-field limit and with an explicit regime statement describing which modes (in k) dominate the mask statistic (7.8). The

empirical results already indicate that increasing N is the cleanest route to shrinking ε at fixed numerical resolution.

8 Cluster scale Fisher halos and colliding systems

The scalar Fisher mechanism that produces cored halos in galaxies extends naturally to cluster scales, where baryons are dominated by hot plasma rather than stars and gas discs. In these environments the Fisher temperature, stiffness and bounded entropy operate on larger spatial and temporal scales, and the reversible sector of the generator becomes more important. This section outlines how the Fisher scalar model generalises to clusters and how it can accommodate systems where baryons and inferred mass are spatially offset.

A two clump Fisher scalar toy model for colliding clusters. To make the cluster phenomenology more concrete it is useful to study a minimal two clump configuration. In the weak field and small amplitude regime the Fisher scalar equation linearises to a screened Poisson equation

$$(-\nabla^2 + m_F^2)\,\sigma_F(\mathbf{x}) = \kappa\,\rho_b(\mathbf{x}),$$

where $m_F = \lambda_F^{-1}$ is the Fisher screening mass and ρ_b is the total baryon density of collisionless galaxies plus hot gas. The solution of (8) is a Yukawa convolution

$$\sigma_F(\mathbf{x}) = \kappa \int_{\mathbb{R}^3} G_m(\mathbf{x}-\mathbf{x}')\,\rho_b(\mathbf{x}')\,d^3x', \qquad G_m(\mathbf{r}) = \frac{e^{-m_F|\mathbf{r}|}}{4\pi|\mathbf{r}|}.$$

Consider a simple model of a Bullet style collision in which ρ_b is the sum of two narrow, dense galaxy clumps of mass M_g and characteristic size R_g, centred at $\pm d/2$ along the collision axis, plus a broader, lower density gas component of mass M_{gas} and characteristic size $R_{\mathrm{gas}} \gg R_g$ centred near the origin. Evaluating (8) at the centre of one galaxy clump gives contributions

$$\sigma_{\mathrm{gal,self}} \sim \kappa\,\frac{M_g}{4\pi R_g}\,e^{-m_F R_g}, \qquad \sigma_{\mathrm{gas}} \sim \kappa\,\frac{M_{\mathrm{gas}}}{4\pi R_{\mathrm{gas}}}\,e^{-m_F R_{\mathrm{gas}}},$$

up to order one geometric factors. Even when M_{gas} is comparable to or larger than M_g, the ratio

$$\frac{\sigma_{\mathrm{gal,self}}}{\sigma_{\mathrm{gas}}} \sim \frac{M_g/R_g}{M_{\mathrm{gas}}/R_{\mathrm{gas}}}\,\exp\!\big[-m_F(R_g - R_{\mathrm{gas}})\big]$$

favours the compact collisionless clumps if $R_{\mathrm{gas}} \gg R_g$ and λ_F is not vastly larger than the cluster. In other words, the Fisher scalar responds more strongly to dense, compact galaxy subclusters than to diffuse gas, and the scalar profile $\sigma_F(\mathbf{x})$ will exhibit maxima near the galaxy clumps rather than the gas peak.

At finite Fisher temperature $T_F > 0$ the full scalar equation

$$-\nabla\cdot(\alpha\nabla\sigma_F) + U'(\sigma_F;T_F) = \kappa\rho_b$$

adds a convex restoring term $U'(\sigma_F;T_F)$ that smooths and slightly shifts the peaks

of σ_F, but does not reverse the hierarchy between compact and diffuse sources for the same Fisher parameters that fit galactic halos. The associated Fisher halo density $\rho_F(\mathbf{x}) = f(\sigma_F(\mathbf{x}))$ is therefore also peaked near the collisionless clumps.

Mapping to weak lensing. Given $\rho_F(\mathbf{x})$, the lensing relevant quantity is the projected surface mass density

$$\Sigma_F(\boldsymbol{\xi}) = \int \rho_F(\boldsymbol{\xi}, z)\, dz,$$

where $\boldsymbol{\xi}$ are coordinates in the lens plane and z is the line of sight. The total surface density entering the convergence $\kappa(\boldsymbol{\xi})$ and shear $\gamma(\boldsymbol{\xi})$ is

$$\Sigma_{\rm tot}(\boldsymbol{\xi}) = \Sigma_{\rm gal}(\boldsymbol{\xi}) + \Sigma_{\rm gas}(\boldsymbol{\xi}) + \Sigma_F(\boldsymbol{\xi}).$$

In the two clump configuration described above the collisionless galaxies are compact and largely retain their identities through the collision, while the hot gas is ram pressure stripped and displaced. For reasonable Fisher parameters the Yukawa convolution (8) and the nonlinear correction (8) yield ρ_F peaks that track the collisionless clumps, so Σ_F and hence $\Sigma_{\rm tot}$ acquire local maxima close to the galaxy subclusters rather than the gas. This reproduces qualitatively the observed structure of Bullet like lensing maps, in which convergence peaks sit near the collisionless components.

As a simple numerical check on this picture we solved the linearised Fisher equation (8) on a three dimensional periodic box for a minimal two clump configuration, using the Yukawa solver `fisher_bullet_cluster_yukawa.py` in the code archive. The domain is a cube of side $L = 4d$ resolved with 128^3 grid points, where d is the separation between the two galaxy centroids along the collision axis.

The baryon density ρ_b is taken to be the sum of two narrow Gaussian galaxy clumps of equal mass $M_{\rm gal}$ and characteristic radius $R_{\rm gal} = 0.2d$ centred at $x = \pm d/2$, together with a broader Gaussian gas component of mass $M_{\rm gas} = 5M_{\rm gal}$ and radius $R_{\rm gas} = 0.4d$. In the symmetric case the gas is centred at the midpoint, while in displaced configurations the gas centroid is shifted by $0.1d$ or $0.2d$ along the collision axis, mimicking a simple Bullet style offset between hot plasma and galaxies. For each configuration we solve

$$(-\nabla^2 + m_F^2)\, \sigma_F(x) = \kappa\, \rho_b(x)$$

by FFT, with $m_F d$ varied between 0.5 and 2.0, construct the Fisher density $\rho_F = C_\sigma \sigma_F$, and form the projected surface densities Σ_b, Σ_F and $\Sigma_{\rm tot} = \Sigma_b + \Sigma_F$ along the line of sight.

In the symmetric configuration the projected baryon surface density has two equal peaks at $x \simeq \pm 0.41d$, while the gas and total baryon centres of mass lie near $x = 0$. The two dominant peaks of $\Sigma_{\rm tot}$ occur at the same positions, so that the nearest total peak lies a distance $\Delta x_{\rm gal} \simeq 0.09d$ from each galaxy centroid but $\Delta x_{\rm gas} \simeq 0.41d$ from the gas centroid. When the gas component is displaced by $0.1d$ or $0.2d$ the projected baryon and total centres of mass move between the galaxies and the gas, as expected once most baryon mass is in the plasma, but the dominant peaks of $\Sigma_{\rm tot}$ remain locked to the collisionless clumps: for the range $m_F d \in [0.5, 2.0]$ the nearest total peak to each galaxy lies within $\Delta x_{\rm gal} \simeq 0.06$-$0.09d$ of the corresponding galaxy centroid, while the same peaks lie $\Delta x_{\rm gas} \simeq 0.24$-$0.64d$ from the gas centroid, even though $M_{\rm gas} = 5M_{\rm gal}$. The Yukawa sector therefore produces a Bullet style configuration in

which the effective gravitating peaks track the compact collisionless clumps rather than the extended gas, without introducing separate couplings for galaxies and plasma or modifying the source term in (8). A more realistic treatment of colliding clusters would require time dependent Fisher fields and hydrodynamical plasma simulations, but this minimal experiment already confirms that the simplest implementation of the scalar Fisher mechanism naturally admits Bullet like lensing geometries.

Conversely, a robust observational pattern in which, for a given set of Fisher parameters compatible with galactic halos, the lensing convergence peaks in colliding clusters systematically coincide with the gas rather than with dense galaxy components would be very difficult to accommodate within (8). Such systems would directly challenge the Fisher halo picture and provide a sharp falsifier for this sector of the theory.

To check how robust this Bullet like behaviour is to changes in the relative size and mass of the gas component we carried out a small parameter scan with the script `fisher_bullet_measure.py` in the code archive. We fix two identical Gaussian galaxy clumps of radius $R_{\rm gal}$ at $x = \pm d/2$ and place a gas Gaussian at $x = 0$ with radius $R_{\rm gas} = \mu_R R_{\rm gal}$ and mass $M_{\rm gas} = \mu_M M_{\rm gal}$. For each triple $(m_F d, \mu_M, \mu_R)$ with $m_F d \in \{0.25, 0.5, 1.0, 2.0\}$, $\mu_M \in \{1, 3, 5, 10\}$ and $\mu_R \in \{1.5, 2, 3\}$ we solve the linearised Fisher equation (8) on a 64^3 periodic box, construct the total surface density $\Sigma_{\rm tot} = \Sigma_b + \Sigma_F$ along the line of sight, and extract the two dominant peaks of $\Sigma_{\rm tot}$ along the collision axis $y = 0$. For each peak we measure its distance to the nearest galaxy centroid, $\Delta_{\rm gal}$, and to the gas centroid, $\Delta_{\rm gas}$, and define a dimensionless "Bullet-likeness" ratio

$$R_{\rm Bullet} = \frac{\Delta_{\rm gas}}{\Delta_{\rm gal}},$$

with the conventions that peaks coincident with the gas have $R_{\rm Bullet} = 0$ and peaks coincident with a galaxy are reported as $R_{\rm Bullet} \gg 1$. Configurations with $R_{\rm Bullet} \gg 1$ have total convergence peaks much closer to the galaxies than to the gas, while values $R_{\rm Bullet} \simeq 0$ correspond to gas dominated peaks.

In this simple model the phase structure is almost entirely controlled by the relative size of the gas component. When the gas is only mildly more extended than the galaxies, $R_{\rm gas}/R_{\rm gal} = 1.5$, the total peaks become gas dominated once $M_{\rm gas} \gtrsim 5 M_{\rm gal}$, while for $M_{\rm gas} \sim 3 M_{\rm gal}$ one peak sits near the gas and the other near a galaxy. When the gas is twice as extended, $R_{\rm gas}/R_{\rm gal} = 2$, there is a broad band of mass ratios $1 \leq M_{\rm gas}/M_{\rm gal} \leq 5$ in which both peaks of $\Sigma_{\rm tot}$ lie between 7 and 100 times closer to the galaxy centroids than to the gas centroid, independently of $m_F d$ in the scanned range. For still more extended gas, $R_{\rm gas}/R_{\rm gal} = 3$, the Fisher Yukawa sector remains Bullet like even when the gas mass is ten times that of either clump: for $M_{\rm gas} = 10 M_{\rm gal}$ both peaks of $\Sigma_{\rm tot}$ are separated from the gas centroid by a distance $\Delta_{\rm gas}$ approximately seven times larger than their separation $\Delta_{\rm gal}$ from the nearest galaxy centroid. These experiments therefore indicate that, once the gas is a few times more extended than the collisionless clumps, there is a wide and rather insensitive region of parameter space in which a single Fisher scalar with a universal source term generically produces Bullet like convergence maps, without introducing separate couplings for galaxies and plasma.

8.1 Fisher scalar structure in clusters

Consider a cluster with baryonic mass density $\rho_b(x)$ supported by an intracluster medium and galaxies. The scalar Fisher field obeys the static equation

$$-\nabla \cdot \big(2\alpha(x)\nabla\sigma_F(x)\big) + T_F\, \partial_{\sigma_F} S_{\mathrm{Bern}}(\sigma_F(x)) = \kappa\rho_b(x)$$

with the same bounded entropy and stiffness structure as in the galactic case, but now with $\alpha(x)$ and T_F varying on megaparsec scales. The effective Fisher density and gravitational acceleration are obtained from the scalar gradients in the same way as in the spherical toy model, by matching the Fisher acceleration to a Newtonian potential.

Clusters differ from galaxies in two important respects. First, the baryon distribution is often extended and multimodal, with subclusters and filaments contributing to the overall potential. Second, the dynamical time and collisional time of the intracluster medium can be comparable to the Fisher relaxation timescale. As a result, the scalar field may not reach a fully static equilibrium during major mergers, and its configuration can retain memory of prior baryon distributions.

In the simplest approximation, one can treat the scalar as quasistatic on scales larger than the core of each subcluster. Within each subcluster the scalar responds to the local baryons through (8.1), generating an effective Fisher halo that tracks the coarse baryon configuration. On larger scales the halos associated with different subclusters interact and superpose, with the nonlinear bounded entropy term regulating the combined structure.

8.2 Off centre baryons and Fisher relaxation

In colliding cluster systems, baryons and collisionless tracers such as galaxies can become spatially separated during the merger. In a conventional dark matter scenario this separation is taken as evidence for a collisionless dark component, whose mass distribution tracks the galaxies rather than the plasma. In the Fisher picture the situation is more subtle, because the scalar responds to the coarse grained baryonic acceleration field and is governed by a hypocoercive generator with both reversible and irreversible sectors.

A schematic description can be developed by considering two subclusters with baryon densities $\rho_{b,1}(x)$ and $\rho_{b,2}(x)$ that pass through each other along a collision axis. Before the collision the scalar field is approximately the sum of two static solutions $\sigma_{\mathrm{F},1}(x)$ and $\sigma_{\mathrm{F},2}(x)$, each solving (8.1) with its own baryon source. During the collision, ram pressure and shocks can displace the baryon peaks relative to the galaxies. The scalar field, however, evolves under the full generator $K = G + J$, and its relaxation toward a new configuration is controlled by the hypocoercive interplay between Fisher diffusion and reversible transport.

If the effective Fisher temperature is low in the overlap region, the scalar halos associated with each subcluster are stiff and respond slowly. In this case the Fisher mass distribution retains a memory of the pre collision configuration for a significant time, with halo peaks that can remain closer to the collisionless galaxy components

than to the displaced plasma. The bounded entropy term prevents arbitrarily sharp features, but does not immediately erase the off set structure. In this regime the Fisher halo behaves qualitatively like a collisionless component on merger timescales, even though it is ultimately sourced by baryonic information and governed by a diffusive operator.

If the Fisher temperature is higher and reversible currents are strong, the scalar field relaxes more rapidly toward a configuration aligned with the post collision baryon distribution. The halo then follows the plasma more closely and does not exhibit large offsets. The degree of misalignment between Fisher halos and baryons in a given system is therefore a diagnostic of the local Fisher temperature and hypocoercive index.

A full quantitative treatment requires solving the time dependent scalar equation coupled to the baryon hydrodynamics in merging clusters, with $\alpha(x,t)$ and $T_F(x,t)$ determined by the underlying UIH dynamics. This provides a natural setting in which to study how Fisher halos interpolate between collisionless and collisional behaviour depending on the local balance of reversible and irreversible sectors.

Finally, the relativistic completion and lensing analysis in Section 7.2 confirms that the projected surface density $\Sigma_{\rm tot}$ used in this section is the correct input for the lensing convergence. The same scalar energy density $\rho_{\rm eff} \approx \frac{1}{2} Z(\sigma_{\rm F})\,|\nabla\sigma_{\rm F}|^2$ that sources the Weyl potential also underlies the Fisher contribution to $\Sigma_{\rm tot}$, so the peak structure in our Bullet like geometries directly encodes the Fisher lensing signal.

8.3 BPS type bounds at cluster scales

The static scalar equation (8.1) can be written in a form that admits BPS type inequalities at cluster scales. In particular, for suitable choices of α and κ one can complete the Fisher free energy into a sum of squares and a topological term, leading to an inequality of the form

$$\mathcal{F}[\sigma_{\rm F}] \;\geq\; \mathcal{F}_{\rm BPS}[\rho_b],$$

with equality when a first order Bogomolny equation is satisfied. In spherical symmetry this reduces to the scalar Bogomolny equation studied earlier, while in more general geometries it provides bounds on the integrated Fisher energy and halo mass in terms of baryonic invariants.

At cluster scales these bounds constrain the possible Fisher configurations for a given baryon distribution, and can be used to estimate how much Fisher mass can be displaced relative to the baryons during a merger without violating the Fisher BPS inequality. This suggests a programme in which cluster mergers are used as laboratories to probe the Fisher BPS structure and the associated hypocoercive relaxation.

Global stability of Fisher halos. The Bogomolny completion for the Fisher free energy implies a lower bound of the form

$$F[\sigma_F] \;\geq\; F_{\rm BPS}[\rho_b] \;=\; -\,Q_F[q_{\rho_b}],$$

where Q_F is the pure Fisher charge determined by the baryon source sector. In particular, at fixed baryon distribution the Fisher scalar cannot relax to energies below

$F_{\mathrm{BPS}}[\rho_b]$, and configurations that solve the scalar BPS equation are global minimisers of the Fisher free energy.

When the scalar sector is embedded in the density manifold described in the metriplectic analysis, with a curvature coercivity bound $\kappa_{\min} \geq \kappa_* > 0$ along the gradient flow, the Bakry-Émery framework then yields exponential relaxation of $F[\sigma_F]$ towards this minimum. In the Fisher gravity picture, a BPS Fisher halo is therefore a globally stable attractor of the scalar gradient dynamics: perturbations that respect the positivity and ellipticity hypotheses decay in the natural H^{-1} geometry, and the halo cannot evaporate or collapse below the Fisher charge set by the baryons. Cluster-scale mergers probe this stability by driving the system far from the BPS configuration and allowing the hypocoercive Fisher dynamics to relax back towards a new halo that again saturates the Bogomolny bound for the post-merger baryon distribution.

8.4 Dwarf galaxy clustering and the Fisher Freeman bound

Recent work on dwarf galaxy clustering has identified a striking inversion relative to the behaviour of massive galaxies. Using deep wide field data, Zhang et al. [31] report that diffuse, low surface brightness blue dwarfs exhibit significantly stronger spatial clustering than compact dwarfs at fixed stellar mass. In a standard cold dark matter picture the amplitude of clustering is primarily controlled by halo mass, so dwarf galaxies of similar stellar mass are expected to occupy halos of comparable mass and to show similar two point correlations. The observed reversal, in which low surface density dwarfs are more strongly clustered than high surface density dwarfs, therefore poses a non trivial challenge for formation models built on collisionless dark matter.

In the Fisher framework this anomaly has a natural interpretation in terms of the surface density driven phase structure of the scalar vacuum. The scalar sector developed above singles out a critical acceleration scale a_F and the associated Fisher Freeman bound, which may be written in the form

$$\Sigma_{\mathrm{crit}} \;=\; \frac{a_F}{2\pi G},$$

where Σ_{crit} is the characteristic central baryon surface density at which the Fisher response saturates. For central surface densities $\Sigma_b(0) \ll \Sigma_{\mathrm{crit}}$ the bounded entropy sector remains in its linear regime and the Fisher vacuum behaves as a soft medium that supports extended scalar halos. For $\Sigma_b(0) \gtrsim \Sigma_{\mathrm{crit}}$ the Bernoulli occupation number is driven towards saturation, the bounded entropy term stiffens, and the scalar gradients are constrained by the Fisher acceleration ceiling. In this stiff regime the extra force is effectively screened outside the dense core and the Fisher halo is compressed relative to the linear case.

To make contact with the ons in [31] it is useful to introduce a dimensionless Fisher saturation ratio

$$\mathcal{R}_\Sigma \;:=\; \frac{\Sigma_0}{\Sigma_{\mathrm{crit}}} \;=\; \frac{2\pi G\,\Sigma_0}{a_F},$$

where Σ_0 is a characteristic central baryon surface density. For a simple disc like

configuration one may take

$$\Sigma_0 \;\approx\; \frac{M_b}{\pi R_{\rm eff}^2},$$

with M_b the baryonic mass and $R_{\rm eff}$ an effective radius that captures the inner surface density scale. The exact profile dependence only enters through order one factors; the classification into soft and stiff regimes is controlled by the ratio $\mathcal{R}_\Sigma$.

As a representative example, consider two dwarf populations at fixed stellar mass $M_\star \approx 2\times10^8\,M_\odot$, reflecting the diffuse and compact systems discussed by Zhang et al [31]. A diffuse dwarf with effective radius $R_{\rm eff} \approx 2.0\,\mathrm{kpc}$ has

$$\Sigma_0^{\rm diff} \;\approx\; \frac{2\times10^8\,M_\odot}{\pi(2000\,\mathrm{pc})^2} \;\approx\; 1.6\times10^1\,M_\odot\,\mathrm{pc}^{-2},$$

while a compact dwarf with $R_{\rm eff} \approx 0.5\,\mathrm{kpc}$ has

$$\Sigma_0^{\rm comp} \;\approx\; \frac{2\times10^8\,M_\odot}{\pi(500\,\mathrm{pc})^2} \;\approx\; 2.5\times10^2\,M_\odot\,\mathrm{pc}^{-2}.$$

Taking $a_F \sim 10^{-10}\,\mathrm{m\,s^{-2}}$ as in the Fisher Freeman analysis above gives a critical surface density

$$\Sigma_{\rm crit} \;\approx\; 10^2\,M_\odot\,\mathrm{pc}^{-2},$$

so that the corresponding saturation ratios are

$$\mathcal{R}_\Sigma^{\rm diff} \;\approx\; \frac{\Sigma_0^{\rm diff}}{\Sigma_{\rm crit}} \;\sim\; 0.1 \quad\text{and}\quad \mathcal{R}_\Sigma^{\rm comp} \;\approx\; \frac{\Sigma_0^{\rm comp}}{\Sigma_{\rm crit}} \;\sim\; 2.5.$$

Within the Fisher scalar theory the diffuse dwarfs with $\mathcal{R}_\Sigma \ll 1$ therefore lie cleanly in the soft, linear response regime, whereas the compact dwarfs with $\mathcal{R}_\Sigma \gtrsim 1$ probe the stiff, saturated regime in which the Fisher acceleration is bounded by a_F.

This separation has direct consequences for the range and strength of the scalar mediated force. In the soft regime the bounded entropy sector remains unsaturated and the Fisher scalar explores the interior of its potential well. The associated halos are extended, with screening length set by m_F^{-1}, and the effective Fisher mass can reach far beyond the stellar component.

Diffuse dwarfs below the Freeman scale are therefore expected to carry long range Fisher clouds that overlap and interact over larger separations, enhancing their two point clustering at fixed baryon mass. In the stiff regime the high central surface density drives the vacuum towards saturation, suppresses scalar gradients in order to respect the Fisher acceleration ceiling, and compresses the halo into the inner regions. Compact dwarfs above the Freeman scale then behave more like screened systems in which the extra force beyond Newtonian gravity has a shortened effective range, reducing their large scale Fisher mediated correlations relative to diffuse dwarfs of the same stellar mass.

In a cold dark matter framework the difference in clustering between diffuse and compact dwarfs must be attributed to differences in the underlying halo population, for example through assembly bias or environment dependent feedback, since halo mass is the primary control parameter. In the Fisher picture the controlling variable is instead

the central baryon surface density through the dimensionless ratio $\mathcal{R}_\Sigma$. The reversal reported by Zhang et al [31], in which low surface density dwarfs cluster more strongly than high surface density dwarfs at fixed stellar mass, is then a natural qualitative consequence of the surface density driven phase structure of the Fisher vacuum. A detailed comparison will require embedding the Fisher halo model into a full large scale structure calculation, but the existing data already point to dwarf clustering as a promising regime in which the Fisher Freeman bound and the associated soft and stiff phases can be tested.

9 Summary and outlook

Universal Information Hydrodynamics [3] provides a framework in which weak field gravity on galactic scales can be viewed as the response of a Fisher structured vacuum to the presence of baryons. The Fisher Kähler construction supplies the geometric backbone, combining a monotone information metric and a symplectic form into a single Fisher structure that links reversible and irreversible sectors through the universal generator

$$K = G + J,$$

with G a Fisher gradient part and J a reversible current part coupled to a bounded entropy functional.

In the scalar reduction studied here the fast microscopic sector is integrated out, leaving an effective scalar Fisher field σ_F coupled to baryonic matter through a free energy functional that combines a Fisher gradient term, a Bernoulli bounded entropy channel and a linear coupling to the baryon density. The corresponding Euler-Lagrange equation defines a Fisher scalar halo model in which the gradients of σ_F generate an additional acceleration via the Fisher coupling. In spherical symmetry this model admits a Bogomolny completion and BPS type bounds that relate the halo profile to baryonic quantities. The Bogomolny structure yields inequalities that bound the total Fisher halo mass, inner slopes and characteristic core surface densities in terms of the baryon distribution and a small set of Fisher parameters. Within this scalar theory one can therefore define a characteristic Fisher surface density scale and Freeman-type bounds that constrain how strongly the vacuum can respond to a given baryonic disc.

A radial gradient flow implementation shows that the Bernoulli bounded entropy channel produces a smooth transition between cuspy and cored halos as the Fisher temperature and baryon compaction are varied. In the low temperature, high surface density regime the scalar halo behaves like a stiff cold component with cuspy profiles. At intermediate Fisher temperature the entropy penalty generates flat cores whose profiles are well approximated by empirical cored halo families. At high Fisher temperature the scalar mass is compressed into the inner regions, with little extended Fisher halo at large radii, reflecting strong reversible mixing and bounded entropy saturation. The Bernoulli model thus provides a controlled cusp to core mechanism in which the choice between cusps, cores and compressed configurations is fixed by Fisher parameters and baryon structure rather than by ad hoc profile fitting.

At the level of disc galaxy rotation curves the scalar Fisher theory motivates a simple one parameter response in which the halo contribution to the circular velocity is proportional to a cumulative nonlocal functional of the baryonic acceleration. The shape of this Fisher response is fixed by the baryonic rotation curve, while the overall

susceptibility is set by a single amplitude parameter per galaxy. In the weak amplitude, screened regime this response can be written as a Helmholtz type convolution with a Yukawa kernel, and the combination of the nonlocal Fisher functional with the empirical size-mass relation yields a baryonic Tully-Fisher scaling as a derived consequence rather than a fitted input. Within the same framework the scalar inequalities translate into bounds on core surface densities and on the shape of the radial acceleration relation for any admissible choice of global Fisher parameters.

A deliberately constrained application of this response model to a heterogeneous SPARC-like sample, using one Fisher susceptibility parameter per galaxy and fixed baryonic mass models, reveals structured trends. Gas dominated dwarfs and low surface brightness systems favour a nonzero soft susceptibility and develop extended cored rotation curves. Intermediate spirals require modest Fisher corrections that smooth the transition between inner and outer regions. High surface density, strongly bulge dominated systems are often driven toward an effectively stiff regime in which the best fit susceptibility is close to zero, consistent with Fisher halos that are compressed into the inner potential wells. These patterns are consistent with the cusp-core phase diagram and with the bounded entropy picture developed earlier, and they illustrate how a single Fisher response sector can interpolate between cored and effectively halo free behaviour as surface density is varied.

On cluster scales the same scalar mechanism extends to more complex baryon distributions and merging environments. In the screened, weak field limit the Fisher scalar obeys a Helmholtz type equation with a Fisher screening length that can be comparable to cluster core sizes. In such regimes the scalar field can retain memory of prior baryon configurations on merger timescales, especially at low Fisher temperature where the halo is stiff. This opens the possibility of systems in which the effective Fisher mass distribution exhibits offsets relative to the plasma without invoking additional collisionless species. The Bogomolny bounds provide control on how much Fisher mass can be displaced relative to the baryons during a merger, and the relaxation back toward a new BPS configuration is governed by the same hypocoercive Fisher dynamics that appear in the broader UIH setting.

A direct Fisher Gauss law test on the SPARC rotation curve sample supports this picture. By converting the fitted susceptibility profiles $C(R)$ into an effective Planck weighted stiffness $\hat{h}(x)$, as defined in Section 6.1, we find that 142 galaxies collapse onto a single dimensionless running profile with a median scatter of about 0.2 dex in $\log_{10} \hat{h}$. In the Fisher regularised Madelung setting the same stiffness scale controls the quantum pressure term through $\alpha = \hbar_{\mathrm{eff}}^2/(2m_{\mathrm{F}})$, so this universality is consistent with the idea that microscopic Fisher regularisation and macroscopic halo response are governed by a common set of information geometric parameters. We have not used this identification to introduce any new free parameters in the present analysis, but it provides a natural target for future work on the microphysical completion of the model.

A natural next step is to move beyond spherical symmetry and analyse rotating disc halos as two dimensional Fisher Kähler media. In that setting the complex Fisher order parameter $\Psi_{\mathrm{F}} = \sqrt{\rho_{\mathrm{F}}}\, e^{\mathrm{i}\varphi}$ lives on a Kähler information manifold and the full generator $K = G + J$ can support hypocoercive toroidal solitons with quantised circulation. The same Fisher stiffness that appears in the scalar halo sector would then control both the core size and the vortex spectrum of disc halos, providing a geometric link between the scalar Fisher halos studied here and a richer class of toroidal UIH configurations. Working out this Fisher Kähler soliton structure, and comparing it with the effective

Planck universality seen in Section 6.1, is left to future work.

Several directions for further work are clear. A first priority is to connect the effective Fisher susceptibility used in rotation curve fits, and the structural inequalities and surface density scale derived here, to the spectral data of the universal generator. In particular, the halo gap and Fisher response indices $(\Lambda_{\mathrm{halo}}, S_{\mathrm{halo}})$ introduced in the Fisher spectrometer construction provide concrete dimensionless invariants that should be computable both from microscopic UIH models and from halo fits. This requires a detailed analysis of the spectrum of K in the presence of baryonic sources, and of how the Fisher parameters flow under coarse graining.

A second priority is to lift the scalar model to a full Fisher Kähler field theory with both amplitude and phase, capturing Fisher currents, vortices and gravitomagnetic effects in rotating systems. This would allow direct modelling of non spherical halo structures, bars and spiral features, and the coupling between halo flows and disc dynamics within the same Fisher geometric framework. A third priority is to construct the optical metric associated with Fisher structured vacua, to compute lensing in Fisher halos derived from microscopic UIH models, and to confront those predictions with systems in which baryons and lensing mass are offset.

Finally, a systematic comparison between Fisher halo predictions and large galaxy and cluster samples that explicitly enforces the Fisher inequalities and Freeman-type bounds will be essential. The scalar Fisher model and susceptibility based response developed here provide practical tools for such comparisons, embedding empirical fits within a geometric framework that links them to information hydrodynamics, bounded entropy and UIH universality diagrams. As these tools are refined and extended, they will either identify a small set of information geometric parameters that organise gravity from laboratory Fisher channels to galaxies and clusters, or reveal where additional degrees of freedom and couplings are required. In either case the scalar Fisher sector provides a controlled starting point for recasting gravitational phenomena in terms of universal information flows rather than additional elementary dark components.

Three tests of vacuum stiffness. The scalar Fisher framework links halo phenomenology to baryon surface density and environment rather than to total mass alone. This suggests three qualitative tests that we leave for future work.

First, the saturation scale derived from the Freeman surface density bound predicts a sharp transition in effective halo mass-to-light ratios as a function of central surface density, potentially explaining why diffuse dwarf spheroidals appear dark matter dominated while compact globular clusters of similar stellar mass show little evidence for an extended halo [35]. Second, because the Fisher halo is an emergent response to the baryon distribution rather than an independently assembling particle component, early structure formation at high redshift should track baryon collapse timescales more closely than halo virialisation, providing an alternative angle on the abundance of very massive systems reported in recent JWST surveys [36].

Third, the stiffness profile is sensitive to the large scale environment, so the same vacuum sector that supports extended halos for isolated ultra diffuse galaxies can be partially screened in the vicinity of massive hosts, offering a possible route to reconcile dark matter poor satellites such as DF2 and DF4 with the Fisher picture [37]. Together these density and environment driven effects provide a set of falsifiable signatures that distinguish Fisher gravity from standard cold dark matter at fixed baryon mass.

A Weak-field Einstein relations by solver

We treat the simulation box as a static weak-field configuration with negligible time derivatives. In Fourier space, with $\nabla^2 \to -k^2$, the solver implements the Poisson relation

$$k^2\Psi(\mathbf{k}) = -4\pi G\,\rho_{\rm tot}(\mathbf{k}), \qquad \rho_{\rm tot} := \rho_{\rm s} + \rho_{\rm J},$$

where $\rho_{\rm s}$ is the scalar gradient energy density and $\rho_{\rm J}$ is the auxiliary "current" energy density.

The slip field is sourced by the trace-free anisotropic stress Π_{ij} via

$$k^4 S(\mathbf{k}) = 12\pi G \left(k_i k_j - \tfrac{1}{3}\delta_{ij}k^2\right)\Pi_{ij}(\mathbf{k}).$$

Equation (A) makes the isotropy condition explicit: if Π_{ij} is locally isotropic, meaning it is proportional to δ_{ij} so that its trace-free part vanishes, then $S(\mathbf{k}) \equiv 0$ for all $\mathbf{k} \neq 0$ and the metric perturbations coincide, $\Phi = \Psi$.

B Vacuum universality and analogue probes

The unifying claim of the broader UIH programme [1–4] is that many apparently different physical systems share a common information-geometric structure. Each system carries a Fisher metric on its state space, a metriplectic generator $K = G + J$ combining reversible currents and Fisher-gradient dissipation, and a small set of spectral and response invariants that classify its behaviour under coarse-graining. The Fisher halo theory developed here suggests that galactic and cluster halos are another member of this family.

The static analysis in Section 5 and the dynamical structure outlined in Section 7.7 associate to each realistic Fisher halo a dimensionless gap parameter $\Lambda_{\rm halo}$ and a susceptibility index $S_{\rm halo}$ via (5.7)-(5.7). The same UIH methods applied to quantum channels and classical Markov generators [3, 4] yield analogous dimensionless gaps and response exponents for those finite-dimensional systems. One can therefore view both laboratory systems and galactic halos as points in a common "Fisher universality plane" with coordinates (Λ, S).

We do not expect these points to coincide numerically. Universality classes are regions, not single values, and systems at very different scales probe different parts of the same Fisher geometry. What the unified picture does suggest is that, after appropriate rescaling, the points corresponding to laboratory realisations of Fisher-Kähler dynamics and those corresponding to Fisher halos should occupy a compatible region in the (Λ, S) plane and exhibit similar qualitative scaling under coarse-graining. For example, systems that flow under Fisher-preserving renormalisation group maps to the same diffusive fixed point in the sense of Ref. [4] should display comparable relations between their gap, their hypocoercive index and their static response exponents.

This perspective turns the idea of laboratory "vacuum microscopes" into a concrete consistency requirement. Given a sufficiently broad collection of laboratory systems for which the Fisher gap and response exponents can be measured, one can delineate an empirical universality region $\mathcal{U}_{\rm lab}$ in the (Λ, S) plane. The Fisher halo fits then define an empirical region $\mathcal{U}_{\rm halo}$ via the coordinates $(\Lambda_{\rm halo}, S_{\rm halo})$ extracted from galaxies

and clusters. If these two regions are grossly incompatible, in the sense that $\mathcal{U}_{\text{halo}}$ lies well outside any reasonable coarse-grained extension of $\mathcal{U}_{\text{lab}}$, then one of two conclusions is natural: either the vacuum degrees of freedom underlying Fisher halos do not belong to the same Fisher universality class as the laboratory systems studied so far, or the entire UIH unification of quantum, Markov and gravitational sectors is incomplete.

Conversely, if future numerical work finds that $\mathcal{U}_{\text{halo}}$ and $\mathcal{U}_{\text{lab}}$ are compatible after taking into account the obvious differences of scale and environment, this would provide non-trivial support for the information-geometric picture developed here. In that case condensed-matter systems, carefully engineered GKLS channels and classical stochastic processes would genuinely act as analogue probes of the same Fisher-Kähler vacuum geometry that governs Fisher halos, with the gap and response spectra measured in the laboratory helping to constrain the plausible ranges of Fisher parameters in the galactic and cosmological sectors.

The present paper does not attempt such a cross-scale comparison. The definitions of Λ_{halo} and S_{halo} are provided as a template for future numerical and experimental work rather than as claimed measurements. They do, however, make precise in what sense the Fisher halo sector can be said to belong to the same information-geometric universality class as the UIH systems already studied, and how the combined programme could in principle be falsified by a mismatch of Fisher invariants across scales.

C Fisher-Kähler disc halos with phase and vortices

The phase lift and its topological sectors follow the reversible classification and circulation quantisation developed in [1], while the density-level no-work and weighted-Liouville constraints on reversible currents are as in [2], embedded in the full Fisher–Kähler UIH framework [3].

The scalar Fisher gravity model treats the halo as a real field σ_F with free energy

$$F_{\text{scalar}}[\sigma_F;\rho_b] = \int_{\mathbb{R}^3} \left[\alpha(x)\,|\nabla\sigma_F|^2 - T_F S_{\text{Bern}}(\sigma_F) - \kappa\,\sigma_F(x)\,\rho_b(x)\right] d^3x.$$

To incorporate reversible Fisher currents more explicitly it is natural to lift this scalar field to a complex Fisher-Kähler order parameter

$$\Psi(x) = \sqrt{\rho_F(x)}\, e^{i\varphi(x)},$$

where ρ_F is a halo density and φ is a phase whose gradients encode J-sector currents. A simple choice compatible with the Bernoulli structure is to map the scalar field σ_F to the halo density via

$$\rho_F(x) = \rho_0\, p(\sigma_F(x)), \qquad p(\sigma_F) = \frac{1}{1+e^{-\beta\sigma_F}},$$

so that ρ_F inherits both the bounded entropy and the BKM mobility of the Bernoulli manifold.

We then consider the augmented free energy

$$F_{\mathrm{tot}}[\sigma_F, \varphi; \rho_b] = F_{\mathrm{scalar}}[\sigma_F; \rho_b] + F_J[\sigma_F, \varphi],$$

with J-sector contribution

$$F_J[\sigma_F, \varphi] = \frac{1}{2m_J} \int_{\mathbb{R}^3} \rho_F(\sigma_F(x)) \, |\nabla\varphi(x)|^2 \, d^3x.$$

The metric gradient flow of F_{tot} in the Fisher-Wasserstein geometry defines the G-sector, while the Hamiltonian flow generated by F_J defines the reversible J-sector. On a time slice, the corresponding continuity equation for the halo density can be written in the form

$$\partial_t \rho_F + \nabla \cdot (\rho_F v_G + \rho_F v_J) = 0,$$

with

$$v_G = -G \, \nabla\mu_{\mathrm{eff}}, \qquad v_J = \frac{1}{m_J} \nabla\varphi,$$

where G is the Fisher mobility operator and

$$\mu_{\mathrm{eff}} = \mu_{\mathrm{scalar}}(\sigma_F; \rho_b) + \frac{1}{2m_J} |\nabla\varphi|^2$$

is the effective chemical potential obtained by varying F_{tot} with respect to ρ_F. Here μ_{scalar} denotes the chemical potential of the pure scalar theory.

A static halo configuration satisfies two conditions. First, the G-sector current must vanish, which requires μ_{eff} to be spatially constant. Second, the J-sector current must be divergence free,

$$\nabla \cdot (\rho_F \nabla\varphi) = 0.$$

The first condition can be written as

$$\mu_{\mathrm{scalar}}(\sigma_F; \rho_b) + \frac{1}{2m_J} |\nabla\varphi|^2 = \mu_0,$$

for some constant μ_0, and shows that the scalar sector experiences an additional effective potential

$$V_J(x) := \frac{1}{2m_J} |\nabla\varphi(x)|^2$$

due to reversible Fisher circulation.

In an axisymmetric disc plus halo it is natural to adopt cylindrical coordinates (R, θ, z) and to consider a vortex type phase field

$$\varphi(R, \theta, z) = \ell \, \theta + \varphi_0(R, z),$$

where $\ell \in \mathbb{Z}$ is a winding number and φ_0 is a smooth correction. For the pure vortex $\varphi_0 \equiv 0$ one has

$$\nabla\varphi = \frac{\ell}{R} \, \hat{\theta}, \qquad |\nabla\varphi|^2 = \frac{\ell^2}{R^2}, \qquad v_J = \frac{\ell}{m_J R} \, \hat{\theta}.$$

The weighted continuity equation for the J-sector,

$$\nabla \cdot (\rho_F v_J) = 0,$$

reduces in this case to

$$\frac{1}{R}\frac{\partial}{\partial R}\Big(R\rho_F(R,z)\, v_J^\theta(R,z)\Big) + \frac{\partial}{\partial z}\big(\rho_F v_J^z\big) = 0.$$

With $v_J^z = 0$ and $v_J^\theta = \ell/(m_J R)$ this simplifies to

$$\frac{\ell}{m_J}\frac{1}{R}\frac{\partial}{\partial R}\rho_F(R,z) = 0,$$

so that any halo profile $\rho_F(R,z)$ which is radially slowly varying over the radii of interest admits such a vortex current as an approximately divergence free J-sector solution.

Inserting the vortex ansatz into (C) shows that the scalar chemical potential obeys

$$\mu_{\text{scalar}}(\sigma_F;\rho_b) + \frac{\ell^2}{2m_J R^2} = \mu_0.$$

Compared with the pure scalar case this introduces a centrifugal term $\ell^2/(2m_J R^2)$ which diverges as $R \to 0$ for $\ell \neq 0$. To keep the effective chemical potential μ_{eff} finite the scalar field σ_F and its associated Bernoulli density ρ_F must adjust so that the combination remains bounded. In particular, nonzero winding ℓ suppresses the halo density in the central region, providing a natural Fisher-Kähler mechanism for core formation in disc halos with significant J-sector circulation.

A full analysis of these Fisher-Kähler disc halos would require solving the coupled amplitude-phase system for (σ_F, φ) in a realistic disc geometry and matching the resulting rotation curves and density profiles to observations. The simple construction above shows that the UIH framework already contains the necessary geometric ingredients to support vortex supported, cored disc halos as stationary hypocoercive bound states of the combined G and J sectors.

D Fisher cosmology roadmap

The scalar Fisher halo model developed in this paper has been formulated entirely in the weak field, quasi Newtonian regime on approximately static backgrounds. To assess whether the same Fisher structure can also account for cosmological dark components one must embed the scalar sector in a homogeneous and isotropic space-time and follow both the background expansion and the growth of perturbations. We briefly outline a minimal roadmap for such a Fisher cosmology, without attempting a full implementation.

A natural starting point is a spatially flat Friedmann-Robertson-Walker metric

$$\mathrm{d}s^2 = -\mathrm{d}t^2 + a(t)^2\,\mathrm{d}\vec{x}^{\,2},$$

together with a coarse-grained homogeneous Fisher scalar $\sigma_F = \sigma_F(t)$ representing

the vacuum order parameter at cosmological scales and an averaged baryon density $\bar{\rho}_b(t)$. At this level the scalar sector is described by the same bounded entropy free energy used for galactic halos, specialised to spatially homogeneous configurations,

$$F_{\mathrm{FRW}}[\sigma_F; \bar{\rho}_b] = \int_{\Sigma_t} a(t)^3 \Big(\alpha_0 \, |\nabla \sigma_F|^2 + V_I(\sigma_F) - \kappa \, \sigma_F \, \bar{\rho}_b \Big) \, \mathrm{d}^3 x,$$

with $\alpha_0 > 0$ constant and V_I the Bernoulli bounded entropy potential introduced in Section 3. For strictly homogeneous fields the gradient term drops out of the background dynamics and the scalar behaves as an effective fluid with energy density and pressure of the form

$$\rho_F(\sigma_F, \dot{\sigma}_F) = \frac{1}{2} \dot{\sigma}_F^2 + V_I(\sigma_F), \qquad P_F(\sigma_F, \dot{\sigma}_F) = \frac{1}{2} \dot{\sigma}_F^2 - V_I(\sigma_F),$$

up to model dependent normalisations set by the underlying Fisher metric. The equation of motion for σ_F then takes the usual damped form

$$\ddot{\sigma}_F + 3H \dot{\sigma}_F + V_I'(\sigma_F) = \kappa \, \bar{\rho}_b(t), \qquad H := \frac{\dot{a}}{a},$$

in which the bounded entropy channel and the baryon coupling jointly determine the effective equation of state parameter

$$w_F(t) := \frac{P_F}{\rho_F} \in [-1, +1],$$

with the accessible range restricted by the Bernoulli geometry and the Fisher temperature T_F.

A first cosmological test of the scalar Fisher sector would therefore proceed at the level of the homogeneous background. For any given choice of Fisher parameters $(\lambda_F, T_F, \alpha_0, \kappa)$ one can integrate the coupled Friedmann and scalar equations to obtain an effective Hubble history $H(a)$ and compare it to the background expansion inferred from supernovae, baryon acoustic oscillations and late time distance ladders. The bounded entropy structure of V_I strongly restricts the allowed time evolution of $w_F(t)$; background histories that fall far outside the observationally allowed band would falsify that choice of Fisher parameters or potential sector.

The second stage is to study linear perturbations of the Fisher scalar and the metric around the FRW background. At this level the scalar Fisher vacuum behaves as a dark component with a specific sound speed and clustering scale, again fixed by the same Fisher stiffness and bounded entropy parameters that appear in the galactic theory. The questions are then whether the resulting matter power spectrum, CMB anisotropies and lensing potentials can be brought into agreement with data for any admissible Fisher parameter set, and whether the scalar sector can simultaneously support the BPS halo structure used in this paper. Failure to achieve such a joint fit would signal that the present scalar Fisher model is at best an effective description of late-time, weak-field halos and that additional degrees of freedom or modified couplings are required at cosmological scales.

Finally, the wider UIH framework suggests a more microscopic route to Fisher cosmology. The same universal generator $K = G + J$ and Fisher-Kähler geometry used to describe GKLS channels and scalar halos define an information theoretic

state space for the vacuum. In principle one can coarse-grain this state space on cosmological scales and derive effective Fisher parameters and bounded entropy channels directly from the spectrum of K in a slowly evolving FRW background. Pursuing this programme lies beyond the scope of the present work, but it provides a concrete way to connect early-universe Fisher cosmology, late-time Fisher halos and laboratory UIH experiments within a single information geometric framework. As such it forms an essential falsifier and extension of the scalar Fisher gravity picture developed here.

A broader motivation for the scalar Fisher programme is the possibility of a genuinely universal information theoretic description of irreversible dynamics across scales. In the finite dimensional UIH setting, the same Fisher gap and hypocoercive indices that control relaxation in quantum channels and classical Markov processes organise a rich phase diagram of approach to equilibrium. The Fisher scalar halos studied here can be viewed as infinite dimensional, weak field, coarse grained realisations of the same UIH geometry, with the Fisher temperature and stiffness hierarchy encoding the effective strength of reversible currents in the vacuum sector.

This suggests a concrete falsifier programme that goes beyond fitting individual galaxies. One can ask whether a single family of Fisher parameters, calibrated for example on hypocoercive experiments in controlled laboratory systems, can be run through the scalar Fisher construction to describe disc galaxy rotation curves, cluster scale lensing and merger offsets, and eventually a Fisher cosmology, without leaving the regime allowed by the Fisher bounds and guardrails. Failure to find such a common Fisher phase would point either to missing structure in the scalar reduction or to a breakdown of the assumed cross scale universality. Success, by contrast, would identify a small set of information geometric parameters that organise gravity from quantum channels to galaxies. The present work takes the first steps in this direction by showing that a bounded entropy Fisher scalar, constrained by Bogomolny structure and simple guardrails, already reproduces several key halo phenomena while remaining tightly linked to the underlying UIH geometry.

E Soft Fisher vacuum, local voids and the H_0 tension

Several recent works have argued that the tension between local distance ladder determinations of the Hubble constant and the Planck ΛCDM value may be signalling a large scale departure from homogeneity in the nearby Universe. Banik and Samaras [33] show that early time modifications such as early dark energy are disfavoured once the cosmic age and matter density are constrained self consistently. In their analysis the remaining viable late time solutions all require a gigaparsec scale local underdensity, of the KBC type, whose evacuation proceeds more rapidly than in standard gravity. In effect the data demand an enhancement of structure growth on scales of order 100 to 300 Mpc.

In the Fisher scalar framework this type of behaviour arises naturally from the density dependence of the stiffness profile $\alpha(x)$. Overdense regions such as walls and filaments drive the Fisher occupation towards saturation and enter a stiff, screened regime in which the scalar contribution to the acceleration is suppressed. In underdense regions the baryon density is lower, the Fisher occupation remains in the linear regime, and the effective stiffness drops. As discussed in Section 2.5, a smaller α enhances the

Fisher response and increases the total gravitational acceleration,

$$g_{\rm tot} \;=\; g_{\rm N} + g_{\rm F} \;\approx\; g_{\rm N}\,(1+\gamma_{\rm vac}),$$

with $\gamma_{\rm vac}$ inversely related to the local stiffness. Voids therefore correspond to a soft Fisher vacuum in which the evacuation towards the surrounding walls proceeds faster than in a purely Newtonian setting. The same soft vacuum mechanism that produces extended halos for diffuse dwarf galaxies thus provides a concrete field theoretic realisation of the enhanced void growth required in Ref. [33].

Mazurenko et al. [34] refine this picture by comparing specific local void models with the redshift dependence of the inferred Hubble parameter $H_0(z)$ reconstructed from Type Ia supernovae and other distance indicators. For an observer near the centre of a KBC scale void the local expansion inferred under the assumption of homogeneity is elevated at low redshift and gradually relaxes towards the Planck value at higher redshift, as light rays probe regions outside the underdensity. Mazurenko et al. show that this $H_0(z)$ behaviour is broadly consistent with void profiles that also fit bulk flow constraints, provided structure formation is enhanced in the void interior.

In a Fisher cosmology the same qualitative pattern is expected once the scalar sector is promoted to an evolving background. Inside the underdense region the soft Fisher vacuum amplifies the outflow, raising the locally inferred expansion rate. As one moves outwards, the baryon density increases, the vacuum stiffens, and the Fisher contribution to the acceleration is screened. The effective gravitational coupling along the line of sight then interpolates from $G_{\rm eff} \approx G(1+\gamma_{\rm vac})$ in the void interior back to G in the homogeneous exterior, producing a mild decline of $H_0(z)$ from the local ladder value towards the Planck value. In this sense the Fisher soft vacuum provides a controlled mechanism for the kind of enhanced late time structure growth and redshift dependent H_0 evolution that the void based resolutions of the Hubble tension require, while remaining consistent with the gigaparsec scale smoothness of the Fisher scalar implied by local solar system tests.

References

[1] J. R. Dunkley. The Converse Madelung Question: Schrödinger Equation from Minimal Axioms. arXiv:2511.03552 (2025).

[2] J. R. Dunkley. The Converse Madelung Answer: Quantum Hydrodynamics and Fisher Information Geometry. 10.5281/zenodo.17643885 (2025).

[3] J. R. Dunkley. Universal Information Hydrodynamics. 10.5281/zenodo.17651781 (2025).

[4] J. R. Dunkley. Hypocoercive Renormalisation. 10.5281/zenodo.17751078 (2025).

[5] Intrinsic Fisher-Kähler Information Geometry Hypocoercive Renormalisation. 10.5281/zenodo.17779841 (2025).

[9] B. R. Frieden. *Physics from Fisher Information*. Cambridge University Press (1998).

[7] M. Reginatto. Derivation of the equations of nonrelativistic quantum mechanics using the principle of minimum Fisher information. Physical Review A **58**, 1775–1787 (1998).

[8] S. Amari. *Differential-Geometrical Methods in Statistics*. Springer (1985).

[9] B. R. Frieden. *Physics from Fisher Information: A Unification*. Cambridge University Press (1998).

[10] B. R. Frieden. *Science from Fisher Information: A Unification*. Cambridge University Press (2004).

[11] T. Jacobson. Thermodynamics of Spacetime: The Einstein Equation of State. Physical Review Letters **75**, 1260–1263 (1995).

[12] T. Padmanabhan. Thermodynamical Aspects of Gravity: New insights. Reports on Progress in Physics **73**, 046901 (2010).

[13] E. P. Verlinde. On the Origin of Gravity and the Laws of Newton. JHEP **04**, 029 (2011).

[14] E. P. Verlinde. Emergent Gravity and the Dark Universe. SciPost Physics **2**, 016 (2017).

[15] J. Khoury and A. Weltman. Chameleon Fields: Awaiting Surprises for Cosmology. Physical Review Letters **93**, 171104 (2004).

[16] L. Berezhiani and J. Khoury. Theory of Dark Matter Superfluidity. Physical Review D **92**, 103510 (2015).

[17] J. W. Moffat. Scalar-Tensor-Vector Gravity Theory. Journal of Cosmology and Astroparticle Physics **03**, 004 (2006).

[18] M. Milgrom. A Modification of the Newtonian Dynamics as a Possible Alternative to the Hidden Mass Hypothesis. The Astrophysical Journal **270**, 365–370 (1983).

[19] R. H. Sanders and S. S. McGaugh. Modified Newtonian Dynamics as an Alternative to Dark Matter. Annual Review of Astronomy and Astrophysics **40**, 263–317 (2002).

[20] B. Famaey and S. S. McGaugh. Modified Newtonian Dynamics (MOND): Observational Phenomenology and Relativistic Extensions. Living Reviews in Relativity **15**, 10 (2012).

[21] K. C. Freeman. On the Disks of Spiral and S0 Galaxies. The Astrophysical Journal **160**, 811–830 (1970).

[22] R. B. Tully and J. R. Fisher. A New Method of Determining Distances to Galaxies. Astronomy & Astrophysics **54**, 661–673 (1977).

[23] A. Burkert. The Structure of Dark Matter Halos in Dwarf Galaxies. The Astrophysical Journal Letters **447**, L25–L28 (1995).

[24] J. F. Navarro, C. S. Frenk, and S. D. M. White. A Universal Density Profile from Hierarchical Clustering. The Astrophysical Journal **490**, 493–508 (1997).

[25] S. S. McGaugh, J. M. Schombert, G. D. Bothun, and W. J. G.deBlok. The Baryonic Tully-Fisher Relation. The Astrophysical Journal **533**, L99–L102 (2000).

[26] F. Lelli, S. S. McGaugh, and J. M. Schombert. SPARC: Mass Models for 175 Disk Galaxies with Spitzer Photometry and Accurate Rotation Curves. The Astronomical Journal **152**, 157 (2016).

[27] S. S. McGaugh, F. Lelli, and J. M. Schombert. The Radial Acceleration Relation in Rotationally Supported Galaxies. Physical Review Letters **117**, 201101 (2016).

[28] D. Clowe, M. Bradač, A. H. Gonzalez, M. Markevitch, S. W. Randall, C. Jones, and D. Zaritsky. A Direct Empirical Proof of the Existence of Dark Matter. The Astrophysical Journal Letters **648**, L109–L113 (2006).

[29] Planck Collaboration (N.Aghanim etal.). Planck 2018 Results. VI. Cosmological Parameters. Astronomy & Astrophysics **641**, A6 (2020).

[30] H. Rue and L. Held. *Gaussian Markov Random Fields: Theory and Applications*. Chapman & Hall/CRC (2005).

[31] Z. Zhang, Y. Chen, Y. Rong, H. Wang, H. Mo, X. Luo and H. Li. Unexpected clustering pattern in dwarf galaxies challenges formation models. arXiv:2504.03305 (2025).

[32] K. Zioutas. Novel dark matter signatures. arXiv:2501.15498 (2025).

[33] I. Banik and N. Samaras. Constraints on the Hubble and matter density parameters with and without modelling the CMB anisotropies. arXiv:2410.00804 (2025).

[34] S. Mazurenko, I. Banik and P. Kroupa. The redshift dependence of the inferred H_0 in a local void solution to the Hubble tension. Mon. Not. R. Astron. Soc., in press (2025), arXiv:2412.12245.

[35] H. Baumgardt, M. Hilker, A. Sollima, and A. Bellini. Mean proper motions, space orbits and velocity dispersion profiles of Galactic globular clusters from Gaia DR2 data. Mon. Not. R. Astron. Soc. 482, 5138 (2019).

[36] M. Xiao et al. Accelerated formation of ultra massive galaxies in the first billion years. arXiv:2309.02492 (2023).

[37] P. van Dokkum et al. A galaxy lacking dark matter. Nature 555, 629 (2018).